Parton Showers and Radiative Corrections in QCD

Zur Erlangung des akademischen Grades eines

DOKTORS DER NATURWISSENSCHAFTEN

bei der Fakultät für Physik
des Karlsruher Instituts für Technologie

genehmigte

DISSERTATION

von

Dipl. Phys. Simon Plätzer

aus Gernsbach

Tag der mündlichen Prüfung: 22. 10. 2010
Referent: Prof. Dr. D.Zeppenfeld
Korreferent: Prof. Dr. M.Steinhauser

Parton Showers and
Radiative Corrections in QCD

Doctoral Thesis submitted to the
Faculty of Physics, Karlsruhe Institute of Technology by

Simon Plätzer

Karlsruhe, October 2010

Some people see things as they are and say: why?
I dream things that never were and say: why not?

Abstract

The simulation of realistic final states is an indispensable tool to extract any conclusion from experimental data obtained at high-energy collider experiments. More precise theoretical predictions will be needed to accompany the ever increasing precision of measurements reported by experiments.

This thesis focuses on the perturbative QCD part involved in these simulations, particularly parton showers, higher order QCD corrections, and their consistent combination. A new parton shower algorithm based on subtraction dipoles is studied theoretically, with emphasis on the proper inclusion of effects due to soft gluon radiation, and numerical results from an implementation of this algorithm in the Monte Carlo event generator Herwig++ are reported.

In order to perform the combination of parton showers and higher order QCD corrections, a theoretical handle is required to calculate expansions of parton shower predictions in the strong coupling constant. Such a formalism is introduced on very general grounds and used to set the theoretical grounds for combining parton showers and QCD corrections at next-to leading (NLO) and next-to-next-to leading order (NNLO) in perturbation theory. A program setting up NLO calculations matched to the dipole-type parton shower in an automatic way has been developed, and numerical results are reported along these obtained from showering events described at leading order.

Zusammenfassung

Die Simulation realisitischer Endzustände stellt ein unverzichtbares Hilfsmittel dar, um Daten zu interpretieren, die mit Experimenten an Hochenergie-Kollidern gemessen werden. Hier sind präzisere theoretische Vorhersagen nötig, die den immer genauer werdenden Messungen gegenüber gestellt werden können.

Diese Arbeit beschäftigt sich mit dem Teil der Simulationen, der durch perturbative Rechnungen in QCD bestimmt ist. Speziell werden hier Partonkaskaden, Korrekturen höherer Ordnung und deren konsistente Kombination betrachtet. Theoretische Eigenschaften eines neuen Partonkaskaden-Algorithmus, basierend auf Subtraktions-Dipolen, werden insbesondere bezüglich der korrekten Wiedergabe von Effekten bedingt durch vielfache Abstrahlung weicher Gluonen untersucht. Numerische Resultate gewonnen aus einer Implementierung dieses Algorithmus' in dem Ereignis-Generator Herwig++ werden diskutiert.

Für die Kombination von Partonkaskaden und Korrekturen höherer Ordnung ist ein theoretischer Formalismus nötig, der es erlaubt, Vorhersagen einer Partonkaskade systematisch in der starken Kopplungs-Konstante zu entwickeln. Solch ein Formalismus wird in einer allgemeinen Art und Weise abgeleitet und benutzt um die theoretische Basis der Kombination von Partonkaskaden und Korrekturen in nächst-führender Ordnung (NLO) und nächst-nächst-führender Ordnung (NNLO) zu berechnen. Im Rahmen dieser Arbeit wurde zusätzlich zur Entwicklung der Dipole-Kaskade eine Monte Carlo Simulation entwickelt, die Rechnungen in NLO automatisch mit dieser Partonkaskade kombiniert. Diese verbesserte Simulation wird mit der Beschreibung von Ereignissen in führender Ordnung verglichen.

Contents

1 Introduction

The understanding of the fundamental building blocks of nature and the interactions between them has constantly increased in the last decade. This knowledge – mainly accumulated at high energy particle collider experiments – has been assembled in the standard model (SM) of particle physics, comprising on the one hand a theory of electromagnetic and weak interactions being treated on equal footing.[1] On the other hand, the theory of strong interactions, which is by now accepted to be modelled by quantum chromodynamics (QCD) is included, but no success has so far been made in consistently including a quantum theory of gravity.

The SM, describing thus three of the fundamental forces of nature, is nowadays established experimentally in a very precise way. Only one degree of freedom, the physical Higgs boson, has so far not been discovered. This leaves as a yet open question the mechanism of electroweak symmetry breaking. Further experimental findings, in particular the very existence of dark matter, and strictly also including the non-vanishing neutrino masses, show that the SM is to some extent incomplete. From a theoretical point of view, the SM may be regarded as an effective low-energy theory of a more fundamental model. Besides the search for the missing Higgs boson (including the question whether this is the Higgs boson as assumed existing in the SM), it is the quest for any 'new physics' beyond the SM, which mainly triggered the development and build of the Large Hadron Collider (LHC), by now in operation at CERN.

Gaining more insight into the dynamics of QCD in this context appears not to be a major question raised, though it is of utmost importance in particular for phenomenology at hadron colliders: QCD is the force confining the fundamental quarks in hadrons and its influence is thus not avoidable in scattering processes involving hadrons. It needs to be understood in detail to draw any conclusion from measurements performed at the

---

[1]The electroweak interactions in the standard model should not be regarded 'unified', as sometimes stated. The correct term is that the electromagnetic and weak forces mix.

LHC experiments. Being of interest on its own as well, QCD dynamics has been explored extensively at the LEP and HERA colliders, just to name two examples.

Predictions from QCD can be calculated by means of a perturbative expansion in terms of its fundamental degrees of freedom – quarks and gluons, commonly referred to as partons. Owing to the fact that QCD becomes strongly coupled at small momentum transfers, partons produced in a scattering process will fragment into the observed hadrons. The dynamics of this hadronization process is calculable from a perturbative expansion only to some extent. The remaining part is subject to phenomenological models in place of the yet not analytically known behaviour of QCD at small energy scales. Though perturbative calculations can be mapped to a certain class of observables by identifying a 'jet' of hadrons as originating from a parton, a full simulation of realistic final states as encountered in the experiments is mandatory to compare theoretical predictions to observed data. It is this need, which is common to all high energy physics collider experiments, may their purpose be just the study of QCD dynamics or the search for physics beyond the SM.

Simulations of this type, being implemented by using Monte Carlo methods and aiming at the prediction of events with a frequency as observed in nature, have been provided since more than 30 years. Since the first attempts, many insights have been gained into the nature of multiple parton emission initiating the fragmentation process and non-perturbative models modelling the last stage of hadron formation in a jet. A shortcoming of these simulations is that almost all processes described are still modelled at the leading order of QCD perturbation theory, though higher-order radiative corrections are by now available from many collaborations. This includes recent approaches to fully automate the calculation of these corrections, yet only for few processes a consistent inclusion of these into realistic simulations has so far been achieved. One may raise the question of an automated combination here as well.

Maintaining the correct description of multiple parton emission, or 'parton showers', while easing the combination with higher order QCD corrections, is a further topic to be considered in this context. Taking these two questions as a starting point, the work at hand is actually structured in a two-fold way, dealing with new approaches to parton showers on the one hand, and the inclusion of radiative corrections, on the other hand. More precisely, the outline of this thesis is as follows:

In chapter 2 the basics of QCD are revisited, while chapter 3 reviews the treatment of higher order QCD corrections, the resummation of leading contributions to all orders, and the combination of both types of calculations. This forms the analytical counterpart of combining parton showers and radiative corrections in a Monte Carlo simulation.

Chapter 4 develops a calculational formalism for predictions as expected from parton shower simulations, forming not only the input to derive and cross-check analytically properties of parton showers against expectations from perturbative calculations, but especially to calculate fixed-order expansions. The knowledge of the latter is mandatory to derive the consistent combination, or the matching, of parton showers and radiative corrections.

In chapter 5, a new parton shower algorithm is introduced. This algorithm is much better suited for including higher order QCD corrections and shown to still correctly predict the leading effects of multiple parton emission to all orders. In chapter 6, use is made of the formalism set up in chapter 4 to calculate the conditions to be met when combining parton showers with next-to-leading order (NLO) calculations, and investigates the same structures at next-to-next-to-leading order (NNLO).

Having set the scene on a theoretical ground, chapter 7 introduces Monte Carlo methods developed to automate the matching to NLO and to allow for more flexibility even in the parton shower simulation itself.

Chapter 8 focuses on completely documenting the parton shower algorithm as used in practise, including all technical details. Chapter 9 shares this motivation, now focusing on matching. Numerical results as obtained from the implementation of these algorithms are discussed in chapter 10, before turning to a summary and outlook on further possible work in chapter 11. Three appendices are devoted to short documentations of the software libraries constituting the core of the developed Monte Carlo simulation code, and one appendix documents the validation of these codes.

1 Introduction

2 Quantum Chromodynamics

Based on the study of non-abelian gauge theories by Yang and Mills [1], and the ground-breaking work of Callan, Gross, Wilczek and Politzer, [2,3] and many others, quantum chromodynamics (QCD) is by now accepted to be the theory of strong interactions. Though not exactly solvable except numerically on a discrete space-time lattice, predictions for collider experiments can be calculated by a perturbative expansion in the strong coupling. This is possible in the high-energy regime where the theory becomes asymptotically free, *i.e.* weakly coupled. These predictions, which in some cases have been calculated up to the fourth order in perturbation theory, are confirmed by experiments with amazingly high precision. In this chapter we will shortly review the basics of QCD.

QCD is a non-abelian gauge theory with (in general) gauge group $SU(N)$, where N is the number of charges to which the interaction couples, usually referred to as 'colours'. Experiments determined that $N = 3$. The QCD gauge field is a connection valued in the Lie algebra $su(N)$,

$$A_\mu = A_\mu^a t^a \; , \qquad D_\mu = \partial_\mu + ig A_\mu \; , \tag{2.1}$$

where we introduced the respective covariant derivative D_μ. The classical Lagrangian is given by

$$\mathcal{L} = -\frac{1}{4} \text{Tr}[F_{\mu\nu} F^{\mu\nu}] + \sum_{i=1}^{n_f} \overline{\psi}_i (i \not{D} - m_i) \psi_i \; . \tag{2.2}$$

The quark fields ψ_i, describing coloured fermions, transform in the fundamental representation. The quanta of the gauge field are called gluons. The field strength is calculated as the curvature associated to the gauge field connection,

$$F_{\mu\nu} = F_{\mu\nu}^a t^a = \frac{-i}{g}[D_\mu, D_\nu] = \partial_\mu A_\nu - \partial_\nu A_\mu + ig[A_\mu, A_\nu] \; . \tag{2.3}$$

The quantisation is usually carried out within the framework of the Fadeev-Popov procedure, where the classical Lagrangian has to be supplemented with a gauge-fixing term and the additional ghost contribution.[1]

Calculation of the renormalisation group evolution of the QCD coupling reveals that QCD is – as opposed to QED – asymptotically free: the running coupling α_s, with

$$\mu^2 \frac{\partial}{\partial \mu^2} \alpha_s(\mu^2) = \beta(\alpha_s(\mu^2)) \; , \tag{2.4}$$

becomes large at small energy scales μ and small in the high-energy regime. Interpreting the quarks as constituents of hadrons, it is this finding which enables the calculation of high-energy scatterings of coloured particles by means of perturbation theory.

Scattering processes of hadrons in the high energy regime are seen as taking place through scattering of the coloured constituents, called partons, accompanied with certain momentum distributions of these constituents inside the hadron. Coloured particles produced in a scattering are assumed to evolve to lower energy scales by successive radiation until eventually the *confinement* of partons in colour-singlet hadrons takes place in the strongly coupled regime. The experimental manifestation of this phenomenon is the observation of jets, collimated sets of hadrons moving in roughly the same direction. In order to identify a jet originating from a parton, so-called infrared safe definitions of a jet resolution are mandatory. Infrared safety is the in-sensitivity of these observables to addition or removal of particles arbitrarily collinear to another particle or of arbitrary small energy. The momentum distributions of partons inside hadrons, parton distribution functions, can to some extent be calculated perturbatively as well. More precisely, their dependence on a typical energy scale of the hard scattering process is driven by the very same phenomenon of multiple parton emission as leading to jet formation. This reveals that a considerable amount of a hadron's momentum is indeed being carried by gluons.

Jet algorithms and the measurement of input momentum distributions to be evolved according to the perturbatively calculable differential equation enable a comparison of experimental data and parton level predictions. The parton level predictions do however not correspond to realistic final states and a large part of QCD dynamics in the low energy regime can only be taken into account by phenomenological models turning a parton level final state into the observed hadronic final state. These models will not be discussed here. A prerequisite is however having evolved a parton involved in a high energy scattering to a scale where perturbation theory ceases to make sense. This evolution is modelled through multiple parton emission, or 'parton showers', in current Monte Carlo simulations.

---

[1]For axial gauges, $n \cdot A = 0$, the ghost fields decouple, which is an advantage when in particular considering singular limits as discussed in the next chapter, though loop calculations become more involved.

3 QCD in Practise

3.1 Overview

In this introductory chapter, practical aspects of perturbative calculations in QCD are reviewed. In particular, higher order corrections at a fixed order, as well as the identification of leading contributions and their resummation to all orders – if possible – are discussed.

The impact of the latter corrections can be carried out analytically using well established frameworks, for a review see [4]. Most importantly for the work at hand, these corrections can be turned into a Monte Carlo simulation, forming the basis of parton shower event generator. Here, the contributions are modelled as multiple soft and/or collinear parton emission. The resulting final state eventually provides the input for non-perturbative models of hadronization as the next step to a fully realistic model of final states as encountered in collider experiments.

3.2 Higher Order Corrections

Owing to the fact that QCD becomes strongly coupled at small momentum transfers, and that the strong coupling is still of $\mathcal{O}(0.1)$ at scales encountered in high energy physics experiments, higher order QCD corrections typically do not turn out to be small. Neglected higher order corrections constitute an uncertainty on the theoretical prediction calculated perturbatively.

Though unknown until actually calculated, their size may be estimated from the dependence of the lower order calculation on the unphysical renormalisation and factorisation scales.

These scales enter in the process of renormalisation of fundamental parameters and parton distribution functions (PDF), needed to make sense of divergences encountered in a fixed-order calculation by an infinite redefinition of these quantities, regarding unrenormalised quantities as unobserved. Renormalisation of fundamental parameters is concerned with divergences of ultraviolet origin, while renormalisation of PDFs (or fragmentation functions for predictions for processes with identified final state hadrons) deals with divergences of infrared origin, particularly stemming from collinear divergences.

We shall here focus on infrared divergences, which turn out to be the most complicated thing to handle when calculating a perturbative prediction for differential cross sections as observed in experiment. The statement that physically observable quantities are finite, provided one looks at a sufficiently inclusive observable is at the heart of the KLN theorem, [5]. This justifies the procedure of factoring collinear divergences into parton distributions and is a major prerequisite for the method of subtraction to work for predictions of differential quantities at higher orders. This method will be discussed in more detail, particularly focusing on next-to-leading order corrections, in the next section.

The obstacle in calculating predictions for differential cross sections lies in the fact that perturbative contributions at the same order enter with a different phase space dependence. Particularly, Feynman diagrams with loops, to which we refer as virtual corrections, and diagrams corresponding to parton emission will have to be considered. We will call the latter real emission contributions. Both classes of diagrams are separately infrared divergent. The infrared divergences of virtual corrections can be extracted in dimensional regularisation as poles in the in the parameter ϵ, being connected to the space-time dimensionality as $d = 4 - 2\epsilon$ upon expanding near $\epsilon = 0$. The infrared divergences in real emission contributions are hidden in the kinematic dependence of the amplitude becoming singular whenever one or more emitted partons become soft and or collinear to another parton[1]. They can be made explicit as poles in ϵ by analytical integration of the resulting differential cross section over the phase space measure in d dimensions and will then cancel the corresponding poles of the virtual contributions. This cancellation will be incomplete for poles of collinear origin which appear whenever an external parton's momentum is not integrated over. This is precisely the case of incoming or outgoing, identified partons, and the divergences are dealt with by means of redefining PDFs and/or fragmentation functions.

The procedure outlined above then leads to finite predictions for inclusive cross sections. In practise, one is however interested in less inclusive quantities: Differential distributions may be used to separate signal from background contributions by kinematic

---

[1]Collinear divergences are present only for massless partons. We will however mostly be working in the so-called chiral limit where quarks are treated as massless.

cuts, or to extract the value of masses and couplings, which are otherwise inaccessible from inclusive measurements. In addition, differential distributions form the key input to fully exclusive Monte Carlo simulations of realistic final states as observed in experiment. A framework to calculate higher order corrections to fully differential quantities in a flexible way is therefore mandatory.

3.3 Differential Cross Sections at NLO

At NLO, an inclusive observable $\langle \mathcal{F} \rangle$ defined for a $2 \to n$ process is calculated as

$$
\begin{aligned}
\langle \mathcal{F} \rangle_{\mathrm{NLO}} = & \int_n \mathrm{d}\sigma_B(p_n)\mathcal{F}(p_n) \\
& + \int_n \mathrm{d}\sigma_V(p_n)\mathcal{F}(p_n) + \int_0^1 \mathrm{d}z \int_n \mathrm{d}\sigma_B(p_n^C(z))\mathcal{F}(p_n^C(z))P(z) \\
& + \int_{n+1} \mathrm{d}\sigma_R(q_{n+1})\mathcal{F}(q_{n+1}) \; ,
\end{aligned}
\tag{3.1}
$$

where $\mathrm{d}\sigma_B$ is the leading order (Born) differential cross section, $\mathrm{d}\sigma_V$ is the one-loop virtual contribution, and $\mathrm{d}\sigma_R$ refers to the real emission contribution. In dimensional regularisation, the renormalised one-loop correction will exhibit poles in $1/\epsilon^2$ and $1/\epsilon$ due to the loop momentum becoming soft, or two neighbouring loop propagators becoming simultaneously on-shell – which is the case for the loop momentum becoming collinear to a (massless) external line. $P(z)$ denotes the counter term originating from factoring the collinear divergences of incoming or identified partons into parton distribution or fragmentation functions, respectively. This contribution is divergent as $1/\epsilon$, and p^C denotes a phase space point with the corresponding incoming or identified parton's momentum rescaled by the convolution variable z. The correction to $\langle \mathcal{F} \rangle$ is finite, if its definition is infrared safe, *i.e.*

$$
\mathcal{F}(q_{n+1}) \to \mathcal{F}(p_n) \; ,
\tag{3.2}
$$

whenever a parton's momentum becomes 'soft', $q_k \to \lambda q_k$ along with $\lambda \to 0$, in case of which the 'soft' parton is just removed from the set q_{n+1}, or whenever two partons become collinear to each other, in case of which the corresponding momenta are combined into a common 'emitter' momentum. The real emission contribution is singular in any of these unresolved limits, and the divergences are converted into poles in ϵ upon carrying out the phase space integration. The KLN theorem then guarantees that all of the ϵ poles cancel in the final expression.

If the *integrands* were all finite, then the integrals could be performed by Monte Carlo methods, and each point generated to evaluate the integral could have been used to book a histogram for the differential version of the observable $\mathcal{F}$. Indeed, this method

need not make any reference to a particular observable $\mathcal{F}$, but could have been used for arbitrary observables. The observation that the divergences present in the real emission contribution do factor in a process independent way is at the heart of the subtraction method to precisely achieve finiteness of all integrands. The factorisation properties can be used to construct an auxiliary cross section which *subtracts* the divergences present in $\mathrm{d}\sigma_R$, and the analytic integration over the unresolved parton's momentum will reveal exactly those ϵ poles present in the virtual contribution and the collinear counter term $\mathrm{d}\sigma_C$ – with opposite sign – again by virtue of the KLN theorem. More precisely, the cross section is rewritten as

$$
\langle \mathcal{F} \rangle_{\mathrm{NLO}} = \int_n \mathrm{d}\sigma_B(p_n)\mathcal{F}(p_n) \tag{3.3}
$$
$$
+ \int_n \left[\mathrm{d}\sigma_V(p_n) + \int_1 \mathrm{d}\sigma_A(q_{n+1}) - \int_0^1 \mathrm{d}z \, \mathrm{d}\sigma_B(p_n^C(z))\mathcal{F}(p_n^C(z))K(z) \right]_{\epsilon=0} \mathcal{F}(p_n)
$$
$$
+ \int_0^1 \mathrm{d}z \int_n \mathrm{d}\sigma_B(p_n^C(z))\mathcal{F}(p_n^C(z)) \left[P(z) + K(z) \right]_{\epsilon=0}
$$
$$
+ \int_{n+1} \left[\mathrm{d}\sigma_R(q_{n+1})\mathcal{F}(q_{n+1}) - \mathrm{d}\sigma_A(q_{n+1}) \right] .
$$

Here $\mathrm{d}\sigma_A$ denotes the auxiliary cross section, and the subscript 1 on the integral denotes the analytic integration over the unresolved parton's momentum. The kernel $K(z)$ is constructed in such a way as to equal those contributions of the analytic phase space integration, which are convolutions with the Born cross section. Note that no analytic phase space integration over the real emission matrix element needs to be performed, and all integrands are finite, provided $\mathcal{F}$ is infrared safe. Commonly used subtraction algorithms are FKS, [6], antenna subtraction [7,8], and dipole subtraction [9,10].

3.4 Parton Showers and Resummation

Considering again the generic NLO correction 3.1, we shall now consider a class of observables which cut out the divergences associated to soft or collinear parton emission by introducing a resolution parameter ρ, *e.g.* the relative $p_\perp$ between two partons. We assume that lowering ρ precisely corresponds to the singular limits, such that the integral of the real emission contribution above ρ is finite. The divergences leave their trace in contributions of the form

$$
\alpha_s \ln^2(\rho) \qquad \text{and} \qquad \alpha_s \ln(\rho) \tag{3.4}
$$

(in one-to-one correspondence with the poles in $1/\epsilon^2$ and $1/\epsilon$). The logarithms may eventually overcome the smallness of α_s for sufficiently small ρ, thereby spoiling the

convergence of the perturbative series. A typical effect is seen *e.g.* in a three-jet rate becoming larger than a two-jet rate below some value of the jet resolution. Indeed, owing to the universal factorisation of soft and collinear divergences, these contributions appear to all orders in α_s as

$$\alpha_s^n \ln^{2n}(\rho) \qquad \text{and} \qquad \alpha_s^n \ln^{2n-1}(\rho) \; . \tag{3.5}$$

This particular class of logarithmically enhanced contributions requires a strong ordering of the energies and/or the transverse momenta of each individual parton emission, and are referred to as 'leading logarithmic' (LL) contributions. Singular limits for which two or more emitted partons do not satisfy this ordering give rise to lower powers of logarithms,

$$\alpha_s^n \ln^{2n-2}(\rho) \; , \; \alpha_s^n \ln^{2n-3}(\rho) \; , \quad ... \tag{3.6}$$

referred to as next-to-leading logarithmic (NLL) contributions, etc.. The appearance of these contributions to all orders requires their resummation to improve the convergence of the perturbative series. Resummation is indeed possible owing to the factorisation properties, and can be carried out analytically, [4]. The relation between fixed-order calculations and all-order resummation is depicted in figure 3.1.

The essence of the resummation procedure is that the LL and NLL contributions exponentiate to a form factor multiplying the leading order cross section,

$$\Delta(Q^2, p_\perp^2) = \exp\left(-\int_{p_\perp^2}^{Q^2} \frac{\mathrm{d}q^2}{q^2} \frac{\alpha_s(q^2)}{2\pi} \Gamma(q^2, Q^2) \right) \; . \tag{3.7}$$

Here, Q^2 is a hard scale typical to the process, and $p_\perp^2$ is a typical transverse momentum of the emitted parton, which is defined through the choice of resolution criterion, $\rho \sim p_\perp^2/Q^2$. Γ is called a *Sudakov anomalous dimension*, and the form factor is usually referred to as a *jet function* in the analytic resummation frameworks.

As cross sections iteratively factor in the strongly ordered limits, the resummation (of at least leading logarithms) can be turned into a probabilistic picture, where the Sudakov form factor is interpreted as the probability of having not emitted a parton between two scales Q^2 and $p_\perp^2$. This is the starting point for parton shower simulations, building up parton cascades from a Monte Carlo algorithm and thereby performing resummation of large logarithmic contributions as well. The probability density describing parton emission at a scale selected according to the Sudakov form factor is given by the splitting function multiplying the cross section in the collinear limit.

The all-order resummation of the effects of soft gluon emission is more involved. Here, a probabilistic interpretation is not evident since the factorisation takes place at amplitude level, leaving its trace in non-trivial colour correlations when squaring the factored amplitude. The analytic resummation of these contributions aims at exponentiating the correlation matrix, known as *soft anomalous dimension*, defining the *soft function* similar to the jet function, the matrix elements of which now need to be taken between the

amplitude expressed in a certain basis of colour factors. In the limit of letting the number of colours to infinity, originally introduced by t'Hooft [11], these colour correlations become diagonal and positive and a direct probabilistic interpretation is feasible. The most important consequence of the radiation pattern encountered for soft gluon emission is angular ordering, which can be traced back to a destructive interference of the real emission amplitudes, suppressing soft radiation outside cones defined by a 'colour dipole' formed out of two partons. Parton showers which incorporate this effect are known as coherent. One important consequence of coherence is that the LL coefficient of the Sudakov anomalous dimension implemented in such parton showers precisely equals the LL coefficient as predicted by the soft anomalous dimension. An algorithm to include the exact colour correlations in a parton shower simulation is proposed in chapter 5.

3.5 Overture: Matching Fixed Order and Resummation

As is evident from figure 3.1, the resummation and fixed order calculation both contain the same orders starting from the fixed order calculation being carried out in next-to-leading order (NLO). Thus, a procedure to match these calculation is required in order to avoid double counting of contributions at the same order.

Figure 3.1 also shows that a given fixed order determines a respective logarithmic order or vice-versa when one attempts a consistent combination of the two: a LL resummation requires a NLO calculation, modelling the first real emission at LO, a NLL resummation requires a NNLO calculation, modelling the first real emission at NLO. These are sometimes referred to as LO+LL and NLO+NLL, respectively ('same number of N's'). Since the fixed-order will however also contain non-logarithmically enhanced contributions, it is desirable to remove the double counting in a way such that the contributions in the respective orders are determined by the fixed order. The probably most simple recipe to achieve this (see [12] for an example) is to perform a fixed-order expansion of the all-order resummation up to the order of the fixed-order calculation and subtract these contributions from the combined result.

The very same recipe may immediately be applied to a Monte Carlo implementation of a NLO calculation and a parton shower simulation to achieve the simulation of fully exclusive final states at NLO or even higher accuracy.

The details of a new approach to coherent parton showering, and the combination of parton showers and higher order corrections form the core of this thesis and are discussed in the chapters to follow.

Figure 3.1: Relation between fixed-order calculations and all-order resummation in the plane of powers of the strong coupling and large logarithms L. Note that a LL resummation requires a NLO calculation to match to, which models the real emission at LO thus being referred to as LO+LL and so on. Gray lines indicate improving a fixed order by a resummation of higher order, for which a consistent matching is not possible.

3 QCD in Practise

4 A Calculational Formalism for Parton Showers

4.1 Overview

The purpose of this chapter is to introduce a new formalism in which predictions as expected from a numerical parton shower simulation can (at least to some extent) be calculated analytically in a rigorous way.

The starting point is to *define* any parton shower algorithm to be a stochastic process, in particular a Markov process. Starting from this definition, which at first only is justified by the way an actual Monte Carlo simulation is typically implemented, we will show that the structures expected from perturbative QCD are indeed emergent.

A general conclusion that this is not accidental, or – stated in another way – a proof, that QCD in a certain regime gives rise to Markovian dynamics of multiple parton emission can however not be drawn.

To this extent, the formalism at hand should be considered as a tool for investigating the properties of parton shower predictions beyond a purely numerical approach. This tool will turn out to be of utmost importance particularly in the context of matching parton showers and fixed order calculations in perturbative QCD.

The (time dependent) stochastic process to be considered occupies a state at a given evolution time. Any such state is a collection of partons with well-defined momenta, the evolution time is directly related to a resolution scale, which, starting from a hard scale eventually may hit a value where perturbative parton emission ceases to take place and models of non-perturbative physics will have to be applied.

The dynamics of transitions between a state occupied at some time to another state occupied at a later time is governed by transition rates, which can be derived from the

factorisation properties of cross sections and are thus calculable in perturbative QCD.

The outline of this chapter is as follows: section 4.2 sets the scene for the formalism by precisely defining the notion of a parton ensemble and the construction of the transition rates from factorising cross sections. Section 4.3 derives the evolution equations for transition probability densities, before introducing generating functionals for the transition probability densities governing the dynamics of the parton shower. Section 4.4 outlines some applications of the formalism, particularly focusing on the extraction of evolution equations for physical quantities such as parton luminosities, as well as fixed order expansions, which will be extensively used in chapter 6.

4.2 Preliminaries

4.2.1 Parton Ensembles and Cross Sections

A m-parton configuration as predicted by a fixed-order calculation or as a state within the parton shower evolution is generically denoted by

$$q_m \equiv \{\hat{q}_a, \hat{q}_b; \hat{q}_1, ..., \hat{q}_m\} \ ,$$

where the $\hat{q}_i$ collectively denote each parton's momentum and quantum numbers, $i = a, b$ refers to incoming, $i = 1, ..., m$ to outgoing partons. The dependence on the quantum numbers is suppressed for readability as long as no ambiguities are present.

The measure on this space of states is taken to be

$$\mathrm{d}\phi(q_m) = \prod_{i=a,b;1}^{m} \frac{\mathrm{d}^{d-1}\hat{\mathbf{q}}_i}{(2\pi)^{d-1}2\hat{q}_i^0} \ , \tag{4.1}$$

where we consider only massless partons in this context. For the purpose of matching to fixed-order calculations carried out in dimensional regularisation, we shall assume a general spacetime dimension d. Integrations over this measure are understood to contain summations over the respective quantum numbers implicitly.

Note that the phase space measure *does* include a (formal) integration over incoming parton momenta and is not constrained by a momentum conserving δ-function. The purpose of this construction is to write a cross section for producing a partonic ensemble[1] out of a collision involving incoming hadrons $P \equiv P_a, P_b$ as the integral over

$$\mathrm{d}\sigma(P, q_m|Q; \mu_F, \mu_R) = \frac{\mathrm{d}\hat{\sigma}(q_m|Q; \mu_F, \mu_R)}{\mathrm{d}\phi(q_m)} F(P, q_{a,b}, \mu_F, \mu_R)\delta_F(P, q_{a,b})\mathrm{d}\phi(q_m|Q) \tag{4.2}$$

---

[1]We do not consider identified final state hadrons within this context.

where

$$\mathrm{d}\phi(q_m|Q) = (2\pi)^d \delta(\sum_i \hat{q}_i - \hat{q}_a - \hat{q}_b - Q)\mathrm{d}\phi(q_m) \ . \tag{4.3}$$

$F(P, q_{a,b}, \mu_F, \mu_R)$ denotes the relevant parton luminosity and $\delta_F(P, q_{a,b})$ implements constraints originating from the particular factorisation framework considered, thereby reducing the integration over incoming momenta to the relevant variables, *e.g.* longitudinal momentum fractions within collinear factorisation. Here, the explicit expression is given by

$$\delta_F(P, q_{a,b}) = \delta_F(P_a, \hat{q}_a; P_b, x_a)\mathrm{d}x_a \ \delta_F(P_b, \hat{q}_b; P_a, x_b)\mathrm{d}x_b \tag{4.4}$$

with

$$\delta_F(P_{a,b}, \hat{q}_{a,b}; P_{b,a}, x_{a,b}) =$$
$$\frac{16\pi^2}{(2P_a \cdot P_b)^{1-\varepsilon}} \left(\frac{(P_a \cdot P_b)^2}{P_a \cdot \hat{q}_{a,b} \ P_b \cdot \hat{q}_{a,b}}\right)^{\varepsilon} \delta\left(\frac{P_{b,a} \cdot \hat{q}_{a,b}}{P_a \cdot P_b} - x_{a,b}\right) \delta\left(\frac{P_{a,b} \cdot \hat{q}_{a,b}}{P_a \cdot P_b}\right) \tag{4.5}$$

and $d = 4 - 2\varepsilon$ as usual. We shall also use the shorthand

$$\mathrm{d}\phi^F(q_m|Q) = \delta_F(q_{a,b})\mathrm{d}\phi(q_m|Q) \tag{4.6}$$

for readability and the dependence on the hadron momenta is now understood implicitly, when not stated otherwise.

The scale dependence of $F(p_{a,b}, \mu_F, \mu_R)$ is assumed to be governed by

$$\mu_F \frac{\partial}{\partial \mu_F} F(p_{a,b}, \mu_F, \mu_R) = \sum_n \int F(q_{a,b}, \mu_F, \mu_R)\mathrm{d}K(q_n|p_{a,b}; \mu_F, \mu_R) \tag{4.7}$$

where K has a perturbative expansion in α_s. The only source of the μ_R dependence in F is renormalisation carried out in the perturbative calculation of K. When not relevant, we drop making explicit this dependence for readability.

4.2.2 Factorisation and the Derivation of Splitting Kernels

The parton shower splitting kernels need to be derived from approximate or exact factorisation properties of the squared amplitude which we assume to be given by

$$|\mathcal{M}(q_m, \mu_R, \mu_F)|^2 = \sum_{n \leq m} \sum_\alpha |\mathcal{M}(p_n, \mu_R, \mu_F)|^2 P_\alpha(q_m|p_n; \mu_R) \ . \tag{4.8}$$

The index α denotes a particular configuration of unresolved partons and this factorisation is accompanied by a kinematic mapping $q_m = q_m^\alpha(p_n)$ such that the phase space measure obeys the convolution

$$\mathrm{d}\phi^F(q_m|Q)F(q_{a,b}, \mu_F) = \int \mathrm{d}\phi^F(p_n|Q)F(p_{a,b}, \mu_F)\mathrm{d}\phi_{m-n}^\alpha(q_m|p_n; \mu_F) \tag{4.9}$$

where

$$\mathrm{d}\phi_{m-n}^{\alpha}(q_m|p_n;\mu_F) =$$

$$\mathcal{J}^{\alpha}(q_{a,b})\frac{F(q_{a,b},\mu_F)}{F(p_{a,b},\mu_F)}\mathrm{d}\phi\left(q_m\left|\sum_i \hat{p}_i - \hat{p}_a - \hat{p}_b\right.\right)\delta\left(q_n, q_n^{\alpha}(p_n)\right) \ . \quad (4.10)$$

The Jacobian $\mathcal{J}^{\alpha}(q_{a,b})$ has its origin in mapping $\delta_F(q_{a,b})$ to $\delta_F(p_{a,b})$. Here, we introduced δ-functions in the sense that

$$\sum_m \int \delta(p_n, q_m)\mathrm{d}\phi(q_m) = 1 \quad (4.11)$$

and

$$\delta\left(q_n, q_n^{\alpha}(p_n)\right) \quad (4.12)$$

fixes n out of the m momenta q_m to be determined by the mapping q^{α} under consideration thereby giving rise to phase space factorisation or convolution properties, respectively. The momentum conservation constraint in the factorised phase space measure may be implemented exactly or approximate compatible with a particular limit considered.

Hence differential cross sections obey the convolution

$$\mathrm{d}\sigma(q_m|Q;\mu_F,\mu_R) = \int \mathrm{d}\sigma(p_n|Q;\mu_F,\mu_R)\mathrm{d}P(q_m|p_n;\mu_F,\mu_R) \quad (4.13)$$

where the differential splitting rate is given by

$$\mathrm{d}P(q_m|p_n;\mu_F,\mu_R) = \sum_{n\leq m}\sum_{\alpha} P_{\alpha}(q_m|p_n;\mu_R)\mathrm{d}\phi_{m-n}^{\alpha}(q_m|p_n;\mu_F) \ . \quad (4.14)$$

Eq. 4.10 has a straightforward interpretation: A cross section acts as a source of partonic ensembles p_n, and the source of different ensembles q_m is obtained by multiplying the original source with a splitting rate producing q_m out of p_n and summing over all possible intermediate states p_n. Note that $\mathrm{d}P$ is in general *not* a probability density. Physical cross sections as the sum over all possible transitions are however required to be positive in a perturbative domain.

A parton shower is assumed to evolve from larger to smaller scales t. This scale is connected to a particular splitting under consideration by the parton shower splitting kernels, which take the form

$$\mathrm{d}P_{\alpha}(q_m|p_n;t) = P_{\alpha}(q_m|p_n;\mu_R)\mathrm{d}\phi_{m-n}^{\alpha}(q_m|p_n;\mu_F)\big|_{\mu_{F,R}=\mu_{F,R}^{\alpha}(t)}\delta(t - t^{\alpha}(q_m)) \quad (4.15)$$

such that

$$\int_{t'}^{t}\mathrm{d}\tau \int \mathrm{d}P_{\alpha}(q_m|p_n;\tau) = \int_{\Omega^{\alpha}(t,t')} P_{\alpha}(q_m|p_n;\mu_R)\mathrm{d}\phi_{m-n}^{\alpha}(q_m|p_n;\mu_F)\big|_{\mu_{F,R}=\mu_{F,R}^{\alpha}(q_m)} \ ,$$

$$(4.16)$$

where $\mu_{F,R}^\alpha(q_m) \equiv \mu_{F,R}^\alpha(t^\alpha(q_m))$ and $\Omega^\alpha(t,t')$ is the phase space region accessible for the $m-n$ additional partons when evolving between t and t'. Throughout we assume that lowering scales indicate an evolution to infrared regions, *i.e.* $t' \to 0$ increases the phase space available for soft and/or collinear emissions.

The definitions

$$\mathrm{d}P(q_m|p_n;t) \equiv P(q_m|p_n;t)\mathrm{d}\phi(q_m) \equiv \sum_\alpha \mathrm{d}P_\alpha(q_m|p_n;t) \tag{4.17}$$

will often be used in the following sections.

4.2.3 An Aside on Cutoff Dependence of Infrared Safe Observables

In the context of matching to fixed order, we will face the problem of identifying changes in infrared safe observables $\mathcal{C}(q_m)$ due to a finite infrared cutoff imposed on the parton shower. Particularly, these effects will appear in the form

$$\delta\mathcal{C}(t,t') = \int_{t'}^t \mathrm{d}\tau \int \left(\mathcal{C}(q_m) - \mathcal{C}(p_n)\right)\mathrm{d}P_\alpha(q_m|p_n;\tau) \tag{4.18}$$

where we are interested in the region $t' \ll t$. Let us first focus on the phase space measure and the splitting kernels involved. In any unresolved limit, for which $\lambda_i(q_m|p_n)$, $i = 1,...,2(m-n)$, with $\lambda_i(q_m|p_n) \to 0$ as $t^\alpha(q_m) \to 0$, the splitting kernels scale as

$$P_\alpha(q_m|p_n;t) = \frac{\alpha_s^{m-n}c_\alpha(p_n)}{\lambda_1(q_m|p_n)\cdots\lambda_{2(m-n)}(q_m|p_n)} + \mathcal{O}\left(\frac{1}{\lambda^{2(m-n)-1}}\right) , \tag{4.19}$$

and by dimensional analysis the phase space measure is then constrained to

$$\mathrm{d}\phi_{m-n}^\alpha(q_m|p_n;\mu_F) \sim \mathrm{d}\lambda_1\cdots\mathrm{d}\lambda_{2(m-n)} , \tag{4.20}$$

by the requirement of giving rise to the expected logarithmic contributions,

$$\int_{t'}^t \mathrm{d}\tau \int \mathrm{d}P_\alpha(q_m|p_n;\tau) \sim c_\alpha(p_n)\alpha_s^{m-n}\ln^{2(m-n)}\left(\frac{T(p_n)}{t'}\right) , \tag{4.21}$$

where $T(p_n)$ is some hard scale associated to the kinematic configuration given by p_n. Conversely, infrared safety demands that $\mathcal{C}$ behaves as

$$\mathcal{C}(q_m) = \mathcal{C}(p_n) + \left(\lambda_1(q_m|p_n)\cdots\lambda_{2(m-n)}(q_m|p_n)\right)\left(\mathcal{C}_{m,0}(p_n) + \mathcal{O}(\lambda)\right) , \tag{4.22}$$

and the contributions to the infrared safe observable in the unresolved limits are now seen to contribute power corrections only, *i.e.* contributions, which are not logarithmically enhanced for $t' \ll t$,

$$\delta\mathcal{C}(t,t') \sim \alpha_s^{m-n}c_\alpha(p_n)\mathcal{C}_{m,0}(p_n)\int_{t'}^t \mathrm{d}\tau \prod_{i=1}^{2(m-n)-1}\int \mathrm{d}\lambda_i(t)\left(1 + \mathcal{O}(\lambda)\right) . \tag{4.23}$$

4.3 Calculating Parton Shower Predictions

We will now establish the theoretical treatment of viewing multiple parton emission as a Markov process on the space of states as defined in the previous section. This treatment will naturally lead to evolution equations for any quantity predicted by a parton shower, as long as it is actually implemented as such a stochastic process.

4.3.1 From Markov Processes to Evolution Equations

Markov processes obey the defining property that considering conditional probability densities of finding a particular state q_m at time t', given any sequence of states $p_n, p_{n_1}, ..., p_{n_k}$ at preceding times $t' < t < t_1 < ... < t_k$ actually only depends on the state occupied just before,

$$p(q_m, t'|p_n, t; p_{n_1}, t_1; ...; p_{n_k}, t_k) = p(q_m, t'|p_n, t) \equiv \Delta(q_m, t'|p_n, t) \qquad (4.24)$$

where $\Delta(q_m, t'|p_n, t)$ is interpreted as the transition probability density from p_n at time t to q_m at time t'.

Thus Δ obeys the product rule

$$\Delta(q_m, t'|p_n, t) = \sum_{i=n}^{m} \int \Delta(q_m, t'|k_i, \tau)\Delta(k_i, \tau|p_n, t)\mathrm{d}\phi(k_i) \qquad (4.25)$$

for any $t' < \tau < t$. Note that we did restrict ourselves to exclude processes where partons are absorbed in a transition. These processes actually pose no problem for the formalism. It can however be shown that in the presence of *both* emission and absorption processes a simple exponentiation of the probability to keep a state is not possible anymore: this quantity will need to solve a a nonlinear evolution equation.

From the product rule we immediately find that

$$\Delta(q_m, t|p_n, t) = \delta(q_m, p_n) . \qquad (4.26)$$

The transition *rates* $\mathcal{P}(q_m|p_n; t)$ are related to Δ by considering expansions around small time intervals,

$$\Delta(q_m, t|p_n, t + \delta t) = \delta(q_m, p_n) + \mathcal{P}(q_m|p_n; t)\delta t + \mathcal{O}(\delta t^2) \qquad (4.27)$$

giving rise to the differential equation

$$\frac{\partial}{\partial t}\Delta(q_m, t'|p_n, t) = \sum_{i=n}^{m} \int \Delta(q_m, t'|k_i, t)\mathcal{P}(k_i|p_n; t)\mathrm{d}\phi(k_i) . \qquad (4.28)$$

The dependence on the smaller scale t' may be inferred from a similar expansion

$$\Delta(q_m, t - \delta t | p_n, t) = \delta(q_m, p_n) + \mathcal{Q}(q_m | p_n; t)\delta t + \mathcal{O}(\delta t^2) \ . \tag{4.29}$$

Note that Δ changes by *decreasing* the smaller scale argument, as we evolve from higher to lower scales. In general, $\mathcal{P} \neq \mathcal{Q}$, *i.e.* Δ changes differently in both evolution directions. Then

$$\frac{\partial}{\partial t'}\Delta(q_m, t' | p_n, t) = -\sum_{i=n}^{m} \int \mathcal{Q}(q_m | k_i; t')\Delta(k_i, t' | p_n, t)\mathrm{d}\phi(k_i) \ . \tag{4.30}$$

Integrating both differential equations, adding the results and expanding around small evolution interval changes, it is easy to prove that $\mathcal{P} = \mathcal{Q}$ is required for consistent solutions.

4.3.2 Virtual Corrections and the Impact of Unitarity

The above findings are valid for a unitary process, which obeys

$$1 = \sum_{m=n}^{\infty} \int \Delta(q_m, t' | p_n, t)\mathrm{d}\phi(q_m) \ , \tag{4.31}$$

thus imposing a sum rule on the splitting rates,

$$0 = \sum_{m=n}^{\infty} \int \mathcal{P}(q_m | p_n, t)\mathrm{d}\phi(q_m) \ . \tag{4.32}$$

From this it is evident, that the splitting rates do need to be of the form

$$\mathcal{P}(q_m | p_n, t) = [P(q_m | p_n, t)]_+ = P(q_m | p_n, t) - \delta(q_m, p_n)\sum_{i=n}^{\infty} \int P(k_i | p_n, t)\mathrm{d}\phi(k_i) \ , \tag{4.33}$$

generalising the +-distribution. If only parton splittings are present this implies that transitions to lower multiplicities are absent and we find for the no-emission density $\Delta(p_n, t, t')$ defined through

$$\Delta(q_m, t' | p_n, t) = \delta(q_m, p_n)\Delta(p_n, t, t') + \Delta_T(q_m, t' | p_n, t) \tag{4.34}$$

(with $\Delta_T(p_n, t' | p_n, t) = \Delta_T(q_m, t | p_n, t) = 0$) the simple differential equation

$$\frac{\partial}{\partial t}\Delta(p_n, t, t') = -\Delta(p_n, t, t')\sum_{i=n}^{m} \int P(k_i | p_n; t')\mathrm{d}\phi(k_i) \ . \tag{4.35}$$

with initial condition $\Delta(p_n, t, t) = 1$ giving rise to the expected functional form of the Sudakov from factor.

Considering a process which obeys non-normalised transition densities,

$$1 \neq N(p_n, t, t') = \sum_{m=n}^{\infty} \int \Delta_0(q_m, t'|p_n, t) \mathrm{d}\phi(q_m) \tag{4.36}$$

we find that the rates driving the normalised one,

$$\Delta(q_m, t'|p_n, t) = \frac{\Delta_0(q_m, t'|p_n, t)}{N(p_n, t, t')} \tag{4.37}$$

do indeed need to sum up to zero when summing over all reachable final states, and N needs to be independent of t'. Conversely, the t-dependence of Δ_0 is governed by kernels

$$\frac{N(p_n, t)}{N(q_m, t)}[P(q_m|p_n; t)]_+ + \delta(q_m, p_n)\frac{\partial \ln N(p_n, t)}{\partial t} \ , \tag{4.38}$$

(where $N(p_n, t) \equiv N(p_n, t, \cdot)$) while the t'-dependence is the same for Δ and Δ_0 and the initial condition is $\Delta_0(q_m, t|p_n, t) = N(p_n, t)\delta(q_m, p_n)$.

The virtual correction to the splitting kernels is thus given by

$$V(p_n, t) = -\sum_{i=n}^{\infty} \int P(k_i|p_n; t)\mathrm{d}\phi(k_i) + \frac{\partial \ln N(p_n, t)}{\partial t} \tag{4.39}$$

such that the origin of N is readily traced back to factoring virtual corrections beyond the constraint imposed by the +-prescription, if these where explicitly taken into account for defining the splitting kernels.

We will from now on collectively denote renormalisation and factorisation scales by μ and assume that the dependence on a particular splitting solely enters as $\mu_\alpha(t_\alpha) = \mu(t_\alpha)$. Cross sections after evolving from a hard scale t down to a lower scale t' are then obtained from

$$\mathrm{d}\sigma(q_m|Q; \mu(t')) = \sum_{n \leq m} \int \Delta(q_m, t'|p_n, t)\mathrm{d}\sigma(p_n|Q; \mu(t))\mathrm{d}\phi(q_m) \ . \tag{4.40}$$

The total inclusive cross section is thus only preserved, if Δ is normalised. If this was not the case, *i.e.* by making the replacement $\Delta \to \Delta_0$ in the above equation, and $\mathrm{d}\sigma \to \mathrm{d}\sigma_0$, where $\mathrm{d}\sigma_0$ is 'stripped' from the factoring virtual correction, $\mathrm{d}\sigma(p_n|Q; \mu(t)) = V(p_n, t)\mathrm{d}\sigma_0(p_n|Q; \mu(t))$, we need to renormalise

$$\mathrm{d}\sigma_0(p_n|Q; \mu(t)) \to \frac{1}{N(p_n, t)}\mathrm{d}\sigma(p_n|Q; \mu(t)) \tag{4.41}$$

to preserve the total inclusive cross section, where $\mathrm{d}\sigma$ now contains the virtual corrections. Noting that the splitting kernels are derived in a perturbative expansion, $\ln N$

needs to be of the highest order considered for the splitting rates P, such that this renormalisation turns out to be a higher order ambiguity.

We therefore conclude that it is sufficient to only use factorising splitting rates which do change the partonic ensemble and to impose unitarity order by order, considering unitary processes with +-regulated splitting kernels P. It should be noted that this issue is not connected to demanding that the evolved differential cross section – considered for a particular configuration q_m – should equal a known cross section. This will be addressed when considering the matching of parton showers to fixed-order calculations in chapter 6.

4.3.3 The Method of Generating Functionals

For the purpose of calculating fixed-order expansions of parton shower predictions, as well as to infer the evolution structure it is useful to introduce the generating functional of transition probabilities,

$$Z(p_n, t', t)[u] = \sum_{m=n}^{\infty} \int u(q_m) \Delta(q_m, t'|p_n, t) \mathrm{d}\phi(q_m) \ . \tag{4.42}$$

The scale dependence of Z can immediately be derived from the evolution equations for Δ with initial conditions

$$Z(p_n, t, t)[u] = u(p_n) \qquad Z(p_n, t', t)|_{u=1} = 1 \ . \tag{4.43}$$

Particularly, the generating functional possesses the implicit solution

$$\ln \frac{Z(p_n, t', t)[u]}{u(p_n)} = \sum_{m=n}^{\infty} \int_{t'}^{t} \mathrm{d}\tau \int \left(\frac{Z(q_m, t', \tau)[u]}{Z(p_n, t', \tau)[u]} - 1 \right) P(q_m|p_n; \tau) \mathrm{d}\phi(q_m) \ . \tag{4.44}$$

The transposition probabilities may be recovered using

$$\Delta(q_m, t'|p_n, t) = \left. \frac{\delta}{\delta u(q_m)} Z(p_n, t', t)[u] \right|_{u=0} , \tag{4.45}$$

whereas m-particle inclusive densities,

$$D(q_m, t'|p_n, t) = \sum_i \int \Delta(q_m \cup k_i, t'|p_n, t) \mathrm{d}\phi(k_i) \ , \tag{4.46}$$

are given by

$$D(q_m, t'|p_n, t) = \left. \frac{\delta}{\delta u(q_m)} Z(p_n, t', t)[u] \right|_{u=1} . \tag{4.47}$$

4.4 Applications

4.4.1 Extracting the Evolution of Parton Luminosities

In order to derive the evolution of parton densities as generated by a parton shower, we make explicit the dependence of the transition rates on the partons luminosities as dictated by the generalised splitting measure $\mathrm{d}\phi_{m-n}^\alpha$, eq. 4.10,

$$P(q_m|p_n;t) = \frac{F(q_{a,b}, \mu(t))}{F(p_{a,b}, \mu(t))} \hat{P}(q_m|p_n;t) \; . \tag{4.48}$$

Considering the quantity

$$\tilde{\Delta}(q_m, t'|p_n, t) = \frac{F(p_{a,b}, \mu(t'))}{F(q_{a,b}, \mu(t))} \Delta(q_m, t'|p_n, t) \tag{4.49}$$

we find that this obeys the product rule eq. 4.25, and thus describes a unitary Markov evolution as well. The kernels $\tilde{\mathcal{P}}$ which govern the dynamics of $\tilde{\Delta}$ are again obtained from expanding around small evolution intervals,

$$\tilde{\mathcal{P}}(q_m|p_n;t) =$$
$$\frac{\delta(q_m, p_n)}{F(q_{a,b}, \mu(t))} \frac{\partial F(p_{a,b}, \mu(t))}{\partial t} + \frac{F(p_{a,b}, \mu(t))}{F(q_{a,b}, \mu(t))} \left[\frac{F(q_{a,b}, \mu(t))}{F(p_{a,b}, \mu(t))} \hat{P}(q_m|p_n;t) \right]_+ \; . \tag{4.50}$$

By the unitarity constraint we then find the evolution equation for the parton luminosity,

$$\frac{1}{F(p_{a,b}, \mu)} \frac{\partial F(p_{a,b}, \mu)}{\partial \mu} =$$
$$- \sum_{m=n}^{\infty} \int \frac{F(p_{a,b}, \mu)}{F(q_{a,b}, \mu)} \frac{\partial t(\mu)}{\partial \mu} \left[\frac{F(q_{a,b}, \mu)}{F(p_{a,b}, \mu)} \hat{P}(q_m|p_n;t(\mu)) \right]_+ \mathrm{d}\phi(q_m) \; , \tag{4.51}$$

or

$$\frac{\partial F(p_{a,b}, \mu)}{\partial \mu} = \sum_{m=n}^{\infty} \int F(q_{a,b}, \mu) \frac{\partial t(\mu)}{\partial \mu} \left[\hat{P}(q_m|p_n;t(\mu)) \right]_+ \mathrm{d}\phi(q_m) \; , \tag{4.52}$$

precisely the functional form of the DGLAP equation. Note that for each splitting type α, the splitting kernels impose a particular scale choice

$$\mu = \mu(t^\alpha(q_m)) \; . \tag{4.53}$$

This choice, along with the chosen relation between the evolution variable and the factorisation scale should be done in such a way that for each splitting type α

$$\frac{\partial t^\alpha(\mu, q_m)}{\partial \mu} = f^\alpha(q_{a,b}) \ , \tag{4.54}$$

since only then transitions involving final state partons *only* will not contribute to the evolution of the parton luminosity due to the +-regularisation. Even then, the choice is of importance and should be done in such a way as to reproduce the exact evolution of the parton luminosity in the region where appropriate.

We further note that the luminosity does factor into independent densities for parton a and b, only if there is no transition involving both incoming partons simultaneously.

4.4.2 Evolution Structure

The implicit solution of the generating functional is very useful when determining the structure of a parton shower evolution. In particular, its factorisation properties will immediately point to what subsets of a partonic ensemble can be considered evolving independently of each other, given a set of splitting kernels.

We will here consider two examples: A shower based solely on $1 \to 2$ splittings, and dipole-type showers. For the first case (in the limit of negligible recoils, such that the partons are always considered on their mass shell), the splitting kernels take the form

$$P(q_m|p_n; t) = \delta_{m-n,1} \sum_{i=1}^{n} \sum_{j \neq i} p(\hat{q}_i, \hat{q}_j|\hat{p}_i; t) \delta(q_m \backslash \{\hat{q}_i, \hat{q}_j\}, p_n \backslash \{\hat{p}_i\}) \ . \tag{4.55}$$

Taking the test functions to factor into single partons,

$$u(p_n) = \hat{u}(\hat{p}_1) \cdots \hat{u}(\hat{p}_n) \tag{4.56}$$

the factorisation of Z into functionals for each individual parton immediately follows,

$$Z(p_n, t', t)[u] = \prod_{i=1}^{n} Z_1(\hat{p}_i, t', t)[u] \tag{4.57}$$

where

$$\ln\left(\frac{Z_1(\hat{p}_i, t', t)[u]}{\hat{u}(\hat{p}_i)}\right) =$$
$$\sum_{j \neq i} \int_{t'}^{t} d\tau \int \left(\frac{Z_1(\hat{q}_i, t', \tau)[u] Z_1(\hat{q}_j, t', \tau)[u]}{Z_1(\hat{p}_i, t', \tau)[u]} - 1\right) p(\hat{q}_i, \hat{q}_j|\hat{p}_i; \tau) d\phi(\{\hat{q}_i, \hat{q}_j\}) \ , \tag{4.58}$$

such that in this case indeed each individual parton is an independently evolving entity of the partonic ensemble.

Dipole-type showers are based on $2 \to 3$ splittings,

$$P(q_m|p_n;t) = \delta_{m-n,1} \sum_{i=1}^{n} \sum_{j \neq i} \sum_{k \neq i,j} d(\hat{q}_i, \hat{q}_k, \hat{q}_j|\hat{p}_i, \hat{p}_j; t)\delta(q_m\backslash\{\hat{q}_i, \hat{q}_k, \hat{q}_j\}, p_n\backslash\{\hat{p}_i, \hat{p}_j\}) ,$$

(4.59)

and provide the simplest form of implementing momentum conservation exactly and local to each splitting.

It is natural to factor the test functions into 'dipole functions',

$$u(p_n) = \prod_{i=1}^{n} \prod_{j \neq i} \hat{u}(\hat{p}_i, \hat{p}_j) ,$$

(4.60)

with $\hat{u}(\hat{p}_i, \hat{p}_j) = \hat{u}(\hat{p}_j, \hat{p}_i)$. *Assuming* that the generating functional factors into independent dipoles,

$$Z(p_n, t', t)[u] \stackrel{?}{=} \prod_{i=1}^{n} \prod_{j \neq i} Z_2(\hat{p}_i, \hat{p}_j, t', t)[u] ,$$

(4.61)

with $Z_2(\hat{p}_i, \hat{p}_j, t', t)[u] = Z_2(\hat{p}_j, \hat{p}_i, t', t)[u]$, the integrand in the exponent, cf. 4.58, is given by

$$\sum_{i=1}^{n} \sum_{j \neq i} \sum_{k \neq i,j} ((\bullet) - 1) \, d(\hat{q}_i, \hat{q}_k, \hat{q}_j|\hat{p}_i, \hat{p}_j; t)\mathrm{d}\phi(\{\hat{q}_i, \hat{q}_k, \hat{q}_j\})$$

(4.62)

with

$$\begin{aligned}
(\bullet) &= \frac{Z_2(\hat{q}_i, \hat{q}_k, t', t)[u]Z_2(\hat{q}_k, \hat{q}_j, t', t)[u]}{Z_2(\hat{p}_i, \hat{p}_j, t', t)[u]} \\
&\times \frac{\prod_{l \neq i,j,k} Z_2(\hat{q}_i, \hat{p}_l, t', t)[u]Z_2(\hat{q}_j, \hat{p}_l, t', t)[u]Z_2(\hat{q}_k, \hat{p}_l, t', t)[u]}{\prod_{l \neq i,j} Z_2(\hat{p}_i, \hat{p}_l, t', t)[u]Z_2(\hat{p}_j, \hat{p}_l, t', t)[u]} .
\end{aligned}$$

(4.63)

This shows that the factorisation takes place under very limiting conditions only. Considering, *e.g.* soft gluon emission only, where no flavour changes of emitting partons are present, and the momenta of the emitting partons are assumed to be unchanged, $\hat{q}_{i,j} = \hat{p}_{i,j}$ when considering $\hat{q}_k$ emitted from the dipole (i, j), we have

$$(\bullet) = \frac{Z_2(\hat{p}_i, \hat{q}_k, t', t)[u]Z_2(\hat{q}_k, \hat{p}_j, t', t)[u]}{Z_2(\hat{p}_i, \hat{p}_j, t', t)[u]} \prod_{l \neq i,j,k} Z_2(\hat{q}_k, \hat{p}_l, t', t)[u] .$$

(4.64)

Finally, only for a colour ordered ensemble of partons, where an emission is always placed between the emitting partons (with respect to the colour ordering), the last factor is absent, giving rise to the naive picture of a tree of $1 \to 2$ *dipole* splittings.

4.4.3 Fragmentation Functions

The perturbative contributions to fragmentation functions are the prototypes of m-particle inclusive quantities as introduced in section 4.3.3, though these quantities introduce a more general concept. Starting from an identified parton with momentum $\hat{p}_k$, we are here interested in the change of the distribution of this partons momentum $\hat{p}_k \to \hat{q}_k$, when evolving between a hard and a soft scale $t \to t'$, where $\hat{p}_k$ is considered to be produced in a hard process with final state p_n.

Denoting by $\hat{D}_{k/H}(Q_H, \hat{p}_k, t)$ the universal fragmentation function for a parton $\hat{p}_k$ fragmenting into a hadron H of momentum Q_H, we make use of the auxiliary concept of $D_{k/H}(Q_H, p_n, t)$, describing fragmentation of $\hat{p}_k$ into Q_H, if it has been produced in association with the other partons $\hat{p}_i$ contained in the final state p_n. The latter is a quantity which needs to be defined order-by-order in perturbation theory through the *total* fragmentation function, which connects the two,

$$\int' D_{k/H}(Q_H, p_n, t)\mathrm{d}\sigma(p_n|Q, t) = \hat{D}_{k/H}(Q_H, \hat{p}_k, t) \int' \mathrm{d}\sigma(p_n|Q, t) , \qquad (4.65)$$

where primed integrals refer to summation and integration except the identified parton. On the other hand, the two types of fragmentation functions are related by the one-particle inclusive quantity

$$D(\{\hat{q}\}_k, t'|p_n, t) = \left. \frac{\delta}{\delta u(\{\hat{q}_k\})} Z(p_n, t', t)[u] \right|_{u=1} . \qquad (4.66)$$

through

$$D_{k/H}(Q_H, p_n, t) = \int \hat{D}_{k/H}(Q_H, \hat{q}_k, t')D(\{\hat{q}\}_k, t'|p_n, t)\mathrm{d}\phi(\{\hat{q}_k\}) \qquad (4.67)$$

by purely probabilistic reasoning. Note that, within collinear factorisation we can define the usual fragmentation functions by

$$D_{k/H}(x, t) = \int \delta_F(Q_H, \hat{q}_k; N, x)\hat{D}_{k/H}(Q_H, \hat{q}_k, t)\mathrm{d}\phi(\{\hat{q}_k\}) \qquad (4.68)$$

upon selecting N to define how the collinear direction is approached. The difference between $D_{k/H}(Q_H, p_n, t)$ and $\hat{D}_{k/H}(Q_H, \hat{q}_k, t)$ is to some extent similar to the difference between the generalised parton luminosity considered previously, and the 'true' parton luminosities, being defined for each incoming parton independently. Indeed, the scale dependence of $D_{k/H}(Q_H, p_n, t)$ is directly given by the definition of $D(\{\hat{q}\}_k, t'|p_n, t)$ and the evolution equation for the generating functional,

$$\frac{\partial}{\partial t}D_{k/H}(Q_H, p_n, t) = \sum_i \int D_{k/H}(Q_H, k_i, t) \left[P(k_i|p_n, t)\right]_+ \mathrm{d}\phi(k_i) . \qquad (4.69)$$

The scale dependence (and the very definition) of $D_{k/H}(Q_H, p_n, t)$ and $\hat{D}_{k/H}(Q_H, \hat{p}_k, t)$ thus coincide in the limit where the splitting kernels can be considered to mediate splittings involving the identified parton only, giving rise precisely to the functional form of the dynamics expected from perturbative QCD.

4.4.4 Fixed Order Expansions

The calculation of fixed order expansions of the parton shower generating functional Z is of utmost importance for matching parton showers and fixed order calculations. We will here give an outline of the general procedure as another application of the formalism at hand, but postpone explicit calculations to chapter 6.

To start with, we introduce the perturbative expansion of the splitting kernels with respect to the strong coupling evaluated at the scale chosen in dependence on the evolution scale,

$$a(t) \equiv \alpha_s(\mu(t)) \, , \tag{4.70}$$

$$P(q_m|p_n, t) = \sum_{k=1}^{k_{\max}} \sum_{j=0}^{k} a^k(t) P^{(k,j)}(q_m|p_n, t)\delta_{m,n+j} + \mathcal{O}\left(a^{k_{\max}+1}(t)\right) \, , \tag{4.71}$$

such that at order $a^k(t)$ at most k additional partons are emitted. We did not include purely virtual kernels $P(p_n|p_n, t)$ according to the findings of section 4.3.2, but allow for the possibility of flavour changing transitions of a state of fixed multiplicity, $P(q_n|p_n, t)$, which are not part of this category. At next-to-leading order (NLO), the expansion of Z in the coupling $a(t)$ can directly be translated into an expansion in the strong coupling at a fixed scale μ_R, $\bar{\alpha}_s = \alpha_s(\mu_R)$. Starting from next-to-next-to-leading order (NNLO), $\mathcal{O}(a^2(t))$, the scale choice $\mu(t)$ does enter the expansion in terms of a fixed coupling such that care has to be taken in how the expansion in a fixed coupling is to be carried out. We note in particular, that the splitting kernels are free to associate a scale depending on the splitting type α considered, such that the splitting kernel expansion is indeed more complicated,

$$a^k(t) P^{(k,j)}(q_m|p_n, t) \to \sum_{\alpha} a^k(t^\alpha(q_m)) P_\alpha^{(k,j)}(q_m|p_n, t) \, . \tag{4.72}$$

Upon performing now the expansion in terms of the fixed coupling $\bar{\alpha}_s$, we also note that there is the possibility that the scale choice for a lower multiplicity, $m_1 < m_2$, a final state q_{m_1} may feed into the contribution to a higher multiplicity one, q_{m_2}. Depending on the order of the β-function chosen to determine the running of the strong coupling, one eventually finds the desired expansion of the splitting kernels,

$$P(q_m|p_n, t) = \sum_{k=1}^{k_{\max}} \sum_{j=0}^{k} \bar{\alpha}_s^k \bar{P}^{(k,j)}(q_m|p_n, t)\delta_{m,n+j} + \mathcal{O}\left(\bar{\alpha}_s^{k_{\max}+1}\right) \, , \tag{4.73}$$

where $\bar{P}^{(k)}$ now denotes the effective splitting kernel to be considered at order $\bar{\alpha}_s^k$, and we have moved back the sum over splitting types α into the definition of $\bar{P}^{(k)}$. Accordingly, the generating functional admits the desired expansion

$$Z(p_n, t', t)[u] = \sum_{k=0}^{k_{\max}} \bar{\alpha}_s^k Z^{(k)}(p_n, t', t)[u] + \mathcal{O}\left(\bar{\alpha}_s^{k_{\max}+1}\right) \ . \tag{4.74}$$

Again, the implicit solution of the generating functional is the method of choice to obtain the different terms $Z^{(k)}$. Note that it is sufficient to expand the exponential at most to its $k_{\max}$'th order, if an expansion up to $\mathcal{O}(\bar{\alpha}_s^{k_{\max}})$ is desired. Plugging in then the expansion of the splitting kernels and the generating functional itself, and equating the contributions order-by-order, the $Z^{(k)}$ can recursively be calculated noting that

$$Z^{(0)}(p_n, t', t)[u] = u(p_n) \tag{4.75}$$

is fixed by the normalisation of Z.

4.5 Conclusions

In this chapter, we considered a rather pragmatic approach to multiple parton emission based on, and triggered by, the fact that a typical parton shower implementation is nothing but simulating these dynamics by means of simulating a Markov process in a time variable referring to an evolution from harder to softer scales.

A thorough treatment of taking this fact as a *defining* property of multiple parton emission revealed that these particular dynamics, along with the constraints being imposed by unitarity, do indeed give rise to the dynamics as expected from perturbative QCD as basically emergent phenomena.

The main application of the formalism at hand is – however – motivated by the fact to obtain an analytic handle on what is actually to be expected by the implementation of a parton shower simulation, being completely defined by a set of splitting kernels and some scale choices. Another result is to gain insight into how the splitting kernels at hand govern the evolution dynamics of the simulation with respect to what subsets of a partonic configuration may be considered to evolve independently. Finally, the formalism provides the possibility to accurately calculate fixed order expansions of parton shower predictions – a possibility which is mandatory to perform the matching to fixed-order calculations.

Within this chapter we did not limit ourselves to any particular choice of a parton shower algorithm. The formalism is rather setup in order to deal with a huge class of these algorithms, even anticipating future generalisations in the direction of unintegrated

parton distributions by not sticking to collinear factorisation as the choice of all factorisation schemes. Furthermore, this new approach is completely based on a probabilistic picture thereby being closely linked to Monte Carlo implementations of parton showers as opposed to formalisms aiming at a similar level of generality, *e.g.* the operator based picture derived in [13–16].

5 Coherent Showers with Local Recoils

5.1 Overview

In this chapter we outline a new formalism for dipole-type parton showers which maintain exact energy-momentum conservation at each step of the evolution. This shower algorithm will be based on the kernels derived by Catani and Seymour, [9], originally in the context of carrying out NLO calculations within the subtraction formalism. Particular emphasis is put on the coherence properties, the level at which recoil effects do enter and the role of transverse momentum generation from initial state radiation. The formulated algorithm is shown to correctly incorporate coherence for soft gluon radiation.

Section 5.2 will focus on the effects of finite recoils and the coherence properties. Section 5.3 will give all technical details for final state radiation, whereas section 5.4 describes a treatment of initial state radiation, which so far has not been used in similar approaches, leading to a more physical picture of initial state radiation. Finally, section 5.5 outlines a possible generalisation of the algorithm to include colour correlations beyond the large-N_c limit.

5.2 Local Recoils, Form Factors and Coherence

We consider a single parton emission off a pair of partons with momenta p_i and p_j. The probability for this emission is taken to be the sum of two splitting functions, each associated with one leg. Using DGLAP splitting kernels and the Sudakov decomposition

for the splitting $p_i \rightarrow q_i, q$,

$$q_i = zp_i + \frac{p_\perp^2}{2p_i \cdot n\ z}n + k_\perp \ , \tag{5.1}$$

$$q = (1-z)p_i + \frac{p_\perp^2}{2p_i \cdot n\ (1-z)}n - k_\perp \ , \tag{5.2}$$

where $k_\perp^2 = -p_\perp^2$ and $k_\perp \cdot p_i = k_\perp \cdot n = 0$ constitutes the usual collinear approximation, which may be extended to the quasi-collinear approximation for emissions off massive partons, [17]. The light-like vector n defines the collinear direction, and therefore is used as the gauge vector in a light-cone gauge when deriving the collinear-singular behaviour of QCD matrix elements. n needs to be chosen along the colour connected partner p_j, the so-called physical gauge, in which interference diagrams are collinearly subleading such that the unregularised splitting kernels are given by cut self-energy diagrams only.[1]

Note that, within this parametrisation, the DGLAP splitting kernels are functions of

$$z = \frac{n \cdot q_i}{n \cdot p_i} \ . \tag{5.3}$$

Indeed, there is not a single choice of light-cone gauge, but rather a class of gauge choices which are connected by rescaling the gauge vector n (*i.e.* longitudinal boosts along the collinear direction), for which the splitting kernels are left invariant.

We are interested in extending this picture such as not to perform an approximation in the choice of kinematics, thereby introducing exact energy-momentum conservation within the splitting $p_i, p_j \rightarrow q_i, q, q_j$. The choice of the recoil strategy is not unique. However, choosing a spectator to absorb the longitudinal recoil of the splitting,

$$n = p_j \qquad q_j = \left(1 - \frac{p_\perp^2}{2p_i \cdot p_j\ z(1-z)} \right) p_j \tag{5.4}$$

is the only choice compatible with the remaining gauge degrees of freedom in the functional form of the splitting kernels. As we shall also see, this is the only choice which guarantees that the splitting functions in a physical gauge do reproduce the correct soft behaviour.

5.2.1 DGLAP Kernels, 'Soft Correctness' and Angular Ordering

As we are primarily interested in soft gluon radiation, we neglect gluon splittings into quark-antiquark pairs in this section.

---

[1]We note that this is a gauge choice for each singular limit of interest. The definition of 'colour-connected' here applies in the large-N_c limit but may be generalised by including the full colour correlations present at finite N_c.

For final state radiation the spin-averaged DGLAP kernels are given by

$$P_{qg}(z) = C_F \left(\frac{2z}{1-z} + (1-z) \right) , \qquad P_{gg}(z) = 2C_A \left(\frac{z}{1-z} + \frac{1-z}{z} + z(1-z) \right) ,$$
(5.5)

such that matrix elements squared, summed over all collinear configurations factorise as

$$_{m+1}\langle \mathcal{M}(q_1, ..., q_{m+1}) | \mathcal{M}(q_1, ..., q_{m+1}) \rangle_{m+1} \rightarrow$$
$$\sum_{i=1}^{m} \sum_{k \neq i} \frac{4\pi\alpha_s}{q_i \cdot q_k} P_{ik}(z) \, _m\langle \mathcal{M}(q_1, ..., p_i, ..., q_{m+1}) | \mathcal{M}(q_1, ..., p_i, ..., q_{m+1}) \rangle_m . \quad (5.6)$$

Note that in writing this expression, we do need to include a symmetry factor of $1/2$ along with the gluon splitting function.

As each amplitude $|\mathcal{M}\rangle$ is a colour singlet, *i.e.*

$$\sum_{i=1}^{m} \mathbf{T}_i^2 + \sum_{i=1}^{m} \sum_{j \neq i} \mathbf{T}_i \cdot \mathbf{T}_j = 0$$
(5.7)

we may rewrite collinear factorisation within the choice of the physical gauge for single collinear configurations as

$$_{m+1}\langle \mathcal{M}(q_1, ..., q_{m+1}) | \mathcal{M}(q_1, ..., q_{m+1}) \rangle_{m+1} \rightarrow$$
$$\sum_{i=1}^{m} \sum_{j,k \neq i} \frac{4\pi\alpha_s}{q_i \cdot q_k} P_{ik}(z)|_{n=p_j} \, _m\langle \mathcal{M}(q_1, ..., p_i, ..., q_m) | \mathbf{C}_{ij} | \mathcal{M}(q_1, ..., p_i, ..., q_m) \rangle_m , \quad (5.8)$$

where

$$\mathbf{C}_{ij} = -\frac{\mathbf{T}_i \cdot \mathbf{T}_j}{\mathbf{T}_i^2}$$
(5.9)

is the colour correlation operator as introduced in [9].

Within this framework, we have that

$$\frac{1}{q_i \cdot q} \frac{z}{1-z}\bigg|_{n=p_j} = \frac{q_i \cdot p_j}{q_i \cdot q \, q \cdot p_j} \qquad \frac{1}{q_i \cdot q} \frac{1-z}{z}\bigg|_{n=p_j} = \frac{q \cdot p_j}{q \cdot q_i \, q_i \cdot p_j}$$
(5.10)

such that the *single* splitting function $P_{ij}(z)|_{n=p_j}$ constitutes the complete, correct soft behaviour for the dipole i,j. Note that the eikonal parts – as well as any other part of a splitting function – is invariant under rescaling of the spectator momentum p_j, which is an even stronger motivation to use the longitudinal recoil strategy defined above.

This will also be a necessary requirement when trying to remove what we call 'soft double counting'. As we will show now, this is closely related to the coherence properties and logarithmic accuracy of a particular shower setup. To be precise, we consider the

form factor $\Delta_{ij}(Q^2, \mu^2)$ associated to a final-final dipole i, j when evolving from a hard scale Q^2 to a soft scale μ^2. Regarding the leading- (double) and next-to-leading (single) logarithmic contributions, $\alpha_s^n L^{2n}$ and $\alpha_s^n L^{2n-1}$ with $L = \ln(Q^2/\mu^2)$ the correct behaviour can be obtained from the coherent branching formalism [18], reproducing the results of soft gluon resummation, [19], by considering the leading behaviour of the z-integrated splitting kernel for $\mu^2 \ll p_\perp^2 \ll Q^2$. The resulting form factor reads

$$-\ln\Delta_{ij}(Q^2, \mu^2) = \int_{\mu^2}^{Q^2} \frac{\mathrm{d}p_\perp^2}{p_\perp^2} \frac{\alpha_s(p_\perp^2)}{2\pi} \left(\Gamma_i(p_\perp^2, Q^2) + \Gamma_j(p_\perp^2, Q^2) \right) \ , \qquad (5.11)$$

where the Sudakov anomalous dimensions $\Gamma_i(p_\perp^2, Q^2)$ are given by

$$\Gamma_q(p_\perp^2, Q^2) = C_F \left(\ln\frac{Q^2}{p_\perp^2} - \frac{3}{2} \right) \ , \qquad (5.12)$$

$$\Gamma_g(p_\perp^2, Q^2) = C_A \left(\ln\frac{Q^2}{p_\perp^2} - \frac{11}{6} \right) \ , \qquad (5.13)$$

receiving contributions both at the LL level from soft collinear, at the NLL level from hard collinear radiation. Note that the latter, *i.e.* the non-logarithmic terms in Γ are determined by the average of the soft-suppressed, z-regular terms of the splitting functions.

5.2.2 Sudakov Anomalous Dimensions in the Presence of Recoils

We now want to include the effects of a finite recoil. Within the minimal recoil strategy outlined above the phase space measure exactly factorises to the phase space with respect to the momenta before emission, $p_{i,j}$ and a measure for the emitted parton's momentum,

$$\frac{\mathrm{d}p_\perp^2}{p_\perp^2}\mathrm{d}z \left(1 - \lambda \frac{p_\perp^2}{z(1-z)s_{ij}} \right) \ , \qquad s_{ik} = 2p_i \cdot p_j \qquad (5.14)$$

where we introduced $\lambda \to 1$ to explicitly keep track of these effects, which are otherwise absent as $p_\perp \to 0$ in the collinear limit. Owing to the invariance under rescaling the spectator's momentum, this is the only place where recoil effects do enter. Choosing a phase space region related to an ordering in virtuality or transverse momentum,

$$4\mu^2 < \frac{p_\perp^2}{z(1-z)} < Q^2 \ , \qquad (5.15)$$

we find

$$\Gamma_q^V(p_\perp^2, Q^2) = C_F \left(2\ln\frac{Q^2}{p_\perp^2} - \frac{3}{2} - 2\lambda\frac{Q^2}{s_{ij}} \right) \ , \qquad (5.16)$$

$$\Gamma_g^V(p_\perp^2, Q^2) = C_A \left(2\ln\frac{Q^2}{p_\perp^2} - \frac{11}{6} - 2\lambda\frac{Q^2}{s_{ij}} \right) \ . \qquad (5.17)$$

Note that here, the recoil effects enter at the level of next-to-leading logarithms and the coefficient of the leading logarithms turns out to be twice the correct result. The latter observation has been noted since long [18]. From this example it is very clear that the simple fact that the DGLAP splitting functions reproduce the correct soft behaviour is not enough for the correct soft anomalous dimension. The wrong coefficient of the leading logarithmic contributions may be attributed to a double counting of soft emissions, originating from the fact that the above chosen phase space region does introduce an overlap of the phase space available for emissions off either parton of the dipole.

Choosing angular ordering in the variable $\tilde{q}$ by disentangling soft and collinear limits[2], and imposing phase space constraints through a cutoff on the transverse momentum in the soft limit(s),

$$\tilde{q}^2 = \frac{p_\perp^2}{z^2(1-z)^2} \qquad \mu^2 < z^2\tilde{q}^2 \; , \; (1-z)^2\tilde{q}^2 \qquad \tilde{q}^2 < Q^2 \qquad (5.18)$$

we recover the correct anomalous dimensions (5.12, 5.13) with recoil effects entering beyond NLL,

$$\Gamma_q^{AO}(p_\perp^2, Q^2) \;\; = \;\; C_F\left(\ln\frac{Q^2}{p_\perp^2} - \frac{3}{2}\right) + C_F\frac{p_\perp}{Q}\left(1 - 2\lambda\frac{Q^2}{s_{ij}}\right) + \mathcal{O}\left(\frac{p_\perp^2}{Q^2}\right) \; , \quad (5.19)$$

$$\Gamma_g^{AO}(p_\perp^2, Q^2) \;\; = \;\; C_A\left(\ln\frac{Q^2}{p_\perp^2} - \frac{11}{6}\right) + 2C_A\frac{p_\perp}{Q}\left(1 - \lambda\frac{Q^2}{s_{ij}}\right) + \mathcal{O}\left(\frac{p_\perp^2}{Q^2}\right) \; , \quad (5.20)$$

the subleading terms giving rise to power corrections in the form factor exponent.

Apart from the recoil effects, this result has a straightforward explanation: The phase space region chosen for the angular ordered evolution provides disjoint regions for emissions off either leg of the dipole, thereby removing the soft double counting observed earlier. Note that this observation would then in principle allow to include local recoils within the angular ordered DGLAP evolution.

5.2.3 A New Formalism Using Catani-Seymour Kernels

As outlined in the previous sections, taking a minimal choice to treat recoils yields a dipole-type picture. Within such a cascade it is however difficult to maintain the strong angular ordering, which is tied to the $1 \to 2$ nature of independent jet evolution.

Choosing the phase space to be restricted by a cutoff on the transverse momentum, thereby assuming an ordering in $p_\perp$ (or virtuality) is a much more natural picture to consider for a dipole-type evolution. In addition, this also removes complications when implementing matrix element corrections, either stand alone or for the purpose of matching to NLO, as the first emission off a dipole then is indeed the hardest emission.

---

[2]Note that in the soft limit(s), $z \to \epsilon$, $1 - \epsilon$, $p_\perp^2$ scales as ϵ^2.

To cure the problem of soft double counting generated by this evolution, one may modify the DGLAP splitting functions and 'continue' them over the whole available phase space in such a way, that the soft-singular pieces reproduce the correct soft behaviour when adding both modified splitting functions.

More precisely, for each leg i we replace the eikonal part by the radiation pattern associated with collinear emissions of p_i

$$\frac{p_i \cdot p_j}{p_i \cdot q \; q \cdot p_j} \to \frac{p_i \cdot p_j}{p_i \cdot q \; (p_i + p_j) \cdot q} \tag{5.21}$$

while keeping the collinear parts exactly. Note that this minimal construction, which does not modify the singular properties following from QCD, is nothing but the construction prescription for the subtraction kernels introduced in [9]: E.g. for gluon emission off a final-final dipole we have in terms of the momentum fraction z and the variable y introduced by Catani and Seymour

$$\frac{p_i \cdot p_j}{q \cdot p_j} = \frac{1}{1 - z} \to \frac{p_i \cdot p_j}{(p_i + p_j) \cdot q} = \frac{1}{1 - z(1 - y)} \; . \tag{5.22}$$

This picture of local recoils using a single spectator parton is ideally supplemented with exact factorisation of the phase space considering no kinematic approximation. One choice, which so far has been implemented [20, 21] is to invert the kinematic mappings as derived in [9].

For initial state radiation, taking the Catani-Seymour factorisation literally does have shortcomings. Most prominently, the choice of keeping the initial state emitter's momentum collinear to the one before emission leads for example to the fact that a final state singlet as in Drell-Yan lepton pair production, does receive a non-vanishing transverse momentum from the very first shower emission only. Further, an initial-initial system emitting a parton left the spectator parton unchanged, which might not be sufficient for the description of the transverse momentum spectrum of the whole final state. The aim of this work is to provide a formalism, which does overcome these problems. Further, we are interested in the logarithmic accuracy and ordering of soft gluon radiation in our setup reflecting coherence properties.

Starting from the final-state parametrisation given above, the outline of our formalism is as follows: We obtain a parametrisation of the kinematics for initial state emitters and/or spectators by considering the physical splitting processes while maintaining exact energy-momentum conservation *locally* to each branching, i.e. involving the emitter-emission system and a single spectator only. The spectator is restricted to take the longitudinal recoil of the splitting only. For initial state radiation we do allow each initial state emission to generate transverse momentum of the emitting incoming parton in a backward evolution. This transverse momentum is then migrated to the complete final state system by realigning the incoming partons to the beam axes at the end of the evolution.

For final-final dipoles, we find that the anomalous dimensions take the correct form apart from the fact, that the dependence on the arbitrary hard scale Q^2 is being replaced by the dipole's invariant mass s_{ik},

$$\Gamma_q^{CS}(p_\perp^2, Q^2) = C_F \left(\ln \frac{s_{ij}}{p_\perp^2} - \frac{3}{2} \right) - C_F \pi \lambda \frac{p_\perp}{\sqrt{s_{ij}}} + \mathcal{O}\left(\frac{p_\perp^2}{Q^2} \right) , \tag{5.23}$$

$$\Gamma_g^{CS}(p_\perp^2, Q^2) = C_A \left(\ln \frac{s_{ij}}{p_\perp^2} - \frac{11}{6} \right) - C_A \pi \lambda \frac{p_\perp}{\sqrt{s_{ij}}} + \mathcal{O}\left(\frac{p_\perp^2}{Q^2} \right) , \tag{5.24}$$

with recoil effects entering beyond NLL.

We note that, in case of DGLAP kernels, the correct coefficient of the leading logarithmic contributions to the anomalous dimension is governed by the choice of boundaries on the momentum fraction for a given (but arbitrary) hard scale Q^2,

$$\int_0^{1-\sqrt{\kappa}} \frac{\mathrm{d}z}{1-z} = \frac{1}{2} \ln \left(\frac{Q^2}{p_\perp^2} \right) , \tag{5.25}$$

with $\kappa = p_\perp^2/Q^2$.

The above findings for the anomalous dimension can essentially be traced back to the fact that the transition from a DGLAP kernel possessing a soft singularity $\sim 1/(1-z)$ to the appropriate Catani-Seymour kernel (while keeping track of all recoil effects, i.e. considering the soft limit at fixed $p_\perp^2$) is the simple replacement

$$\frac{1}{1-z} \rightarrow \left(1 - \frac{\kappa_{ij}}{(1-z)} \right) \frac{1-z}{(1-z)^2 + \kappa_{ij}} , \tag{5.26}$$

where $\kappa_{ij} = p_\perp^2/s_{ij}$. Here, the first factor is the effect of the finite recoil stemming from the exact factorisation of the phase space measure.

Within the variables to be outlined in detail in the next section, we find that this pattern generalises to the cases of initial state emitter or spectator partons, up to a sign on the recoil term owing to timelike or spacelike virtualities of the emitter or whether the relevant dipole scale is a spacelike momentum transfer or invariant mass.

Choosing the z boundaries (in the approximation considered above) to be given by

$$z < 1 - \frac{p_\perp^2}{Q^2} = 1 - \kappa \tag{5.27}$$

it is evident that the recoil contribution only gives rise to power corrections, while the logarithmic contribution is given by

$$\frac{1}{2} \int_{\kappa^2}^1 \frac{\mathrm{d}\xi}{\xi + \kappa_{ij}} = \frac{1}{2} \ln \left(\frac{s_{ij}}{p_\perp^2} \right) + \text{power corrections} , \tag{5.28}$$

thereby reproducing the correct coefficient up to the disappearance of the arbitrary hard scale, an immediate consequence of the screening of the soft singularity at fixed transverse momentum.

5.2.4 Structure of the Evolution

For final state radiation with final state spectator, our findings of the previous section immediately signal a choice of the hard scale for a single dipole originating from a hard process. Choosing an arbitrary hard scale $Q^2 \neq s_{ik}$ will immediately result in the appearance of spurious logarithmic contributions when performing the $p_\perp^2$ integration.

For example, at fixed α_s the leading logarithmic contributions for a dipole i, j, with Casimir operators $C_{i,j}$ associated to the partons, take the form

$$- \ln \Delta_{ij} = \frac{\alpha_s}{4\pi}(C_i^2 + C_j^2) \ln \left(\frac{Q^2}{\mu^2} \right) \ln \left(\frac{s_{ij}^2}{\mu^2 Q^2} \right) + \text{NLL} \qquad (5.29)$$

instead of the expected result

$$- \ln \Delta_{ij} = \frac{\alpha_s}{4\pi}(C_i^2 + C_j^2) \ln^2 \left(\frac{Q^2}{\mu^2} \right) + \text{NLL} , \qquad (5.30)$$

the mismatch being manifest as an ambiguity at the level of next-to-leading logarithms. We are therefore lead to the choice $Q^2 = s_{ij}$, *i.e.* the hard scale associated to a dipole is the respective invariant mass.

For initial state emitter or spectator partons, we assume that this generalises to choosing the hard scale in such a way as to fill the complete phase space, modulo the infrared cutoff.

Note that this choice does not determine the ordering *per se*, but only the choice of hard scale and the shape of the phase space restriction when evolving between two scales. The ordering is to be chosen in such a way, that the leading effects of multiple emissions off each leg of the dipole do exponentiate. Due to the structure of the splitting kernels given above and the additional complications from all finite recoil effects the explicit exponentiation is beyond the scope of this paper.

Having however observed that we can reproduce the correct Sudakov anomalous dimension, while avoiding soft double counting we additionally note that within the variables chosen

$$p_\perp^2 = 2 \frac{p_i \cdot q \; q \cdot p_j}{p_i \cdot p_j} \qquad (5.31)$$

for emission of a gluon of momentum q off a dipole (i, j). Ordering emissions in this variable therefore corresponds to an ordering reproducing the most probable history of multiple gluon emission according to the eikonal approximation in the limit of soft gluons strongly ordered in energy.

It should further be noted that the angular ordering constraints for soft gluons are indeed inherent to the $p_\perp$-ordered evolution of a dipole cascade, as has been explicitly shown in [?], provided that the transverse momentum is chosen to be spacelike in the rest frame of a dipole. This is indeed the case for the evolution to be outlined in detail in the following section.

We therefore conclude that branchings within the physical kinematics outlined above and based on the corresponding CS dipole splitting functions allow us to construct a parton shower that has the right coherence properties. The final state emissions should in this case be taken as outlined above, i.e. with the hard scale of a single cascade chosen to be the dipole invariant mass and the evolution should be strictly ordered in transverse momentum. However, in the naive adoption of the CS picture to a parton shower not every initial state emission would contribute to the final state transverse momentum. We will formulate a more suitable approach below.

5.3 Final State Radiation

5.3.1 Final State Spectator

Final state radiation with a final state spectator does represent the generic version of the splitting kinematics chosen here. For a splitting $(p_i, p_j) \to (q_i, q, q_j)$ we choose the standard Sudakov decomposition

$$q_i = z p_i + \frac{p_\perp^2}{z s_{ij}} p_j + k_\perp \tag{5.32}$$

$$q = (1 - z) p_i + \frac{p_\perp^2}{(1 - z) s_{ij}} p_j - k_\perp \tag{5.33}$$

$$q_j = \left(1 - \frac{p_\perp^2}{z(1 - z) s_{ij}} \right) p_j \ , \tag{5.34}$$

where $k_\perp^2 = -2 p_i \cdot p_j \equiv -s_{ij}$ and $k_\perp \cdot p_{i,j} = 0$. The transverse momentum is defined in the dipole's rest frame to be purely spacelike,

$$\hat{p}_{i,j} = \left(\frac{\sqrt{s_{ij}}}{2}, \pm \mathbf{p} \right) \ , \qquad \hat{k}_\perp = (0, \mathbf{p}_\perp) \ , \qquad \mathbf{p} \cdot \mathbf{p}_\perp = 0 \ . \tag{5.35}$$

Note that this does preserve the momentum of the emitting system, $q_i + q + q_j = p_i + p_j$. The parametrisation gives rise to the phase space factorisation [9]

$$d\phi(q_i, q, q_j | Q) = d\phi(p_i, p_j | Q) \frac{1}{16\pi^2} \frac{d\phi}{2\pi} dp_\perp^2 \frac{dz}{z(1 - z)} \left(1 - \frac{p_\perp^2}{z(1 - z) s_{ij}} \right) \tag{5.36}$$

Note that, in the collinear limit, this is the massless version of the kinematics as chosen in [17]. It further constitutes the inversion of the 'tilde'-mapping, where the variables y and z chosen in [9] are given by

$$y = \frac{q_i \cdot q}{q_i \cdot q + q_j \cdot q + q_i \cdot q_j} = \frac{p_\perp^2}{z(1 - z) s_{ij}} \ , \qquad z = \frac{p_j \cdot q_i}{p_i \cdot p_j} \ . \tag{5.37}$$
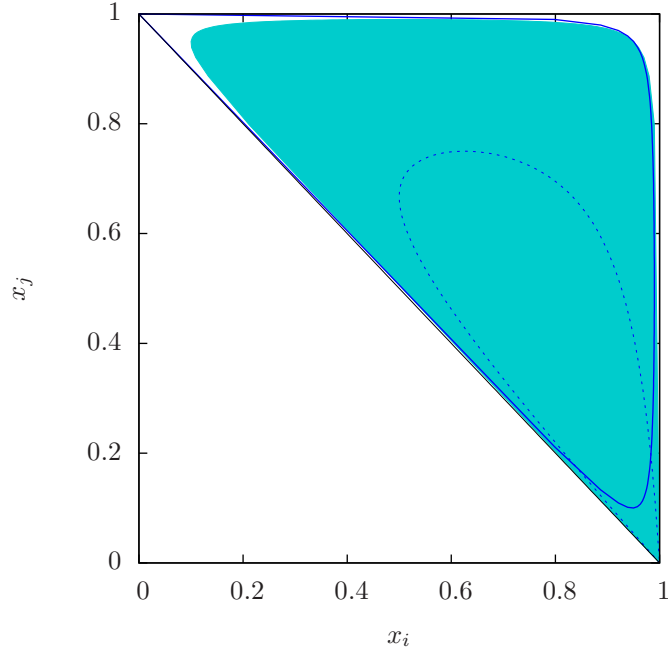
Figure 5.1: Allowed phase space regions for emissions from a final-final dipole expressed
in the Dalitz variables $x_k = 2Q \cdot p_k/Q^2$ for a dipole of mass $s_{ij} = 100$ GeV
and infrared cutoff $\mu = 5$ GeV. The shaded region is accessible for emissions
off the parton i, whereas the area enclosed by the solid line is accessible for
emissions off parton j. The area enclosed by the dotted line is an example of
the phase space excluded when starting at a scale lower than s_{ij}. Note that
the infrared cutoff is exaggerated for illustrative purposes only. In practise,
almost the whole physical phase space will be available.

The allowed phase space region (cf. Fig. 5.1) is obtained by considering the limits on
the emitter's virtuality before emission (*i.e.* the invariant mass of the emitter-emission
pair),

$$4\mu^2 < \frac{p_\perp^2}{z(1-z)} < Q_{\text{max}}^2 = s_{ij} \tag{5.38}$$

such that

$$\mu^2 < p_\perp^2 < \frac{Q_{\text{max}}^2}{4} , \qquad z_\pm = z_\pm = \frac{1}{2} \left(1 \pm \sqrt{1 - \frac{4p_\perp^2}{Q_{\text{max}}^2}} \right) . \tag{5.39}$$

Averaging over azimuth, the final-final splitting kernels take the form

$$\frac{8\pi\alpha_s}{2q_i \cdot q} \langle V(p_\perp^2, z) \rangle \tag{5.40}$$

such that the splitting probability is

$$\mathrm{d}P_{ij}(p_\perp^2, z) = \frac{\alpha_s}{2\pi} \langle V(p_\perp^2, z) \rangle \left(1 - \frac{p_\perp^2}{z(1-z)s_{ij}}\right) \frac{\mathrm{d}p_\perp^2}{p_\perp^2} \mathrm{d}z \;. \tag{5.41}$$

Note that, comparing to the collinear limit, the effect of finite recoils is to act as a damping factor for large-angle hard emissions, provided that $y < 1$ which is a consequence of the phase space boundary.

5.3.2 Initial State Spectator

For an initial state spectator we consider the crossing $q_j \to -q_a$, $p_j \to -p_a$, such that

$$q_i = zp_i + \frac{p_\perp^2}{zs_{ia}}p_a + k_\perp \tag{5.42}$$

$$q = (1-z)p_i + \frac{p_\perp^2}{(1-z)s_{ia}}p_a - k_\perp \tag{5.43}$$

$$q_a = \left(1 + \frac{p_\perp^2}{z(1-z)s_{ia}}\right) p_a \;, \tag{5.44}$$

where $s_{ia} = 2p_i \cdot p_a$. Note that exact momentum conservation is trivially implemented by just the fact that the parametrisation for a final state spectator does respect this constraint. The transverse momentum is defined be purely spacelike in a frame where,

$$\hat{p}_{i,a} = \left(\frac{\sqrt{s_{ia}}}{2}, \pm\mathbf{p}\right) \;, \qquad \hat{k}_\perp = (0, \mathbf{p}_\perp) \;, \qquad \mathbf{p} \cdot \mathbf{p}_\perp = 0 \;. \tag{5.45}$$

The phase space measure then obeys the convolution

$$\mathrm{d}\phi^F(q_i, q, q_a|Q; x_a) = \mathrm{d}\phi^F(p_i, p_a|Q; xx_a)\frac{\mathrm{d}\phi}{2\pi}\frac{x}{16\pi^2}\frac{\mathrm{d}z}{z(1-z)}\mathrm{d}p_\perp^2 \;, \tag{5.46}$$

where

$$x = \frac{1}{1 + \frac{p_\perp^2}{z(1-z)s_{ia}}} \;, \qquad z = \frac{p_a \cdot q_i}{p_a \cdot p_i} \tag{5.47}$$

and it is straightforward to verify that this indeed gives rise to the phase space convolution as given in [9]. Including the parton distributions and the kinematic factor of the partonic flux, the relevant measure is

$$\frac{f_a(x_a)}{4q_a \cdot p_b}\mathrm{d}\phi^F(q_i, q, q_a|Q; x_a)\mathrm{d}x_a =$$
$$\left(\frac{f_a(x_a/x)}{f_a(x_a)}\theta(x - x_a)\frac{\mathrm{d}\phi}{2\pi}\frac{x}{16\pi^2}\frac{\mathrm{d}z}{z(1-z)}\mathrm{d}p_\perp^2\right) \frac{f_a(x_a)}{4p_a \cdot p_b}\mathrm{d}\phi^F(p_i, p_a|Q; x_a)\mathrm{d}x_a \;, \tag{5.48}$$

where P_a and x_a are the momentum of the incoming hadron and the momentum fraction of the incoming parton respectively. p_b denotes the momentum of the second incoming particle in the collision entering the flux factor. The phase space limits can be obtained as for the final state case,

$$4\mu^2 < \frac{p_\perp^2}{z(1-z)} < Q_{\text{max}}^2 \ , \tag{5.49}$$

where, owing to $x > x_a$, the hard scale of a dipole is now given by

$$Q_{\text{max}}^2 = s_{ia} \frac{1 - x_a}{x_a} \ . \tag{5.50}$$

The allowed phase space is shown in Fig. 5.2. Averaging over azimuth, the final-initial splitting kernels take the form

$$\frac{8\pi\alpha_s}{2q_i \cdot q} \frac{1}{x} \langle V(p_\perp^2, z) \rangle \tag{5.51}$$

such that the splitting probability is

$$\mathrm{d}P_{ia}(p_\perp^2, z) = \frac{\alpha_s}{2\pi} \langle V(p_\perp^2, z) \rangle \frac{f_a(x_a/x)}{f_a(x_a)} \theta(x - x_a) \frac{\mathrm{d}p_\perp^2}{p_\perp^2} \mathrm{d}z \ . \tag{5.52}$$

Note that the finite recoil enters only in the PDF ratio, reproducing the correct collinear limit when $x \to 1$. Once again, the effect of the finite recoil is a damping of hard emissions for $x \sim x_a$.

5.4 A New Treatment of Initial State Radiation

5.4.1 Motivation

A construction of initial state radiation by just crossing prescriptions is not obvious owing to the fact that the shower evolution is formulated as a *backward* evolution.

The physical variables thus need to be defined from the physical *forward* kinematics. For the physical emission process $q_a \to p_a, q$ the relevant Sudakov decomposition for the emission momentum q is

$$q_{\text{forward}} = (1-z)q_a + \frac{p_\perp^2}{2n \cdot q_a(1-z)} n - k_\perp \ , \tag{5.53}$$

where n is the backward lightcone direction defining the collinear direction, *i.e.* the final or initial state spectator's momentum.

The parametrisation above is most conveniently inverted to backward evolution $p_a \to q_a, q$ by considering the process in a frame where $q_a = p_a/x$, giving rise to

$$q_{\text{backward}} = \frac{(1-z)}{x}p_a + \frac{p_\perp^2}{2n \cdot p_a(1-z)}n - \frac{1}{\sqrt{x}}k_\perp \ . \tag{5.54}$$

We therefore define the Lorentz invariant physical variables to be given by

$$x \, q_a \cdot q = \frac{p_\perp^2}{1-z} \qquad x \, n \cdot q = (1-z)n \cdot p_a \ . \tag{5.55}$$

The parametrisation keeping the emitter aligned with the beam axis can then be related to a parametrisation where the initial state parton after (backward evolution) emission does acquire a finite transverse momentum while keeping the spectator after emission aligned with the one before emission.

It is this type of splitting kinematics which allows any emission off an initial state parton to contribute transverse momentum to a final state system after having applied a proper realignment boost once the parton shower evolution has terminated. Ideally, this final boost should *not* be related to the parametrisation chosen but being determined in a process dependent way such as to leave the interesting kinematic quantities of the hard process invariant.

5.4.2 Final State Spectator

For initial state emissions with final state spectator, $p_a, p_j \to q_a, q, q_j$, using the variables introduced in [9],

$$x = \frac{p_a \cdot p_j}{(p_a - p_j) \cdot q_a} \qquad u = \frac{q_j \cdot q_a}{(p_a - p_j) \cdot q_a} \ , \tag{5.56}$$

we use the parametrisation

$$q_a = \frac{1-u}{x-u}p_a + \frac{u}{x}\frac{1-x}{x-u}p_j + \frac{1}{u-x}k_\perp \tag{5.57}$$

$$q = \frac{1-x}{x-u}p_a + \frac{u}{x}\frac{1-u}{x-u}p_j + \frac{1}{u-x}k_\perp \tag{5.58}$$

$$q_j = \left(1 - \frac{u}{x}\right)p_j \ , \tag{5.59}$$

which does preserve the momentum transfer, $q + q_j - q_a = p_j - p_a$. The transverse momentum obeys

$$k_\perp^2 = -u(1-u)\frac{1-x}{x}s_{aj} \qquad s_{aj} = 2p_a \cdot p_j \ . \tag{5.60}$$

5 Coherent Showers with Local Recoils

Considering the collinear limit $u \to 0$, it is evident that the relevant momentum fraction is x and we are therefore lead to choose the physical variables to be given by

$$u = \frac{\kappa}{1-z} , \qquad x = \frac{z(1-z) - \kappa}{1 - z - \kappa} , \qquad \kappa = \frac{p_\perp^2}{s_{aj}} . \tag{5.61}$$

Indeed, the Lorentz transformation

$$R^\mu{}_\nu =$$

$$\delta^\mu_\nu + \frac{x}{(1-u)(x-u)} \frac{k_\perp^\mu k_{\perp\nu}}{p_a \cdot p_j} + \frac{u(1-x)}{x-u} \frac{K^\mu K_\nu}{p_a \cdot p_j} + \frac{x}{x-u} \frac{k_\perp^\mu K_\nu - K^\mu k_{\perp\nu}}{p_a \cdot p_j} \tag{5.62}$$

with $K = p_a + p_j$ relates the above parametrisation to one preserving the direction of the incoming parton,

$$R q_a = \frac{1}{x} p_a \tag{5.63}$$

$$R q = u p_j + (1-u)\frac{1-x}{x} p_a - k_\perp \tag{5.64}$$

$$R q_j = (1-u) p_j + u\frac{1-x}{x} p_a + k_\perp . \tag{5.65}$$

In order to derive the phase space convolution properties associated with the parametrisation given above, we employ the formalism outlined in the appendix. Substituting

$$u = \frac{y}{w + y(1-w)} , \qquad x = \frac{1}{w + y(1-w)} \tag{5.66}$$

the parametrisation above is mapped to

$$(-q_a) = w(-p_a) + (1-w)\, y\, p_j - q_\perp \tag{5.67}$$

$$q = (1-w)(-p_a) + w\, y\, p_j + q_\perp \tag{5.68}$$

$$q_j = (1-y)\, p_j , \tag{5.69}$$

with $q_\perp^2 = -s_{aj} y w (1-w)$ such that the generalised phase space measure factors as

$$\mathrm{d}\phi(q_j, q, -q_a | Q) = \frac{s_{aj}}{16\pi^2} \frac{\mathrm{d}\phi}{2\pi} \frac{\mathrm{d}x}{x^3} \, \mathrm{d}u \, \mathrm{d}\phi(p_j, -p_a | Q) . \tag{5.70}$$

Having identified x to be the relevant momentum fraction from the parametrisation 5.63-5.65, we consider the hadronic collision in a frame where[3]

$$P_a \cdot q_a = \frac{1}{x} P_a \cdot p_a , \qquad N \cdot q_a = \frac{1}{x} N \cdot p_a , \tag{5.71}$$

---

[3]Note that there is no a priori relation between incoming hadron and parton momenta in our formulation. N denotes the light-like momentum defining the collinear direction and is taken along the momentum of the beam not containing the emitter parton.

such that the phase space convolution properties of both parametrisations become equivalent at *hadron* level,

$$\mathrm{d}\phi^F(q_i, q, a_a|Q; x_a) = \mathrm{d}\phi^F(p_i, p_a|Q; x x_a)\frac{\mathrm{d}\phi}{2\pi}\frac{1}{16\pi^2}\frac{\mathrm{d}z}{z(1-z)-\kappa}\mathrm{d}p_\perp^2 \ , \tag{5.72}$$

We stress that the crucial difference is related to the fact that, considering the physical forward evolution, our parametrisation does generate a finite transverse momentum for the parton entering the hard process after additional parton emission.

Averaging over azimuth, the initial-final splitting kernels take the form

$$\frac{8\pi\alpha_s}{2q_a \cdot q}\frac{1}{x}\langle V(p_\perp^2, z)\rangle \tag{5.73}$$

such that the splitting probability is

$$\mathrm{d}P_{ai}(p_\perp^2, z) = \frac{\alpha_s}{2\pi}\langle V(p_\perp^2, z)\rangle\frac{f_a(x_a/x)}{f_a(x_a)}\theta(x - x_a)\frac{\mathrm{d}p_\perp^2}{p_\perp^2}\frac{(1-z)\mathrm{d}z}{z(1-z)-\kappa} \ . \tag{5.74}$$

Note that in the collinear limit, $\kappa \to 0$ we have $x \to z$ such that the collinear behaviour is properly reproduced.[4]

The phase space boundaries are given by the requirement that $x_a < x$,

$$\mu^2 < p_\perp^2 < \frac{(1-x_a)s_{aj}}{4} \ , \qquad z_\pm = \frac{1}{2}\left(1 + x_a \pm (1 - x_a)\sqrt{1 - \frac{4p_\perp^2}{(1-x_a)s_{aj}}}\right) \ . \tag{5.75}$$

5.4.3 Initial State Spectator

Initial state radiation with initial state spectator, $p_a, p_b \to q_a, q, q_b$ is described by the parametrisation

$$q_a = \frac{1}{v + x}p_a + \frac{v}{x}\frac{1 - v - x}{v + x}p_b + \frac{1}{v + x}k_\perp \tag{5.76}$$

$$q = \frac{1 - v - x}{v + x}p_a + \frac{v}{x}\frac{1}{v + x}p_b + \frac{1}{v + x}k_\perp \tag{5.77}$$

$$q_b = \left(1 + \frac{v}{x}\right)p_b \ , \tag{5.78}$$

preserving $q - q_a - q_b = -p_a - p_b$. The transverse momentum is defined to be purely spacelike in the dipole's rest frame and obeys

$$k_\perp^2 = -(1 - v - x)\frac{v}{x}s_{ab} \qquad s_{ab} = 2p_a \cdot p_b \ . \tag{5.79}$$

---

[4]For readability we have suppressed indexing a possible flavour change of the incoming parton.
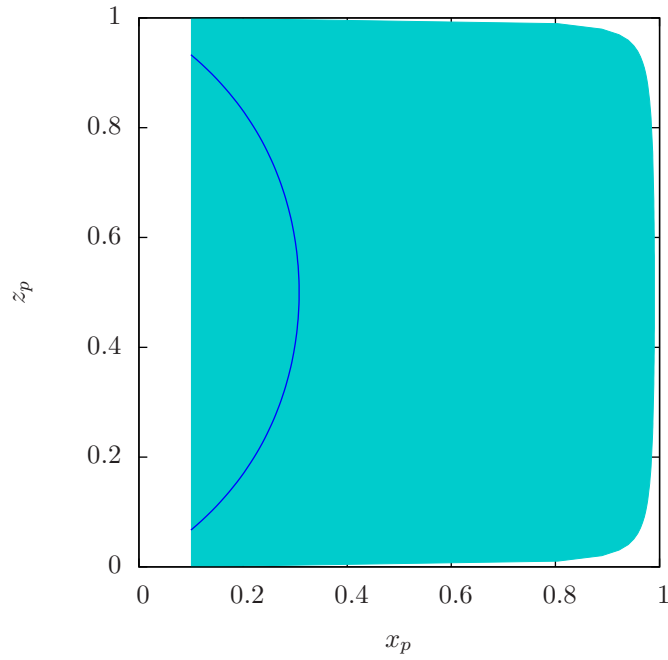
Figure 5.2: Available phase space for a final-initial dipole with invariant momentum transfer $\sqrt{s_{aj}} = \sqrt{-t} = 100$ GeV and an infrared cutoff of 5 GeV. The shaded region is accessible starting at the hard scale, the region enclosed by the solid line is an example of the phase space excluded when starting at a lower scale. The phase space regions for an initial-final dipole are identical. For a final-initial dipole, the variables are $x_p = x$, $z_p = z$, for the initial-final one $x_p = x$, $z_p = 1 - u$. Note that in the latter case $u \rightarrow 1$ and $u \rightarrow 0$ correspond to a collinear limit.

The variables x and v are those introduced in [9],

$$x = \frac{p_a \cdot p_b}{q_a \cdot q_b} \ , \quad v = \frac{q_a \cdot q}{q_a \cdot q_b} \ , \tag{5.80}$$

and we define the physical variables to be given by

$$x = \frac{z(1-z) - \kappa}{1-z} \ , \qquad v = \frac{\kappa}{1-z} \ , \qquad \kappa = \frac{p_\perp^2}{s_{ab}} \ . \tag{5.81}$$

Note that the Lorentz transformation

$$S^\mu_{\ \nu} =$$
$$\delta^\mu_\nu + \frac{p_b \cdot p_a}{p_b \cdot q_a \, q_a \cdot p_a} q_a^\mu q_{a,\nu} + \frac{p_b \cdot q_a}{p_b \cdot p_a \, q_a \cdot p_a} p_a^\mu p_{a,\nu} - \frac{1}{q_a \cdot p_a} \left(q_a^\mu p_{a\nu} + p_a^\mu q_{a\nu} \right) \tag{5.82}$$

does transform this parametrisation to a parametrisation where

$$S q_a = \frac{1}{x+v} p_a \ , \qquad S q_b = \frac{x+v}{x} p_b \ . \tag{5.83}$$

Following the arguments of the previous section we then find the phase space convolution

$$\mathrm{d}\phi^F(q_a, q, q_b | Q; x_a, x_b) =$$
$$\mathrm{d}\phi^F \left(p_a, p_b | Q; (x+v)x_a, \frac{x}{x+v} x_b \right) \frac{\mathrm{d}\phi}{2\pi} \frac{1}{16\pi^2} \frac{\mathrm{d}z}{z(1-z)-\kappa} \mathrm{d}p_\perp^2 \ . \tag{5.84}$$

Averaging over azimuth, the initial-final splitting kernels take the form

$$\frac{8\pi\alpha_s}{2q_a \cdot q} \frac{1}{x} \langle V(p_\perp^2, z) \rangle \tag{5.85}$$

such that the splitting probability is

$$\mathrm{d}P_{ab}(p_\perp^2, z) = \frac{\alpha_s}{2\pi} \langle V(p_\perp^2, z) \rangle \mathcal{F}_{ab} \frac{\mathrm{d}p_\perp^2}{p_\perp^2} \frac{(1-z)\mathrm{d}z}{z(1-z)-\kappa} \ , \tag{5.86}$$

with

$$\mathcal{F}_{ab} = \frac{f_a(x_a/(x+v))}{f_a(x_a)} \theta(x+v-x_a) \frac{f_b(x_b(x+v)/x)}{f_b(x_b)} \theta\left(\frac{x}{x+v} - x_b \right) \tag{5.87}$$

the ratio of incoming parton flux. [5] Note that in the collinear limit, $v, \kappa \to 0$ and $x \to z$ such that we find the correct collinear behaviour.

---

[5] As for the final state spectator, we have suppressed indexing a possible flavour change of the incoming parton.

We remark that it would be possible to keep the spectator unchanged upon properly substituting the integrations over the incoming momentum fractions (the Jacobian being equal to one). This, however, would invalidate the fact that the above given parametrisation of the splitting kinematics does preserve energy-momentum locally involving the emitter-emission-spectator system only (in fact, after applying the relevant Lorentz transformation S this would constitute the inversion of the kinematics as used in the dipole subtraction context). A further argument to not keeping the spectator unchanged is that, following the discussion on soft and collinear factorisation, we see no reason why the emission off the *colour connected* system p_a, p_b should leave p_b unchanged except for a strictly soft and/or collinear emission.

The phase space limits are now determined from $x > x_a x_b = \tau$ to be given by

$$z_\pm = \frac{1}{2}\left(1 + \tau \pm (1-\tau)\sqrt{1 - \frac{4p_\perp^2}{(1-\tau)^2 s_{ab}}}\right) \ , \qquad p_\perp^2 < \frac{(1-\tau)^2 s_{ab}}{4} \ , \qquad (5.88)$$

and are shown in Fig. 5.3.

5.5 An Aside on $1/N_c$-Suppressed Terms

5.5.1 Motivation

The shower algorithm as outlined in the previous sections is defined in the large-N_c limit, thereby neglecting colour correlations

$$_m\langle\mathcal{M}(q_1, ..., q_m)|\mathbf{C}_{ij}|\mathcal{M}(q_1, ..., q_m)\rangle_m \qquad (5.89)$$

between partons (i, j) which are not colour connected in the large-N_c limit. Experience shows that from a purely phenomenological point of view, this approximation seems to be justified by the fact that all existing parton showers (to which this approximation is indeed common) give a reasonable description of all collider data collected so far[6]. A quantitative analysis has however not been carried out so far. Though algorithms have been suggested to fully include these correlations [15], they seem far from being practical.

We will here outline an algorithm which is indeed practical, if a program dealing with colour structures in a certain basis of $SU(N)$ tensors is available. Since colour correlations do have their origin in factorisation of QCD amplitudes for soft gluon emission, we shall limit ourselves to this case only. Owing to the structure of the colour correlations for factorisation at $\mathcal{O}(\alpha_s)$, this picture fits nicely into the algorithm outlined already.

---

[6]It should be noted, that the parton showers do not work in a *strict* large-N_c limit, keeping $C_F \neq C_A/2$ for $N_c = 3$.
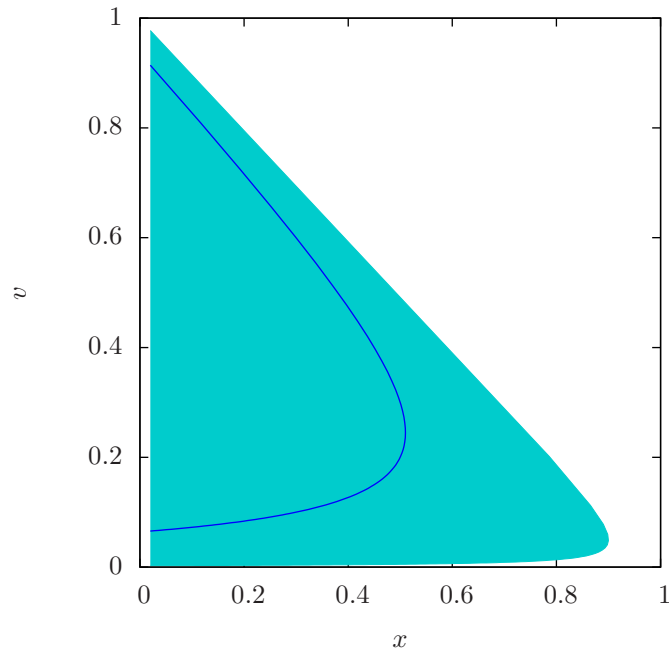
Figure 5.3: Available phase space for emissions off an initial-initial dipole of mass 100 GeV with $\tau = 0.02$ and infrared cutoff 5 GeV. The shaded region is the available phase space when starting from the hard scale, the region enclosed by the solid line is an example of the phase space excluded when starting at a lower scale.

5.5.2 Modification of the Dipole Splitting Kernels

As already noted, the Catani-Seymour splitting kernels do contain the correct soft behaviour. We will therefore use the soft-singular parts of these kernels, as well as the kinematic parametrisation and phase space boundaries outlined previously, but modify them to include the ratio of colour correlated matrix elements squared at each step of the evolution. To be precise, gluon emission at a scale $p_\perp$ off an emitter-spectator pair, $p_i, p_j \rightarrow q_i, q, q_j$ in association with m other partons is now described by a splitting probability

$$\mathrm{d}S_{ij}(p_\perp, z) = \mathrm{d}P_{ij}^{\mathrm{soft}}(p_\perp, z) \frac{{}_m\langle \mathcal{M}(p_1, ..., p_m)|\mathbf{C}_{ij}|\mathcal{M}(p_1, ..., p_m)\rangle_m}{{}_m\langle \mathcal{M}(p_1, ..., p_m)|\mathcal{M}(p_1, ..., p_m)\rangle_m} \tag{5.90}$$

where $\mathrm{d}P_{ij}^{\mathrm{soft}}(p_\perp, z)$ denotes the soft singular part of the splitting probabilities introduced earlier. This form of the splitting kernels is motivated by considering successive soft-gluon approximations to the ratio of exact tree-level matrix elements squared,

$$\frac{|\mathcal{M}(q_1, ..., q_m, q)|^2}{|\mathcal{M}(p_1, ..., p_m)|^2} , \tag{5.91}$$

thereby iteratively constructing final states which are distributed according to the tree level matrix elements in the soft gluon approximation, provided we consider all emitter-spectator combinations for all pairs of partons. The modified dipole splitting kernels will thus generate the soft gluon emission distributed according to the full colour correlations.

A major technical obstacle in this algorithm is the fact that the modified splitting kernels will not be positive definite, posing a problem to a Monte Carlo implementation along traditional lines. Extensions of the Monte Carlo algorithm being used here to the case of non-positive definite splitting kernels are proposed in section 7.3.1.

5.5.3 Calculation of the Soft Gluon Amplitudes

In order to evaluate the amplitude $|\mathcal{M}\rangle_{m+1}$, which will enter the generation of splittings after having emitted a soft gluon with momentum q off a partonic ensemble $p_1, ..., p_m$ in association with an emitter i and spectator j, we will have to define a physical gluon polarisation, which we take to be given in terms of helicities $\pm$ and a phase ψ as

$$\epsilon(q, \psi) = \epsilon_+(q) + e^{i\psi}\epsilon_-(q) . \tag{5.92}$$

Note that the contributions to the polarisation dependent square of the eikonal current,

$$\frac{\epsilon(q, \psi) \cdot p_i \; \epsilon^*(q, \psi) \cdot p_j}{p_i \cdot k \; p_j \cdot k} \tag{5.93}$$

admit the same partial fractioning underlying the construction of the splitting kernel S_{ij}, such that we select ψ with density given by the ratio of polarisation dependent to polarisation summed amplitude squared, *i.e.*

$$\frac{\mathrm{Re}(\epsilon(q, \psi) \cdot p_i \ \epsilon^*(q, \psi) \cdot p_j)}{p_i \cdot p_j} \frac{\mathrm{d}\psi}{2\pi} \ . \tag{5.94}$$

$|\mathcal{M}\rangle_{m+1}$ is then calculated by acting the resulting eikonal current on $|\mathcal{M}\rangle_m$,

$$|\mathcal{M}\rangle_{m+1} = \sum_{l=1}^{m} \frac{\epsilon^*(q, \psi) \cdot p_l}{q \cdot p_l} \mathbf{T}_l |\mathcal{M}\rangle_m \ . \tag{5.95}$$

The initial condition for this recursion is set by the amplitude associated to the hard process from which the cascade did start evolving.

5.6 Conclusions

In this chapter we have specified a parton shower algorithm based on Catani–Seymour subtraction kernels. The coherence properties of soft gluon radiation have been studied in detail, and the algorithm has been shown to correctly take soft gluon coherence into account. As opposed to similar approaches followed by other groups, [20, 21], a much more physical treatment of initial state radiation has been constructed. Here, the final state transverse momentum indeed builds up from multiple initial state emissions, as is required to properly resum the leading contributions to all orders.

The advantage of the algorithm is an ordering in transverse momentum, such that the first emission generated is indeed the hardest one – it is this fact which will greatly simplify the matching to NLO QCD calculations. Finally, a possible extension of the algorithm to include colour correlations beyond the large-N_c limit has been proposed.

All technical details necessary for an implementation have been given, and the full algorithm as implemented as an add-on module to the Herwig++ [22] event generator, will be specified in chapter 8.

6 Matching Parton Showers and Higher Orders

6.1 Overview

Matching parton showers and fixed order QCD calculations has been a vital research field in recent years. Starting from the pioneering work of Frixione and Webber, [23], which introduced the first successful implementation of matching parton showers and NLO QCD calculations, many developments have been achieved. Motivated by schemes for combining parton showers and tree-level matrix elements, [24, 25], first studies in the direction of performing a similar merging at the level of NLO QCD have also been carried out, [26].

The purpose of this chapter is to discuss in detail the matching of parton showers and NLO calculations. We will here derive the matching conditions on very general grounds, using the formalism introduced in chapter 4. We will show that we can exactly reproduce the matching types known so far, MC@NLO [23], and POWHEG, [27], identifying them to be both members of the same class – the essential difference being indeed an improvement to the subsequent parton shower, which is present for the latter scheme.

Since the general formalism considered indeed provides the right conditions for NLO matching, we calculate the expansion of parton shower to $\mathcal{O}(\alpha_s^2)$, deriving matching conditions to NNLO QCD calculations. Such an approach has not yet been considered in the literature.

Before turning to detailed calculations, the next section will introduce the subject of NLO matching in terms of a simple toy model.

6.1.1 A Toy Model of NLO Matching

The toy model starts by considering a very simple, one-dimensional phase space for the Born degrees of freedom x, and another degree of freedom y referring to the real emission contribution. $y \to 0$ is considered the limit of unresolved parton emission.

Let $O(x)$ an observable on the Born phase space, and $O(x, y)$ on the real emission phase space. Most importantly, O will have to be infrared safe, *i.e.*

$$O(x, y) = O(x) + yC(x, y) + \mathcal{O}(y^2) \tag{6.1}$$

with C regular at $y = 0$.

At LO, the prediction for O is simply given by

$$\langle O \rangle_{\mathrm{LO}} = \int_0^1 \mathrm{d}x B(x)O(x) . \tag{6.2}$$

At NLO, O receives contributions from Born, one-loop, and real-emission contributions, respectively,

$$
\begin{aligned}
\langle O \rangle_{\mathrm{NLO}} &= \int_0^1 \mathrm{d}x B(x)O(x) \\
&+ \alpha_s \int_0^1 \mathrm{d}x V(x)O(x) \\
&+ \alpha_s \int_0^1 \mathrm{d}x \int_0^1 \mathrm{d}y \frac{R(x, y)}{y} O(x, y) ,
\end{aligned}
\tag{6.3}
$$

where the real emission residue in $y = 0$ is $R(x, 0) = B(x)$ and within dimensional regularisation (restricted to this two-dimensional model), the virtual contribution will as well exhibit a divergence in terms of a pole in $\epsilon = (d - 4)/2$,

$$V(x) = -\frac{B(x)}{\epsilon} + \bar{V}(x) . \tag{6.4}$$

Within the subtraction formalism the NLO prediction is turned into

$$
\begin{aligned}
\langle O \rangle_{\mathrm{NLO}} &= \int_0^1 \mathrm{d}x B(x)O(x) \\
&+ \alpha_s \int_0^1 \mathrm{d}x V(x)O(x) + \alpha_s \int_0^1 \mathrm{d}x \int_0^1 \mathrm{d}y \frac{A(x, y)}{y^{1-\epsilon}} O(x) \\
&+ \alpha_s \int_0^1 \mathrm{d}x \int_0^1 \mathrm{d}y \frac{R(x, y)O(x, y) - A(x, y)O(x)}{y} .
\end{aligned}
\tag{6.5}
$$

The singular behaviour of the subtraction term is fixed by the singularities of the real emission, *i.e.* $A(x, y) = B(x) + \mathcal{O}(y)$, such that

$$
\begin{aligned}
\langle O \rangle_{\mathrm{NLO}} &= \int_0^1 \mathrm{d}x\, B(x) O(x) \\
&+ \alpha_s \int_0^1 \mathrm{d}x (\bar{V}(x) + A_{finite}(x)) O(x) + \mathcal{O}(\epsilon) \\
&+ \alpha_s \int_0^1 \mathrm{d}x \int_0^1 \mathrm{d}y \frac{R(x, y) O(x, y) - A(x, y) O(x)}{y} \ ,
\end{aligned}
\tag{6.6}
$$

where all contributions are now numerically integrable.

A parton shower with splitting kernels $P(x, y)/y$, starting evolving off the Born process, will predict O as

$$
\langle O \rangle_{\mathrm{PS}} = \int_0^1 \mathrm{d}x \int_0^1 \mathrm{d}y\, B(x) \left(\delta(y) \Delta(x) + \theta(y - \mu) \alpha_s \frac{P(x, y)}{y} \Delta(x) \right) O(x, y)
\tag{6.7}
$$

with the Sudakov from factor

$$
-\ln \Delta(x) = \int_\mu^1 \mathrm{d}y\, \alpha_s \frac{P(x, y)}{y} \ .
\tag{6.8}
$$

Expanding in α_s, we find

$$
\langle O \rangle_{\mathrm{PS}} = \int_0^1 \mathrm{d}x\, B(x) - \alpha_s \int_0^1 \mathrm{d}x \int_\mu^1 \mathrm{d}y \frac{P(x, y)}{y} \left(O(x) - O(x, y) \right) + \mathcal{O}(\alpha_s^2) \ .
\tag{6.9}
$$

The α_s coefficient in this contribution will be double counted, when naively letting the parton shower act on events distributed according to the subtracted NLO calculation.[1].

Matching NLO and parton shower now proceeds through subtracting this double counted contribution from the fixed order,

$$
\begin{aligned}
\langle O \rangle_{\mathrm{NLO,matched}} &= \int_0^1 \mathrm{d}x\, B(x) O(x) \\
&+ \alpha_s \int_0^1 \mathrm{d}x (\bar{V}(x) + A_{finite}(x)) O(x) + \mathcal{O}(\epsilon) \\
&+ \alpha_s \int_0^1 \mathrm{d}x \int_0^1 \mathrm{d}y \frac{P(x, y) - A(x, y)}{y} O(x) \\
&+ \alpha_s \int_0^1 \mathrm{d}x \int_0^1 \mathrm{d}y \frac{R(x, y) - P(x, y)}{y} O(x, y) \ .
\end{aligned}
\tag{6.10}
$$

---

[1]Note that the parton shower starting off the real emission contribution will change this only at formally higher order $\mathcal{O}(\alpha_s^2)$

Here we assumed that letting the infrared cutoff of the parton shower μ to zero only produces power corrections. This has already been shown on general grounds in section 4.2.3. As these contributions are in any way subject to the dynamics of a hadronization model, this poses no inconsistency when considering a complete event simulation. Note that it is now also possible to generate events with finite weights, provided the splitting kernels resemble the singular behaviour of the real emission contribution (and hence the subtraction terms, as well).

Eq. 6.10 is the most general matched NLO prediction. Simplifications may however be obtained by choosing a parton shower behaving 'nice' in this context, in particular either $P(x, y) = A(x, y)$, or $P(x, y) = R(x, y)$, removing one of the contributions needed to be calculated in the fixed-order part of the simulation.

6.2 The General Procedure

For a fixed-order cross section at the r-th order in perturbation theory, several contributions of different final state multiplicity, $\mathrm{d}\sigma^k(p_n|Q; \mu)$ (in relative $\mathcal{O}(\bar{\alpha}_s^k)$ with respect to the lowest order, $\bar{\alpha}_s$ denoting the running coupling at a fixed reference scale cf. section 4.4.4) have to be considered. In order to deal with these contributions on equal footing, and to make use of the formalism introduced in chapter 4, we define the generating functional of fixed-order cross sections up to k_{max}'th order by

$$\sigma(Q, \mu(t))[u] = \sum_{k=0}^{k_{\mathrm{max}}} \sum_n \int \frac{\mathrm{d}\sigma^k(p_n|Q; \mu(t))}{\mathrm{d}\phi(p_n)} u(p_n) \mathrm{d}\phi(p_n) + \mathcal{O}(\bar{\alpha}_s^{k_{\mathrm{max}}+1}) , \qquad (6.11)$$

where t sets a hard scale for the process at hand.

Making use of the generating functional of parton shower transition probabilities, $Z(p_n, t', t)[u]$ the cross sections after parton showering can now easily be obtained by replacing the the test functions u by Z,

$$\sigma_{+\mathrm{PS}}(Q, \mu(t))[u] =$$

$$\sigma(Q, \mu(t))[Z(\mu_{\mathrm{IR}}, t)[u]] \equiv \sum_{k=0}^{k_{\mathrm{max}}} \sum_n \int \frac{\mathrm{d}\sigma^k(p_n|Q; \mu(t))}{\mathrm{d}\phi(p_m)} Z(p_n, \mu_{\mathrm{IR}}, t)[u] \mathrm{d}\phi(p_n) . \quad (6.12)$$

μ_{IR} denotes the infrared cutoff of the parton shower. The matching condition is given by demanding that the matched prediction, $\sigma_{\mathrm{matched}}(Q, \mu(t))[u]$, when evolved by the parton shower, is equal to the fixed-order prediction up to the desired order $\bar{\alpha}_s^{k_{\mathrm{max}}}$,

$$\sigma_{\mathrm{matched}+\mathrm{PS}}(Q, \mu(t))[u] = \sigma(Q, \mu(t))[u] + \mathcal{O}(\bar{\alpha}_s^{k_{\mathrm{max}}}) \qquad (6.13)$$

It can always be written as

$$\sigma_{\text{matched}}(Q, \mu(t))[u] = \sigma(Q, \mu(t))[u] - \sigma_c(Q, \mu(t))[u] \ , \tag{6.14}$$

where $\sigma_c(Q, \mu(t))[u]$ contains the contributions double counted by the parton shower, *i.e.* it is the fixed-order expansion of $\sigma_{+\text{PS}}(Q, \mu(t))[u]$ up to the desired order, excluding the fixed-order itself,

$$\sigma_c(Q, \mu(t))[u] = \sigma_{+\text{PS}}(Q, \mu(t))[u]|_{\mathcal{O}(\bar{\alpha}_s^{k_{\max}})} - \sigma(Q, \mu(t))[u] \ , \tag{6.15}$$

where the vertical line to the right denotes truncation of the expansion at the indicated order. The task of calculating the matching conditions to a fixed-order prediction thus is in calculating the fixed order expansion of the parton shower generating functional Z, which is carried out explicitly up to $\mathcal{O}(\alpha_s^2)$ in the following section.

For practical purposes we shall see that the infrared cutoff has to be removed in the matched fixed-order prediction, such that the matching is formally correct only up to power corrections, cf. section 4.2.3,

$$\sigma_{\text{matched+PS}}(Q, \mu(t))[u] = \sigma(Q, \mu(t))[u] + \mathcal{O}(\bar{\alpha}_s^{k_{\max}}) + \text{power corrections} \ . \tag{6.16}$$

6.3 Fixed-Order Expansions of a Parton Shower

In this section the fixed-order expansions of a parton shower to NLO ($\mathcal{O}(\alpha_s)$) and NNLO ($\mathcal{O}(\alpha_s^2)$), as needed to facilitate the matching to NLO and NNLO calculations, respectively, are calculated. The underlying formalism has already been outlined in section 4.4.4.

6.3.1 Parton Showers to $\mathcal{O}(\alpha_s)$

We will here consider a parton shower being built on splitting kernels in $\mathcal{O}(\alpha_s)$. The scale choice for α_s at the NLO level is of formally higher order, such that

$$\begin{aligned} P(q_m|p_n, t) &= a(t)P^{(1,1)}(q_m|p_n, t)\delta_{m,n+1} + \mathcal{O}\left(a^2(t)\right) \\ &= \bar{\alpha}_s \bar{P}^{(1,1)}(q_m|p_n, t)\delta_{m,n+1} + \mathcal{O}\left(\bar{\alpha}_s^2\right) \end{aligned} \tag{6.17}$$

with $P = \bar{P}$. The contributions $Z^{(0,1)}$ to the generating functional in leading and next-to-leading order satisfy

$$
\begin{aligned}
Z^{(0)}(p_n, t', t) & = u(p_n) && (6.18)\\
Z^{(1)}(p_n, t', t) & = \int_{t'}^{t} \mathrm{d}\tau \int \bar{P}^{(1,1)}(q_{n+1}|p_n, \tau) && (6.19)\\
& \quad \times \left(Z^{(0)}(q_{n+1}, t', \tau) - Z^{(0)}(p_n, t', \tau)\right) \mathrm{d}\phi(q_{n+1}) \\
& = \int_{t'}^{t} \mathrm{d}\tau \int \bar{P}^{(1,1)}(q_{n+1}|p_n, \tau)\left(u(q_{n+1}) - u(p_n)\right) \mathrm{d}\phi(q_{n+1}) \ .
\end{aligned}
$$

This will be the main ingredient to derive NLO matching. Note that the structure is similar to that of a subtracted real emission – a 'Born type' configuration p_n is subtracted from the 'real emission configuration', q_{n+1}.

6.3.2 Parton Showers to $\mathcal{O}(\alpha_s^2)$

Starting from NNLO, the scale choice for the strong coupling cannot be considered being of formally higher order. To start with, we consider the parton shower built from splitting kernels up to order $a^2(t)$, *i.e.*

$$
\begin{aligned}
P(q_m|p_n, t) & = a(t)P^{(1,1)}(q_m|p_n, t)\delta_{m,n+1} && (6.20)\\
& + a^2(t)P^{(2,1)}(q_m|p_n, t)\delta_{m,n+1} \\
& + a^2(t)P^{(2,2)}(q_m|p_n, t)\delta_{m,n+2} + \mathcal{O}(a^3(t)) \ ,
\end{aligned}
$$

The first contribution is the leading order splitting emitting one additional parton, the second is a one-loop correction to this splitting, while the third corresponds to a splitting emitting two additional partons. These kernels are related to the desired fixed-order expansion by the running chosen for α_s,

$$
a(t) = \bar{\alpha}_s + C(\mu(t), \mu_R)\bar{\alpha}_s^2 + \mathcal{O}\left(\bar{\alpha}_s^3\right) \ , \tag{6.21}
$$

$$
\begin{aligned}
\bar{P}^{(1,1)}(q_{n+1}|p_n, t) & = P^{(1,1)}(q_{n+1}|p_n, t) && (6.22)\\
\bar{P}^{(2,1)}(q_{n+1}|p_n, t) & = P^{(2,1)}(q_{n+1}|p_n, t) + C(\mu(t), \mu_R)P^{(1,1)}(q_{n+1}|p_n, t) && (6.23)\\
\bar{P}^{(2,2)}(q_{n+2}|p_n, t) & = P^{(2,2)}(q_{n+2}|p_n, t) \ . && (6.24)
\end{aligned}
$$

The required next step in the recursive evaluation of the generating functional is then given by

$$
Z^{(2)}(p_n, t', t) = \frac{1}{2} \frac{\left(Z^{(1)}(p_n, t', t)\right)^2}{Z^{(0)}(p_n, t', t)}
$$
$$
+ \int_{t'}^{t} d\tau \int \bar{P}^{(1,1)}(q_{n+1}|p_n, \tau) \left(Z^{(1)}(q_{n+1}, t', \tau) - Z^{(1)}(p_n, t', \tau) \frac{Z^{(0)}(q_{n+1}, t', \tau)}{Z^{(0)}(p_n, t', \tau)} \right) d\phi(q_{n+1})
$$
$$
+ \int_{t'}^{t} d\tau \int \bar{P}^{(2,1)}(q_{n+1}|p_n, \tau) \left(Z^{(0)}(q_{n+1}, t', \tau) - Z^{(0)}(p_n, t', \tau) \right) d\phi(q_{n+1})
$$
$$
+ \int_{t'}^{t} d\tau \int \bar{P}^{(2,2)}(q_{n+2}|p_n, \tau) \left(Z^{(0)}(q_{n+2}, t', \tau) - Z^{(0)}(p_n, t', \tau) \right) d\phi(q_{n+2}) .
$$
$$(6.25)$$

Inserting the results for $Z^{(0)}$ and $Z^{(1)}$ we find

$$
Z^{(2)}(p_n, t', t) = \int_{t'}^{t} d\tau \int_{t'}^{\tau} d\tau' \int \bar{P}^{(1,1)}(q_{n+2}|q_{n+1}, \tau') \bar{P}^{(1,1)}(q_{n+1}|p_n, \tau)
$$
$$
\times \left(u(q_{n+2}) - u(q_{n+1}) \right) d\phi(q_{n+1}) d\phi(q_{n+2})
$$
$$
- \int_{t'}^{t} d\tau \int_{t'}^{\tau} d\tau' \int \bar{P}^{(1,1)}(k_{n+1}|p_n, \tau) \bar{P}^{(1,1)}(q_{n+1}|p_n, \tau')
$$
$$
\times \left(u(q_{n+1}) - u(p_n) \right) d\phi(q_{n+1}) d\phi(k_{n+1})
$$
$$
+ \int_{t'}^{t} d\tau \int \bar{P}^{(2,1)}(q_{n+1}|p_n, \tau) \left(u(q_{n+1}) - u(p_n) \right) d\phi(q_{n+1})
$$
$$
+ \int_{t'}^{t} d\tau \int \bar{P}^{(2,2)}(q_{n+2}|p_n, \tau) \left(u(q_{n+2}) - u(p_n) \right) d\phi(q_{n+2}) .
$$
$$(6.26)$$

Here, the first term corresponds to a subtracted real emission for parton emission off a configuration which has already been produced by a first parton shower emission according to the lowest order splitting kernel. The second term amounts to a subtracted real emission contribution according to the lowest order kernel including a 'virtual' contribution originating from integrating over unresolved emissions which could have happened at scales larger than the emission scale. The third term is completely analogous to the one already encountered for the expansion up to $\mathcal{O}(\alpha_s)$, now considering the one-loop corrected single parton emission kernel. Finally, the last term represents subtracting a Born-type configuration from a double real emission configuration. As for the NLO case, all of these contributions are very similar to the ones encountered in a NNLO calculation carried out within subtraction. This will further be discussed in section 6.5.

6.4 NLO Matching

In this section we will analyse the matching of a parton shower and NLO QCD corrections. We will first introduce the generating functional for the NLO cross section in the context of the subtraction formalism, before deriving the general 'master formula' as already sketched in the toy model given in the introduction. We will not consider a particular subtraction scheme, as the general structure for these is dictated by the singularity structure anyway. Examples of schemes being widely in use are dipole subtraction, [9] and FKS, [6].

6.4.1 The NLO Generating Functional

The subtraction terms being used in the context of NLO calculations are indeed similar to the $\mathcal{O}(\alpha_s)$ splitting kernels used in a parton shower and may – regarding the general structure – be thought of as being the inverse of a splitting kernel: a mapping is performed from a $n+1$ parton configuration to a n-parton configuration being accompanied by extracting the singular behaviour of the real emission matrix element.

More precisely, the subtraction terms are introduced as auxiliary cross sections to be added and subtracted from the NLO calculation, together with an exact factorisation of the real emission phase space similar to the one introduced when deriving parton shower splitting kernels in section 4.2.2:

$$\mathrm{d}\sigma_A^{(1,1)}(q_{n+1}|Q;\mu) = \bar{\alpha}_s D^{(1,1)}(p_n|q_{n+1};\mu)\mathrm{d}\phi^F(q_{n+1}|Q;\mu) \tag{6.27}$$

$$= \bar{\alpha}_s \sum_\alpha \int D_\alpha^{(1,1)}(p_n|q_{n+1};\mu)\mathrm{d}\phi_1^\alpha(q_{n+1}|p_n;\mu)\mathrm{d}\phi^F(p_n|Q;\mu) \ .$$

In the last line the phase space convolution associated to the kinematic mapping has been introduced similarly to the case already used for the derivation of the splitting kernels. Owing to the presence of spin correlations in the case of collinear parton emission off a gluon, the $D^{(1,1)}$ have to be considered functions of the Born *amplitude*, a factorisation in terms of the Born amplitude squared (and hence a factorisation of the auxiliary cross section w.r.t. the Born cross section) being present only upon performing the integration of the azimuthal degrees of freedom.

Since the subtraction terms D are constructed to reproduce the singular behaviour of the real emission matrix element squared, their analytic integration over the one-parton phase space in d dimensions will cancel the poles in ϵ being present in the virtual corrections and the counter term used to renormalise the parton distribution functions by virtue of the KLN theorem, as discussed in chapter 3. Within the subtraction formalism

the final form of the NLO generating functional is then given by

$$
\begin{aligned}
\sigma_{\mathrm{NLO}}(Q,\mu)[u] \;=\; & \int u(p_n)\mathrm{d}\sigma^{(0,0)}(p_n|Q;\mu) \qquad\qquad\qquad\qquad\qquad (6.28)\\
+\; & \bar{\alpha}_s \int u(p_n)\left(\mathrm{d}\sigma^{(1,0)}(p_n|Q;\mu)+\mathrm{d}\sigma_{FC}^{(1,0)}(p_n|Q;\mu)\right.\\
& \qquad\qquad \left.+\;D^{(1,1)}(p_n|q_{n+1};\mu)\mathrm{d}\phi^F(q_{n+1}|Q;\mu))\right|_{\epsilon=0}\\
+\; & \bar{\alpha}_s\int\left(\mathrm{d}\sigma^{(1,1)}(q_{n+1}|Q;\mu)u(q_{n+1})\right.\\
& \qquad\qquad \left.-\;D^{(1,1)}(p_n|q_{n+1};\mu)u(p_n)\right)\mathrm{d}\phi^F(q_{n+1}|Q;\mu)\;.
\end{aligned}
$$

As for the splitting kernels, we adopted the convention that superscripts (n,m) indicate a contribution of order n in the strong coupling accompanied by emission of m additional partons both with respect to the leading order considered. The contributions in eq. 6.28 in order of their appearance are the leading order cross section, the sum of one-loop, factorisation counter term and analytic integral of the subtraction term (to be considered for $\epsilon=0$ after analytic cancellation of the poles), as well as the real emission contribution accompanied by the unintegrated subtraction term.

The test functions appearing along with the individual contributions can directly be translated in terms of Monte Carlo events being of either Born ($u(p_n)$) or real emission ($u(q_{n+1})$) type. We will from now on drop the factorisation counter term and the reference to the parton luminosity, when not relevant – these contributions pose no conceptual problem, the factorisation counter term, after a proper deconvolution, can always be attributed to be part of the virtual correction and the parton luminosity is considered to be part of the phase space measure anyway.

6.4.2 Structure of the Matched Generating Functional

The contribution double counted by the parton shower can directly be inferred from section 6.3.1:

$$
\begin{aligned}
\sigma_{\mathrm{NLO,c}}(Q,\mu(t))[u]\big|_{\mathcal{O}(\bar{\alpha}_s)} = \bar{\alpha}_s\int\mathrm{d}\sigma^{(0,0)}(p_n|Q;\mu(t)) \qquad\qquad (6.29)\\
\times\int_{\mu_{IR}}^t\mathrm{d}\tau\int\bar{P}^{(1,1)}(q_{n+1}|p_n,\tau)\left(u(q_{n+1})-u(p_n)\right)\mathrm{d}\phi(q_{n+1})
\end{aligned}
$$

Denoting by $\mathrm{d}\sigma_{\mathrm{finite}}^{(1,0)}$ the contributions of virtual corrections, collinear counter term, and integrated subtraction dipole after cancellation of the ϵ poles, the matched generating functional is readily obtained from the general recipe, subtracting the double counted

contributions from the NLO generating functional:

$$
\sigma_{\mathrm{NLO,matched}}(Q, \mu(t))[u] = \int u(p_n) \left(\mathrm{d}\sigma^{(0,0)}(p_n|Q; \mu(t)) + \bar{\alpha}_s \mathrm{d}\sigma^{(1,0)}_{\mathrm{finite}}(p_n|Q; \mu(t)) \right)
$$

$$
+ \bar{\alpha}_s \sum_{\alpha} \int_{\Omega(\mu_{\mathrm{IR}}, t)} P^{(1,1)}_{\alpha}(q_{n+1}|p_n; t^{\alpha}(q_{n+1})) \mathrm{d}\phi^{\alpha}_1(q_{n+1}|p_n) u(p_n) \mathrm{d}\sigma^{(0,0)}(p_n|Q; \mu^{\alpha}(q_{n+1}))
$$

$$
- \bar{\alpha}_s \sum_{\beta} \int D^{(1,1)}_{\beta}(p_n|q_{n+1}; \mu(t)) \mathrm{d}\phi^{\beta}_1(q_{n+1}|p_n) u(p_n) \mathrm{d}\phi(p_n|Q)
$$

$$
+ \bar{\alpha}_s \int u(q_{n+1}) \mathrm{d}\sigma^{(1,1)}(q_{n+1}|Q; \mu) u(q_{n+1}) \mathrm{d}\phi(q_{n+1}|Q)
$$

$$
- \bar{\alpha}_s \sum_{\alpha} \int_{\Omega(\mu_{\mathrm{IR}}, t)} P^{(1,1)}_{\alpha}(q_{n+1}|p_n; t^{\alpha}(q_{n+1})) \mathrm{d}\phi^{\alpha}_1(q_{n+1}|p_n) u(q_{n+1}) \mathrm{d}\sigma^{(0,0)}(p_n|Q; \mu^{\alpha}(q_{n+1})) \;,
$$

$$(6.30)$$

where $\mu^{\alpha}(q_{n+1})) \equiv \mu(t^{\alpha}(q_{n+1}))$. Several remarks are in order. First, we considered the general possibility that the kinematic mappings used by the parton shower (corresponding to the summation index α) may not coincide with those used by the subtraction terms (index β). We also kept the full dependence on the parton shower infrared cutoff and the scale choices imposed by the splitting kernels.

It should be observed, that the matched generating functional delivers basically three categories of events: Born events with weights given by the Born and finite virtual cross sections, Born-type events with weights given by the difference of splitting kernels times the Born cross section and subtraction terms (including a proper Jacobian after having mapped either contribution to use the kinematic mapping of the other one), and real emission type events with weights given by the real emission cross section minus the splitting kernels times the Born cross section.

For practical purposes, the associated weights should be finite. Provided that the parton shower kernels properly reproduce the singular behaviour of the real emission matrix element, this is possible only upon removing the parton shower cutoff. Note, however, that this change merely gives rise to a power correction as discussed in section 4.2.3, which we will neglect. Attributing the possibility that t and $t^{\alpha}(q_{n+1})$ are chosen such that not all phase space may be available to parton shower emissions to a vanishing splitting kernel in the non-accessible region, while including a Jacobian to translate parton shower kinematic mappings to the ones used in the subtraction terms and taking the scale μ to be independent of the parton shower scales, we can rewrite

$$
\int_{\Omega(\mu_{\mathrm{IR}}, t)} P^{(1,1)}_{\alpha}(q_{n+1}|p_n; t^{\alpha}(q_{m+1})) \mathrm{d}\phi^{\alpha}_1(q_{n+1}|p_n) \mathrm{d}\sigma^{(0,0)}(p_n|Q; \mu(t^{\alpha}(q_{m+1}))) =
$$

$$
\int P^{(1,1)}_{\beta,\mathrm{eff}}(q^{\beta}_{n+1}(p_n)|p_n; \mu) \mathrm{d}\phi^{\beta}_1(q_{n+1}|p_n) \mathrm{d}\phi(p_n|Q) \quad (6.31)
$$

and, inverting the kinematic mapping q^β,

$$P_{\beta,\text{eff}}^{(1,1)}(q_{n+1}^\beta(p_n)|p_n;\mu)\mathrm{d}\phi_1^\beta(q_{n+1}|p_n)\mathrm{d}\phi(p_n|Q) = P_{\beta,\text{eff}}^{(1,1)}(q_{n+1}|p_n^\beta(q_{n+1});\mu)\mathrm{d}\phi(q_{n+1}|Q) \, , \tag{6.32}$$

where $P_{\beta,\text{eff}}^{(1,1)}$ now is a product of the splitting kernel, the Jacobian needed to translate the mappings $\alpha \to \beta$, and the Born differential cross section.

This contribution does, however, in general not reproduce the *point-wise* singular behaviour of the real emission contribution including the spin correlations. In order to practically perform the matching, we therefore further assume that $P_{\beta,\text{eff}}$ has been modified in such a way as to reproduce the spin correlations with the constraint that the azimuthal average reproduces the kernel being used by the parton shower. The matching condition is then correct upon azimuthal average, as has for example been discussed in the context of the MC@NLO matching, [23].

In any case, the structure of the matched generating functional can now be cast into a more transparent form,

$$
\begin{aligned}
\sigma_{\text{NLO,matched}}(Q,\mu)[u] \;=\; & \int u(p_n)\left(\mathrm{d}\sigma^{(0,0)}(p_n|Q;\mu) + \bar\alpha_s\mathrm{d}\sigma_{\text{finite}}^{(1,0)}(p_n|Q;\mu)\right) && (6.33) \\
+ \; & \bar\alpha_s \sum_\beta \int \left(P_{\beta,\text{eff}}^{(1,1)}(q_{n+1}^\beta(p_n)|p_n;\mu) - D_\beta^{(1,1)}(p_n|q_{n+1}^\beta(p_n);\mu)\right) \\
& \qquad \times u(p_n)\mathrm{d}\phi_1^\beta(q_{n+1}|p_n)\mathrm{d}\phi(p_n|Q) \\
+ \; & \bar\alpha_s \int \left(\mathrm{d}\sigma^{(1,1)}(q_{n+1}|Q;\mu) - \sum_\beta P_{\beta,\text{eff}}^{(1,1)}(q_{n+1}|p_n^\beta(q_{n+1});\mu)\right) \\
& \qquad \times u(q_{n+1})\mathrm{d}\phi(q_{n+1}|Q) \, .
\end{aligned}
$$

The finiteness of the three contributions separately is now evident. Eq. 6.33 is the general version of the 'master matching formula' derived in the toy model, eq. 6.10. When considering this matching formula for the case of the HERWIG parton shower and FKS subtraction it constitutes the theoretical basis underlying the MC@NLO matching, [23]. The formalism is however more general and does not make any reference to a particular subtraction nor parton shower algorithm.

In practise, the meaning of the above equation is to basically re-implement the program calculating the NLO corrections. This is not desirable, and the obvious simplification is to consider a parton shower with kernels given by the subtraction terms,

$$P_{\beta,\text{eff}}^{(1,1)} = D_\beta^{(1,1)} \, , \tag{6.34}$$

upon which the contribution in the second line of eq. 6.33 vanishes, leaving a minor modification to interface an NLO program in a consistent way to a parton shower: instead of separately considering real emission phase space points, and 'underlying Born' phase space points weighted by the subtraction terms, real emission events are generated

only with a weight given by the sum of the real emission cross section minus all individual subtraction term weights.

6.4.3 Matching with Matrix Element Corrections

Building a parton shower based on NLO subtraction kernels for just the purpose of simplifying NLO matching is in general not guaranteed to provide precise predictions. With the notable exception of the coherent dipole shower introduced in chapter 5, such a shower may not properly take into account the contributions expected to be relevant for multiple collinear and soft parton emission. A much more elegant simplification of the matching can be obtained by *improving* the parton shower in such a way that it will reproduce the exact real emission matrix element for the hardest emission. This emission will in general not be the first one, such that so-called 'truncated showers' will have to be added, [27, 28].

Since these showers indeed happen *after* the hardest emission has been generated, they can formally be regarded to be built of splitting kernels mediating transitions from a real emission configuration, starting with kernels of the form $P(q_{n+2}|q_{n+1})$. Thus, the fixed-order expansion and matching conditions are still well defined in the context of truncated showers.

Improving the parton shower to reproduce the real emission matrix element,

$$\mathrm{d}\sigma^{(1,1)}(q_{n+1}|Q;\mu) = \sum_{\beta} P_{\beta,\mathrm{eff}}^{(1,1)}(q_{n+1}|p_n^{\beta}(q_{n+1});\mu)\mathrm{d}\phi(q_{m+1}|Q) \qquad (6.35)$$

will remove the contribution given in the last line of eq. 6.33, such that effectively only Born type events are generated with a weight which is given by the Born differential cross section including basically the NLO K-factor differential in the Born degrees of freedom.

A complication arises due to the presence of the different kinematic mappings $q^{\beta}(p)$ and the need that – for practical purposes – an association of an emitted parton to an emitter parton has to be chosen in a full simulation. This association can simply be introduced by assigning additional weights accompanying each kinematic mapping. In particular, we define the aforementioned improvement by constraining the splitting kernels to satisfy

$$P_{\beta,\mathrm{eff}}^{(1,1)}(q_{n+1}|p_n^{\beta}(q_{n+1});\mu)\mathrm{d}\phi(q_{m+1}|Q) = \frac{w_{\beta}(q_{n+1}|p_n^{\beta}(q_{n+1});\mu)}{\sum_{\beta'} w_{\beta'}(q_{n+1}|p_n^{\beta'}(q_{n+1});\mu)}\mathrm{d}\sigma^{(1,1)}(q_{n+1}|Q;\mu)$$

$$(6.36)$$

for arbitrary weight functions w. Working backwards to the definition of the parton shower kernels these are then readily identified to be given by

$$P_{\beta}^{(1,1)}(q_{n+1}|p_n;\mu) = \frac{w_{\beta}(q_{n+1}|p_n;\mu)}{\sum_{\beta'} w_{\beta'}(q_{n+1}|p_n^{\beta'}(q_{n+1});\mu)}\frac{|\mathcal{M}^{(1,1)}(q_{n+1},\mu)|^2}{|\mathcal{M}^{(0,0)}(p_n,\mu)|^2} \ , \qquad (6.37)$$

i.e. being driven by the ratio of the real emission to the Born matrix element squared.

Splitting kernels of this kind, which we have motivated here by trying to simplify the matching to NLO QCD corrections, are not a new concept. Indeed, they are a well-known ingredient to almost all currently available parton shower simulations being known as 'matrix element corrections' [29–32]. To this extent, we refer to NLO matchings of this kind as 'matching with matrix element corrections', instead of referring to the POWHEG scheme, [27], which we here have reproduced in a most general way.

6.5 Is NNLO Matching Possible?

Having derived NLO matching conditions in a most general way, we will in this section investigate, if a matching to a NNLO calculation would be possible. It is indeed the calculational formalism, general matching procedure and the ability to rigorously calculate the fixed-order expansion of a parton shower prediction which enables this study and similar attempts have not been reported in the literature so far.

6.5.1 The NNLO Generating Functional

Before discussing subtraction in the context of second-order corrections and defining the NNLO cross section generating functional, we will here introduce the contributions to be considered besides the ones already present for NLO corrections:

- The interference of two-loop amplitudes with the Born amplitude, and the modulus squared of one-loop amplitudes,

$$\mathrm{d}\sigma^{(2,0)}(p_n|Q,\mu)$$

  containing poles of order ϵ^{-4} through ϵ^{-1},

- the interference of one-loop amplitudes along with an additional parton and the corresponding tree-level amplitudes,

$$\mathrm{d}\sigma^{(2,1)}(q_{n+1}|Q,\mu)$$

  containing poles of order ϵ^{-2}, ϵ^{-1} and divergences if the additional parton becomes unresolved, *i.e.* either soft or collinear to another parton, and

- the tree-level amplitudes squared for emission of two additional partons,

$$\mathrm{d}\sigma^{(2,2)}(q_{n+2}|Q,\mu)$$

containing divergences in single-unresolved limits, as well as divergences in double-unresolved limits, *i.e.* whenever two partons are emitted collinear to another parton, collinear to different partons, if one parton becomes soft in combination with the other being emitted collinear, or if both partons are soft. All these divergences have been classified and extracted *e.g.* in [33].

As opposed to the NLO case, there is no general algorithm on how subtraction at NNLO is to be carried out. Developments towards such a general recipe are however ongoing [34, 35], and proposed schemes have been shown to work in practise for few selected processes [36, 37]. The general structure of any subtraction scheme will however be dictated by the singularity structure outlined before. In particular, subtraction terms will be needed for

- The singularities associated to double unresolved parton emission present in the double-real emission contribution $d\sigma^{(2,2)}(q_{n+2}|Q,\mu)$,

$$d\sigma_{AA}^{(2,2)}(q_{n+2}|Q;\mu) = \bar{\alpha}_s^2 D^{(2,2|2)}(p_n|q_{n+2};\mu)d\phi(q_{n+2}|Q) , \qquad (6.38)$$

mapping back to Born-type kinematics. Note that this is a sum of subtraction terms for genuine double unresolved singularities, and products of two single unresolved singularities.

- The singularities associated to single-unresolved parton emission present in the double-real emission contribution $d\sigma^{(2,2)}(q_{n+2}|Q,\mu)$,

$$d\sigma_A^{(2,2)}(q_{n+2}|Q;\mu) = \bar{\alpha}_s^2 D^{(2,2|1)}(q_{n+1}|q_{n+2};\mu)d\phi(q_{n+2}|Q) , \qquad (6.39)$$

mapping back to the configuration with one additional parton. This subtraction term can actually be chosen to be the same as entering the NLO corrections to the process at hand including an additional jet. It thereby cancels the ϵ-poles present in $d\sigma^{(2,1)}$, requiring a subtraction term for

- the single-unresolved parton singularities present in the ϵ-finite remainder of the subtracted interference of one-loop and tree-level single real-emission amplitudes $d\sigma^{(2,1)}(q_{n+1}|Q,\mu) + D^{(2,2|1)}(q_{n+1}|q_{n+2};\mu)d\phi(q_{n+2}|Q)$,

$$d\sigma_{AV}^{(2,1)}(q_{n+1}|Q,\mu) = \bar{\alpha}_s^2 D^{(2,1|1)}(p_n|q_{n+1};\mu)d\phi(q_{n+1}|Q) , \qquad (6.40)$$

mapping back to Born-type configurations.

The generating functional for cross sections at NNLO thus takes the form

$$
\begin{aligned}
\sigma_{\text{NNLO}}(Q,\mu)[u] = {} & \sigma_{\text{NLO}}(Q,\mu)[u] \\
& + \bar{\alpha}_s^2 \int u(p_n) \left(\mathrm{d}\sigma^{(2,0)}(p_n|Q,\mu) \right. \\
& \qquad + D^{(2,2|2)}(p_n|q_{n+2};\mu)\mathrm{d}\phi(q_{n+2}|Q) \\
& \qquad + D^{(2,1|1)}(p_n|q_{n+1};\mu)\mathrm{d}\phi(q_{n+1}|Q)) \big|_{\epsilon=0} \\
& + \bar{\alpha}_s^2 \int \left(\left(u(q_{n+1})\mathrm{d}\sigma^{(2,1)}(q_{n+1}|Q,\mu) \right. \right. \\
& \qquad + u(q_{n+1})D^{(2,2|1)}(q_{n+1}|q_{n+2};\mu)\mathrm{d}\phi(q_{n+2}|Q)) \big|_{\epsilon=0} \\
& \qquad - u(p_n)D^{(2,1|1)}(p_n|q_{n+1};\mu)\mathrm{d}\phi(q_{n+1}|Q)) \\
& + \bar{\alpha}_s^2 \int \left(u(q_{n+1})\mathrm{d}\sigma^{(2,2)}(q_{n+2}|Q,\mu) \right. \\
& \qquad - u(q_{n+1})D^{(2,2|1)}(q_{n+1}|q_{n+2};\mu)\mathrm{d}\phi(q_{n+2}|Q) \\
& \qquad - u(p_n)D^{(2,2|2)}(p_n|q_{n+2};\mu)\mathrm{d}\phi(q_{n+2}|Q)) \ .
\end{aligned}
\tag{6.41}
$$

6.5.2 Structure of the Matched Generating Functional

In order to obtain the double counted contributions, we will need to consider the leading order cross section functional evaluated with the expansion of Z up to $Z^{(2)}$, as well as the NLO generating functional evaluated with the expansion up to $Z^{(1)}$. Similarly to $Z^{(1)}$, the contributions in $Z^{(2)}$ appear in a form, which allows to remove the infrared cutoff at the cost of introducing a power correction. The matched generating functional finally takes the form

$$
\begin{aligned}
\sigma_{\text{NNLO,matched}}(Q,\mu)[u] = {} & \sigma_{\text{NLO,matched}}(Q,\mu)[u] \\
& + \bar{\alpha}_s^2 \left(\sigma_{\text{NNLO,matched},0}(Q,\mu)[u] \right. \\
& \qquad + \sigma_{\text{NNLO,matched},1}(Q,\mu)[u] \\
& \qquad + \sigma_{\text{NNLO,matched},2}(Q,\mu)[u]) \ ,
\end{aligned}
\tag{6.42}
$$

where the last three contributions refer to the generation of events of Born, single, and double real emission type, respectively. The explicit expressions of the individual

contributions are given by

$$
\sigma_{\text{NNLO,matched},0}(Q,\mu)[u]
$$

$$
= \int u(p_n)\,\big(\mathrm{d}\sigma^{(2,0)}(p_n|Q,\mu) \tag{6.43}
$$

$$
+ D^{(2,2|2)}(p_n|q_{n+2};\mu)\mathrm{d}\phi(q_{n+2}|Q)
$$

$$
+ D^{(2,1|1)}(p_n|q_{n+1};\mu)\mathrm{d}\phi(q_{n+1}|Q))\big|_{\epsilon=0}
$$

$$
+ \int_0^t \mathrm{d}\tau \int u(p_n)\bar{P}^{(1,1)}(q_{n+1}|p_n,\tau) \tag{6.44}
$$

$$
\times \big(\mathrm{d}\sigma^{(1,0)}(p_n|Q,\mu)
$$

$$
+ \int D^{(1,1)}(p_n|k_{n+1},\mu)\mathrm{d}\phi(k_{n+1}|Q)\big)\Big|_{\epsilon=0}\mathrm{d}\phi(q_{n+1})
$$

$$
- \int_0^t \mathrm{d}\tau \int u(p_n)\bar{P}^{(1,1)}(q_{n+1}|p_n,\tau) \tag{6.45}
$$

$$
\times \left(\int D^{(1,1)}(p_n|k_{n+1},\mu)\mathrm{d}\phi(k_{n+1}|Q)\right.
$$

$$
\left. + \int_0^\tau \mathrm{d}\tau' \int \bar{P}^{(1,1)}(k_{n+1}|p_n,\tau')\mathrm{d}\phi(k_{n+1})\mathrm{d}\sigma^{(0,0)}(p_n|Q,\mu)\right)\mathrm{d}\phi(q_{n+1})
$$

$$
+ \int u(p_n)\left(\int_0^t \mathrm{d}\tau \bar{P}^{(2,1)}(q_{n+1}|p_n,\tau)\mathrm{d}\phi(q_{n+1})\mathrm{d}\sigma^{(0,0)}(p_n|Q,\mu)\right. \tag{6.46}
$$

$$
\left. - D^{(2,1|1)}(p_n|q_{n+1},\mu)\mathrm{d}\phi(q_{n+1}|Q)\right)
$$

$$
+ \int u(p_n)\left(\int_0^t \mathrm{d}\tau \bar{P}^{(2,2)}(q_{n+2}|p_n,\tau)\mathrm{d}\phi(q_{n+2})\mathrm{d}\sigma^{(0,0)}(p_n|Q,\mu)\right. \tag{6.47}
$$

$$
\left. - D^{(2,2|2)}(p_n|q_{n+2},\mu)\mathrm{d}\phi(q_{n+2}|Q)\right)\ ,
$$

$$\sigma_{\text{NNLO,matched,1}}(Q,\mu)[u]$$

$$= \int u(q_{n+1}) \left(\mathrm{d}\sigma^{(2,1)}(q_{n+1}|Q,\mu) + D^{(2,2|1)}(q_{n+1}|q_{n+2},\mu)\mathrm{d}\phi(q_{n+2}|Q)) \right)\Big|_{\epsilon=0} \tag{6.48}$$

$$- \int_0^t \mathrm{d}\tau \int u(q_{n+1}) \bar{P}^{(1,1)}(q_{n+1}|p_n,\tau) \tag{6.49}$$

$$\times \left(\mathrm{d}\sigma^{(1,0)}(p_n|Q) + \int D^{(1,1)}(p_n|k_{n+1},\mu)\mathrm{d}\phi(k_{n+1}|Q) \right)\Big|_{\epsilon=0} \mathrm{d}\phi(q_{n+1})$$

$$+ \int_0^t \mathrm{d}\tau \int u(q_{n+1}) \left(\bar{P}^{(1,1)}(q_{n+1}|p_n,\tau) \int D^{(1,1)}(p_n|k_{n+1},\mu)\mathrm{d}\phi(k_{n+1}|Q) \right. \tag{6.50}$$

$$\left. + \int_0^\tau \mathrm{d}\tau' \int \bar{P}^{(1,1)}(k_{n+1}|p_n,\tau)\bar{P}^{(1,1)}(q_{n+1}|p_n,\tau')\mathrm{d}\phi(k_{n+1}) \right)$$

$$\times \mathrm{d}\phi(q_{n+1})\mathrm{d}\sigma^{(0,0)}(p_n|Q,\mu)$$

$$+ \int_0^t \mathrm{d}\tau \int u(q_{n+1}) \left(\bar{P}^{(1,1)}(q_{n+1}|p_n,\tau) \int_0^\tau \mathrm{d}\tau' \int \bar{P}^{(1,1)}(k_{n+2}|q_{n+1},\tau')\mathrm{d}\phi(k_{n+2}) \right. \tag{6.51}$$

$$\left. - \bar{P}^{(2,1)}(q_{n+1}|p_n,\tau) \right) \mathrm{d}\phi(q_{n+1})\mathrm{d}\sigma^{(0,0)}(p_n|Q)$$

$$+ \int u(q_{n+1}) \left(\int_0^t \mathrm{d}\tau \bar{P}^{(1,1)}(q_{n+2}|q_{n+1},\tau)\mathrm{d}\sigma^{(1,1)}(q_{n+1}|Q)\mathrm{d}\phi(q_{n+2}) \right. \tag{6.52}$$

$$\left. - D^{(2,2|1)}(q_{n+1}|q_{n+2},\mu)\mathrm{d}\phi(q_{n+2}|Q) \right) \ ,$$

and

$$\sigma_{\text{NNLO,matched,2}}(Q,\mu)[u]$$

$$= \int u(q_{n+2}) \left(\mathrm{d}\sigma^{(2,2)}(q_{n+2}|Q) \right. \tag{6.53}$$

$$- \int_0^t \mathrm{d}\tau \bar{P}^{(2,2)}(q_{n+2}|p_n,\tau)\mathrm{d}\sigma^{(0,0)}(p_n|Q)\mathrm{d}\phi(q_{n+2})$$

$$\left. - \int_0^t \mathrm{d}\tau \bar{P}^{(1,1)}(q_{n+2}|q_{n+1},\tau)\mathrm{d}\sigma^{(1,1)}(q_{n+1}|Q)\mathrm{d}\phi(q_{n+2}) \right) \ .$$

These equations provide the 'master formula' for NNLO matching, which is possible, if the individual contributions corresponding to generation of Born, single and double real emission events can separately be rendered finite. Note that the divergence structure of $P^{(1,1)}(q_{n+1}|p_n,t)$ is fixed by the NLO matching as outlined in the previous section. The finiteness of eq. 6.53 requires that $P^{(1,1)}(q_{n+2}|q_{n+1},t)$ is of the same kind for the process involving an additional parton emission, along with $P^{(2,2)}(q_{n+1}|p_n,t)$ being constrained to contain the singularities originating from double unresolved parton emission. This implies that eqs. 6.47 and 6.52 represent finite contributions as well. The subtracted two-loop virtual part, eq. 6.43 is finite by definition. It therefore remains to prove that the other contribution can also be rendered finite.

We will first analyse terms 6.48 and 6.49. These contributions are free of poles in ϵ, though separately divergent for a single unresolved parton. Note however that the second contribution subtracts precisely the divergences originating from diagrams, where the unresolved emission vertex is a tree-level object. The remaining divergences in the sum of eqs. 6.48 and 6.49 thus stem from diagrams, where one of the external partons attached to an unresolved splitting vertex is at the same time an external leg of the loop integral. Since these contributions factor in the singular limits as well, see *e.g.* [38], part of the splitting kernel $P^{(2,1)}$ in $\bar{P}^{(2,1)}$ can be chosen accordingly to obtain a finite contribution from terms 6.48 and 6.49.

Provided that the convolution of the Born cross section and the first line in term 6.50 can be rewritten as a convolution of the same form as in the second line of term 6.50, this contribution can, along with the first term in contribution 6.51 be absorbed into the final definition of $P^{(2,1)}$ and the scale choice of the running coupling. Since now $\sigma_{\text{NNLO,matched,2}}(Q,\mu)[u]$ and $\sigma_{\text{NNLO,matched,1}}(Q,\mu)[u]$ are independently finite, $\sigma_{\text{NNLO,matched,0}}(Q,\mu)[u]$ will be finite as well owing to a finite total cross section.

This shows that NNLO matching should in principle be possible. The study of a detailed setup with definite choices of splitting kernels is however beyond the scope of this section but may be subject to future work.

6.6 Conclusions

In this chapter, making use of the formalism defined in chapter 4, we have set up the theoretical framework for combining parton showers and higher order QCD corrections. The advantage of this general treatment is the possibility for precise calculations of fixed-order expansions of a parton shower, which is the only ingredient required to derive the matching conditions on the level of generating functionals introduced for fixed-order cross sections.

The contributions to these generating functionals can directly be interpreted in terms of events to be generated by a Monte Carlo implementation associated with finite weights obtained from the perturbative contributions.

After re-deriving the NLO matching schemes proposed so far in a most general way – in particular independent of the choice of parton shower kernels and subtraction scheme – the possibilities of combining NNLO QCD corrections and parton showers have been evaluated. NNLO matching has been shown to be possible, though any implementation seems to be out of reach at the moment, owing to the lack of a general subtraction scheme.

7 Monte Carlo Methods

7.1 Overview

For a complete simulation of the complex final states as implemented in the dipole shower and matching algorithms to be introduced in chapters 8 and 9, efficient Monte Carlo methods are mandatory. In particular, owing to the number of variables typical probability densities (*i.e.* differential cross sections or splitting kernels) depend on, and the fact that these are usually only known through a numerical implementation with small or no knowledge on their analytical properties, standard approaches to sample random variates according to a given density are not suitable.

For the case of just sampling according to a given density directly, two similar approaches of generating unweighted events 'on the fly' are known and implemented in computer programs [39, 40]. These approaches have mainly motivated the work described here. The main purpose of the development outlined in the next section is however to have a similar level of self-adapting and automatic sampling for a Sudakov-type density associated to a density yet only known through a function call and depending on probably a large number of variables. It is this functionality which finally enables the implementation of automatic matrix element corrections and it is used to generate splittings in the parton shower evolution as well.

The resulting software library, called exsample (for *ex*ponential *sample*r), is capable of doing standard sampling, as well as Sudakov-type sampling and is documented in detail in appendix A.

7.2 Standard Sampling

In the context fixed-order calculations implemented using Monte Carlo methods, one is at first interested in obtaining the integral of a differential cross section. Events to enter histograms for observables are the points being generated to evaluate the differential cross section accompanied by a weight given by the evaluated differential cross section. We will call these weighted events. In performing realistic event simulations, besides knowing the cross section for a given process, the main interest is in obtaining an event sample where the relative occurrence of individual events reflects the properties of the differential cross section, with an equal weight per event which is usually taken to be a unit weight.

The procedure to transform a sample of weighted into such a sample of unweighted events is usually being performed by the most simple form of von Neumann's veto algorithm: First, the maximum of the event weights is determined, and out of the weighted events events are accepted with a probability given by the event weight divided by the maximum event weight. This procedure can however be (and typically is) very inefficient. One may think of instead processing weighted events through the successive parton shower simulation. Owing to the complexity of the parton shower simulation and all connected non-perturbative models this is as well not feasible given the fact that for satisfactory Monte Carlo uncertainties one usually needs a much larger number of weighted than unweighted events.

In a more refined version, being the general version of von Neumann's veto algorithm, one tries to determine an overestimate to the probability density to be sampled. Proposal events are then drawn from this overestimate and accepted with probability given by the true density to its overestimate. This method is obviously more efficient, the closer the overestimate resembles the properties of the target density. In the context of Monte Carlo integration, this procedure will reduce the variance of the integral's estimate, if the proposal points are used to obtain an average of the integrand.

When dealing with higher-order corrections, some contributions to a differential cross section, such as a subtracted real emission, may turn out not to be positive definite. A probabilistic interpretation is thus not directly possible anymore. One can however consistently include such effects by assigning accordingly a negative weight to points where the 'density' turns negative, the absolute value of which will be subtracted from the contents of the corresponding histogram bin. Given an overestimate to the 'densities' absolute value, the unweighting procedure now uses the ratio of the absolute value to this overestimate as acceptance probability, and unweighted events have weights ± 1. Any differential quantity – being always positive, negative or of indefinite sign – thus determines a probability density in a generalised sense, and we will from now on generically use the term density without quotation marks.

Up to the precise way on how the overestimate is determined and how proposal events are generated accordingly, this standard algorithm for drawing samples from a density, along with obtaining the density's integral, is given in algorithm 1 and entering at the heart of the exsample implementation of standard sampling. Note that, though the algorithm formally returns a set of events, in practise it acts like a *continuous source of events*. This ability is mandatory to obtain a self-contained program package which does not need to temporarily store events, being read in by yet another independent program for further processing.

Algorithm 1 The standard sampling and integration algorithm.

---

sampleAndIntegrate(density, overestimate, N_points) {

Require: support(density) $\subseteq$ support(overestimate)
Require: overestimate(x) $\geq$ |density(x)| for all $x \in$ support(overestimate)
  norm $\leftarrow \int$ overestimate(x)dx
  $N \leftarrow 0$
  $N_\text{integral} \leftarrow 0$
  integral $\leftarrow 0$
  events $\leftarrow \{\}$
  while $N < N_\text{points}$ **do**
    repeat
      Draw $x \in$ support(overestimate) according to overestimate(x)
      overestimateWeight $\leftarrow$ overestimate(x)
      weight $\leftarrow$ density(x)
      integral $\leftarrow$ integral +weight/overestimateWeight
      $N_\text{integral} \leftarrow N_\text{integral} + 1$
      $r \leftarrow$ uniform random number on $(0, 1)$
    until $r <$ |weight|/overestimateWeight
    $N \leftarrow N + 1$
    Append $(x, \text{sign}(\text{weight}))$ to events
  end while
  integral $\leftarrow$ integral $\times$ volume(support(overestimate))/(norm $\times N_\text{integral}$)
  return integral and events
}

7.2.1 Adapting Overestimates

The standard sampling and integration algorithm outlined in the previous section will only be efficient and producing an integral estimate with a small variance, if the overestimate is very close to the absolute value of the target density. Since, in practise, little

or nothing is known about the target density except that it is available as a function call from some library, a method to obtain an overestimate from which proposal events can be drawn in a simple and efficient way is needed. One solution is to gain information on the target density by presampling it, *i.e.* evaluating it a equally distributed random points and recording the maximum in a histogram which in turn is used as the overestimate.

Several limitations of a naive implementation of this procedure are evident:

- The true maximum of the target density will only be found when using an infinite number of points to presample it. Even if a large number of points have been used for presampling, such that the obtained maxima in the histogram are reasonably close to the true maximum, there is no guarantee that in the procedure of generating events a maximum exceeding the recorded one will be found. In this case the unweighting procedure is ill defined since the unweighting probability thus calculated will be larger than one. The points used for presampling will also at most be available for a very inaccurate calculation of the integral estimate, since they are uniformly distributed in each bin of the histogram. The next section will address in more detail the problems mentioned here.

- For densities depending on many parameters, setting up a truly d-dimensional histogram (for d parameters) will not be feasible owing to the memory required to store this information, and sampling from such a histogram will then also become a computationally expensive procedure. A potential solution would be an approach similar to the VEGAS Monte Carlo integration program [41], recording the maximum of projections of the density per parameter dimension and using the product of the histograms obtained to define the proposal density. The overestimate obtained in each individual bin may however be far off the true maximum value in the considered bin, thereby rendering the unweighting procedure inefficient again. As will be shown in the next section, these bins will have to be equipped with an additional counter to properly include newly encountered maxima exceeding the original recorded ones, giving rise to the memory problems already mentioned.

To overcome the problems inherent to a naive implementation, exsample implements a mechanism of a histogram-type overestimate function, which is iteratively adapted to the target density in a way that a higher 'bin' density is present, where the target density's variance is larger than in regions where it may be considered flat. The structure of this histogram-type overestimate is also chosen in a way that a fast sampling of it is feasible.

More precisely, exsample makes use of 'cells', which represent a sub-hypercube of the volume where events are to be sampled in. Cells are organised in a binary tree, each cell having either two or no children, in the latter case terminating the tree at this branch. The union of the two hypercubes U_b and U_c represented by the two children cells $c_{b,c}$ always equals the hypercube $U_{(bc)}$ represented by the parent cell $c_{(bc)}$. Each

cell c contains the maximum of the target density encountered by a presampling as its value w_c, and the leaf cells of the tree, constituting a certain fractal-type partition of the sampling volume into hypercubes define the overestimate function,

$$\text{overestimate}(x) = \sum_{\text{leaf cells } c} w_c \, \theta(x \in U_c) \; . \tag{7.1}$$

Each parent cell keeps track of the integrals $I_{c,b} = w_{c,b}\text{volume}(U_{b,c})$ of its children cells. This allows for an efficient sampling of the overestimate function, as given in algorithm 2. The root cell of the tree spans the whole sampling volume and is the only cell present at the initial stage of the algorithm. Children cells are produced in an adaption step, iteratively building up the cell tree through splitting a cell into two children cells and aiming at improving the algorithm's efficiency along with gaining more detailed information on the target density, *i.e.* a more fine-grained overestimate closer to it.

In order to achieve this, each cell always monitors its efficiency. In the current implementation, this efficiency is taken to be the unweighting efficiency, *i.e.* the ratio of accepted to attempted events in the unweighting step of the standard sampling algorithm. If this efficiency drops below a user-supplied threshold, the cell is considered 'bad'. With a frequency increasing from a user-supplied start value along the successive generation of events and on encounter of a bad cell, a potential splitting of the cell is determined to increase the efficiency of the algorithm.[1]

To obtain an optimal hyper-plane along which the cell should be split, each cell histograms projections of the average target density value onto each variable dimension i, $\langle\text{density}(x)\rangle_i$. The dimension k orthogonal to this hyperplane, and the split point x_k defined by the intersection of the hyperplane and this direction are determined to maximise a 'gain' measure, defined as

$$\text{gain}_k(x_k) = \frac{\left| \int_{x_k^-}^{x_k} \langle\text{density}(x)\rangle_k \mathrm{d}x - \int_{x_k}^{x_k^+} \langle\text{density}(x)\rangle_k \mathrm{d}x \right|}{\int_{x_k^-}^{x_k^+} \langle\text{density}(x)\rangle_k \mathrm{d}x} \; , \tag{7.2}$$

where $x_k^{\pm}$ denote the cell's boundaries in the variable x_k. Again, a user-supplied parameter can steer the behaviour of the adaption by considering only those splits to be worth performed, if the gain exceeds some value. In practical purposes it turned out to be sufficient that the histogram recording the average of the target density consists of two bins only and splits are always being performed at the midpoint of a cell's extension in some variable dimension. The general implementation has thus been removed from the final version for performance considerations.

Out of the two children cells the target density is being presampled in that cell which did not contain the maximum point used before to get a new estimate of the maximum.

---

[1]The introduction of this frequency is necessary to avoid too many split determinations and to let newly created cells accumulate information on the function with sufficient statistics.

The number of presampling points per cell is another user-defined parameter. The choice of this parameter has to be carried out in view of the compensation procedure to be defined in the next section with a trade-off between the time needed for presampling and the time lost by the number of events to be vetoed by the compensation procedure. There is no general rule on how it is to be determined. Experience gained so far show that few thousand presampling points are an acceptable compromise.

7.2.2 Compensating for Erroneous Overestimates

Since the true maximum of the target density can never be determined with probability one from the presampling procedure, care has to be taken on what constraints need to be imposed on the sampling procedure once a point has been encountered exceeding the currently used maximum. For a sufficiently large number of presampling points one may reside on the statement that these points are rare and generated distributions will not show any effect on the erroneous overestimate. Thinking about the overall efficiency of the algorithm in performing its function of acting as a continuous source of unweighted events with the smallest possible overhead, this is certainly not a criterion to base an implementation on.

To define the method of compensation, we first introduce the notion of missing events in a given cell. As for the cell's integral, each parent cell carries the sum of the missing events of its children cells. The number of missing events is not limited to be positive. In case it is positive, the corresponding cell needs to be oversampled, *i.e.* the algorithm is forced to sample events in cells with a positive number of missing events, lowering this number in the selected cell if it is larger than zero. Oversampling is imposed on the algorithm as long as there are cells with a positive count of missing events. Conversely, if the missing event count is negative, a cell needs to be undersampled. If such a cell is selected, its missing event count is increased, if it is smaller than zero and the selection is vetoed, triggering a new cell selection. The complete cell selection algorithm is formally given in algorithm 2.

Upon encounter of a new maximum $w'_c > w_c$, the number of missing events associated to this change is calculated for each cell as

$$N_c^{\text{miss}} = N_c \left(\frac{p'_c}{p_c} - 1 \right) \ . \tag{7.3}$$

Here, N_c is the number of proposal events already generated in the cell, and p_c (p'_c) denotes the probability to select cell c using the old (new) overestimate value. This number is then added to each cell's current missing event count. Note that undersampling, $N_c^{\text{miss}} < 0$ appears in the cells not containing the newly encountered maximum owing to the change in normalisation of the overestimate density. Eq. 7.3 ensures that within the currently accumulated statistics proposal events are always distributed according to the last encountered maximum, provided the algorithm has been stopped in a

state where it is not anymore forced to perform over- or undersamplings. This is evident by rewriting eq. 7.3 as

$$N_c^{\text{miss}} = \frac{N_c}{\langle N \rangle_c} \left(\langle N' \rangle_c - \langle N \rangle_c \right) \tag{7.4}$$

where $\langle N \rangle_c = N p_c$ ($\langle N' \rangle_c = N p'_c$) is the number of expected events in cell c for the total number of generated events, N. The difference in brackets is the number of missing events in the absence of fluctuations due to a finite number of generated events, and the factor in front of it takes into account the currently accumulated statistics, *i.e.* how much the population of the cell differs from its expected population.

Algorithm 2 The compensating cell selection algorithm. Once a cell has been selected an event is generated inside its volume with uniform density.

---

selectCell() {

  cell ← root cell

  while cell is not a leaf **do**

    if $N_{\text{miss}}(\text{firstChild(cell)}) > 0 \wedge N_{\text{miss}}(\text{secondChild(cell)}) \leq 0$ **then**

      cell ← firstChild(cell)

    else if $N_{\text{miss}}(\text{firstChild(cell)}) \leq 0 \wedge N_{\text{miss}}(\text{secondChild(cell)}) > 0$ **then**

      cell ← secondChild(cell)

    else

      r ← uniform random number on $(0, 1)$

      if $r <$ integral(firstChild(cell))/integral(cell) **then**

        cell ← firstChild(cell)

      else

        cell ← secondChild(cell)

      end if

    end if

  end while

  if $N_{\text{miss}}(\text{cell}) > 0$ **then**

    $N_{\text{miss}}(\text{cell}) \leftarrow N_{\text{miss}}(\text{cell}) - 1$

  else if $N_{\text{miss}}(\text{cell}) < 0$ **then**

    $N_{\text{miss}}(\text{cell}) \leftarrow N_{\text{miss}}(\text{cell}) + 1$

    cell ← **selectCell**()

  end if

  return cell

}

7.3 Sudakov-type Distributions

In sampling splittings during the parton shower evolution, including the matrix element corrections entering for the POWHEG-type NLO matching, drawing random variates from Sudakov-type distributions is the main Monte Carlo method needed. These distributions (which we will call just Sudakov distributions from now on) are defined given a family of 'kernel' densities f depending on a number of parameters $\{\xi\}$, an evolution variable x and d further variables $\vec{z}$ constituting the variables $(x, \vec{z})$ to be sampled, as functionals of the density f,

$$\mathrm{dSudakov}[f](x|y, \vec{z}, \{\xi\}) \equiv \theta(y - x) f(x, \vec{z}, \{\xi\}) \Delta[f](x|y) \mathrm{d}t \mathrm{d}^d z \equiv$$

$$\theta(y - x) f(x, \vec{z}, \{\xi\}) \exp\left(-\int_x^y \mathrm{d}t \int \mathrm{d}^d w f(t, \vec{w}, \{\xi\})\right) \mathrm{d}t \mathrm{d}^d z . \quad (7.5)$$

The standard way of sampling these densities is known in the literature, see *e.g.* [29,42], as the Sudakov veto algorithm and formalised in algorithm 3, making use of a Sudakov distribution calculated from an overestimate to the kernel density. Note that in the form quoted in the literature, the algorithm is not guaranteed to terminate and in practise a lower cut on the evolution variable (*i.e.* the parton shower's infrared cutoff) has to be imposed, being determined in this abstract form as the maximum value of the evolution variable x below which f is always zero. Upon selection of a scale below this cut, the algorithm terminates in an error state (indicating in practise that radiation above the infrared cutoff has not been selected). This condition will be met in a finite number of rejection steps, since the algorithm keeps on selecting lower and lower values of the evolution variable after each rejection step.

The cell-tree overestimates introduced for the standard sampling are ideally suited to implement this algorithm in an adaptive way which does not require analytic knowledge of the kernel density. The integral entering the exponent of the proposal Sudakov distribution can easily be calculated from the cell-tree overestimate and is then recorded as a linear interpolation which is easily inverted to sample the next value of the evolution variable. The number of missing events is now calculated with respect to the proposal Sudakov density, and the efficiency measure is evaluated as the acceptance efficiency of the overall algorithm and not only the sampling of the additional parameters $\vec{z}$.

The major obstacle in generalising the standard sampling to the case of sampling Sudakov densities is that functionality is required to sample a proposal event given that a set of parameters (in this case the selected value of the evolution variable and the other parameters $\{\xi\}$) has been fixed. Consequently, the number of missing events should also be available in dependence of any parameter point. exsample's cell trees provide the possibility of determining the sub tree of cells containing the parameter point and calculating unique hash values for each possible sub tree. Sampling of random

---

Algorithm 3 The Sudakov veto algorithm.

---

sampleSudakov$(y, \{\xi\}$, density, overestimate$)$ {

Require: support(density) $\subseteq$ support(overestimate)

Require: density$(\mathbf{x}) \geq 0$ for all $\mathbf{x} \in$ support(density)

Require: overestimate$(\mathbf{x}) \geq$ density$(\mathbf{x})$ for all $\mathbf{x} \equiv (x, \vec{z}, \{\xi\}) \in$ support(overestimate)

Require: $x_c = \max(x_< \in$ support(overestimate) $|$ density$(x, \cdot, \cdot) = 0 \;\forall x \leq x_<)$ known

   $r \leftarrow$ uniform random number on $(0,1)$

   if $r > \Delta[\text{overestimate}](y|x_c)$ **then**

     $x \leftarrow$ solution to $r = \Delta[\text{overestimate}](y|x)$

   else

     return below evolution cutoff

   end if

   Draw $\vec{z}$ according to overestimate$(x, \vec{z}, \{\xi\})$

   $r' \leftarrow$ uniform random number on $(0,1)$

   if $r' <$ density$(x, \vec{z}, \{\xi\})/$overestimate$(x, \vec{z}, \{\xi\})$ **then**

     return $(x, \vec{z})$

   else

     return **sampleSudakov**$(x, \{\xi\}$, density, overestimate$)$;

   end if

}

---

variates can then be constrained to take place only along the marked sub-tree for a given parameter point, and the exponent integral and number of missing events are kept track of in dependence on the hash value for a fast query of these quantities.

7.3.1 Do Splitting Kernels of Indefinite Sign Pose a Problem?

The Sudakov algorithm is limited to the case that Δ can be interpreted as a probability, taking values between zero and one. This is certainly guaranteed, if the kernel density f is always positive. Given the general standard sampling algorithm there are no limitations in making sense of Sudakov densities where f is not positive definite and the question of extending the Sudakov veto algorithm to this case may be raised.

In order to see that this is indeed possible, we shall go back to sketch the proof of the veto algorithm, dropping any dependence on parameters or other variables to be sampled: Let $g(x)$ be the overestimate to the desired kernel density $f(x)$. Then, if the algorithm performs no rejection step, the generated density is

$$\text{dVeto}^{(0)}(y|x) = \theta(y - x)\Delta[g](y|x)g(x)\frac{f(x)}{g(x)}\mathrm{d}x = \theta(y - x)\Delta[g](y|x)f(x)\mathrm{d}x \;. \quad (7.6)$$

If it did perform one rejection step, we have

$$\mathrm{dVeto}^{(1)}(y|x) =$$

$$\int_x^y \theta(y-z)\Delta[g](y|z)g(z)\left(1-\frac{f(z)}{g(z)}\right)\theta(z-x)\Delta[g](z|x)g(x)\frac{f(x)}{g(x)}\mathrm{d}x\mathrm{d}z =$$

$$\theta(y-x)\Delta[g](y|x)f(x)\left(\int_x^y(g(z)-f(z))\mathrm{d}z\right)\mathrm{d}x \ . \quad (7.7)$$

It is easy to see that this generalises to n rejection steps as

$$\mathrm{dVeto}^{(n)}(y|x) = \theta(y-x)\Delta[g](y|x)f(x)\frac{1}{n!}\left(\int_x^y(g(z)-f(z))\mathrm{d}z\right)^n\mathrm{d}x \ , \quad (7.8)$$

and summing over any number of rejection steps yields the desired result.

This proof now exhibits the two possible modifications of the algorithm to cope with non-positive definite kernel densities $f(x)$. The most simplest solution, in case of which the algorithm still produces unweighted events with weights ± 1 however requires the knowledge of the zeros of $f(x)$, an overestimate $g(x)$ with $|g(x)| \geq |f(x)|$ and $\mathrm{sign}(g(x)) = \mathrm{sign}(f(x))$, and a way to draw events from $\mathrm{dSudakov}[g](y|x)$. If all these requirements are met, then the algorithm requires no modification[2] except multiplying the event weight by the sign of the overestimate encountered in generating proposal events.

In a most general case, the above requirements for the simple algorithm cannot be satisfied. Yet still a modification exists, at the expense that the algorithm will now produce events with unit positive or negative weights and non-unit weights. It requires the knowledge of an overestimate to the modulus of the kernel density, $g(x) > |f(x)|$ (note that a strictly larger overestimate is required). Proposal events are drawn from $\mathrm{dSudakov}[g](y|x)$ without any conceptual problem, since now $g(x) > 0$. Proposal events are accepted with probability $|f(x)|/g(x)$, which is well defined in this case, and the event weight is multiplied by the following prescription:

- If a proposal event x is rejected, multiply the event weight by

$$w_{\mathrm{reject}} = \begin{cases} 1 & : f(x) \geq 0 \\ \frac{g(x)-f(x)}{g(x)-|f(x)|} & : f(x) < 0 \end{cases} \ . \quad (7.9)$$

- If a proposal event x is accepted, multiply the event weight by

$$w_{\mathrm{accept}} = \mathrm{sign}(f(x)) \ . \quad (7.10)$$

Note that the fraction of events with weights $|w| \neq 1$ will be smaller, the closer $g(x)$ gets to $|f(x)|$.

In both proposed modifications, the proof again condenses to the fact that the density generated after n rejection steps is the desired one given in eq. 7.8.

---

[2]Note that in this case $f(x)/g(x)$ is always a probability.

7.4 Exsample in Use

The exsample library implementing the adaptive sampling algorithms as outlined in the previous sections has been tested with various densities. In this section, we will show few mostly simple examples to show the basic features of exsample and prove its functionality. Cross-checks for more complicated setups are also given in appendix D.

To begin with, we consider sampling of a two-dimensional Gaussian density aligned on a diagonal of the sampling volume. Such densities are known to produce problems to adaption algorithms based on purely projecting the density to the axes, as *e.g.* done in the VEGAS algorithm. Figure 7.1 shows the sampling results, validated against a numerical integration. The cell grid produced by exsample's adaption algorithm is clearly seen to well capture the structure of the integrand beyond what would be visible in projecting it to either axis.

Figure 7.2 shows the results obtained by the adaptive Sudakov veto algorithm, using a kernel density showing the generic behaviour of a QCD splitting function with running α_s,

$$f(\kappa, z) = \frac{1}{\kappa(1-z)} \frac{1}{\beta \ln(\kappa/\lambda)} \theta(\kappa - \mu)\theta(z - \kappa) \ , \qquad (7.11)$$

where κ is taken to be the evolution variable (similar to the $p_\perp$ of the branching) and z is similar to a momentum fraction. $\mu > \lambda$ is an infrared cutoff. β and λ correspond to the zero'th β-function coefficient and the QCD scale, respectively. Again, perfect agreement with a numerical integration is found. In addition, figure 7.3 shows the functionality of the compensation procedure by comparing results for the same distribution but different numbers of presampling points used in the algorithm, which are all consistent with each other.

In order to further test exsample's capabilities in adapting integrands in high-dimensional integration volumes, a 'stress test' has been performed using QCD antennae. For a dipole being formed by partons of momenta p and $\bar{p}$, the QCD antenna for emitting n soft gluons is given by

$$\text{antenna}(p, \bar{p}, q_1, ..., q_n) = \sum_{\sigma \in S_n} \frac{(Q^2)^n \ p \cdot \bar{p}}{p \cdot q_{\sigma(1)} \ q_{\sigma(1)} \cdot q_{\sigma(2)} \cdots q_{\sigma(n-1)} \cdot q_{\sigma(n)} \ q_{\sigma(n)} \cdot \bar{p}} \ , \qquad (7.12)$$

where $Q = p + \bar{p} + \sum_k q_k$. A cut is applied constraining all invariants to a minimum value, and the phase space is generated using the RAMBO algorithm, [43]. This setup has been chosen for various reasons. First of all, since RAMBO requires an abundant number of random numbers (four per final state momentum), the integrand scales to high dimensionality already for a small number of soft gluons. Further, RAMBO by definition does a flat phase space population, such that no dynamics present in the integrand is being mapped out. The relevant behaviour of the integrand is in addition not present in
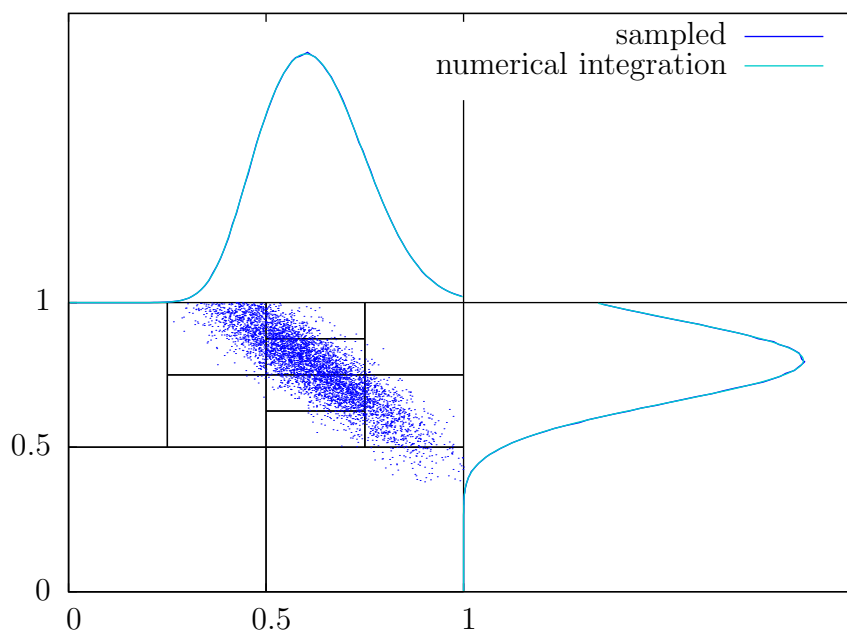
Figure 7.1: A two-dimensional Gaussian distribution sampled by exsample. The lower left box of the plot shows the plane of sampled variables $x_{1,2}$ along with few sampled events and the cell grid produced. To the top and right, projections of the generated distribution versus the result from a numerical integration are shown. Note that adaption methods based on projections (as, *e.g.* used in VEGAS) would not have been able to resolve the full structure of the density being aligned on a diagonal of the sampling volume.
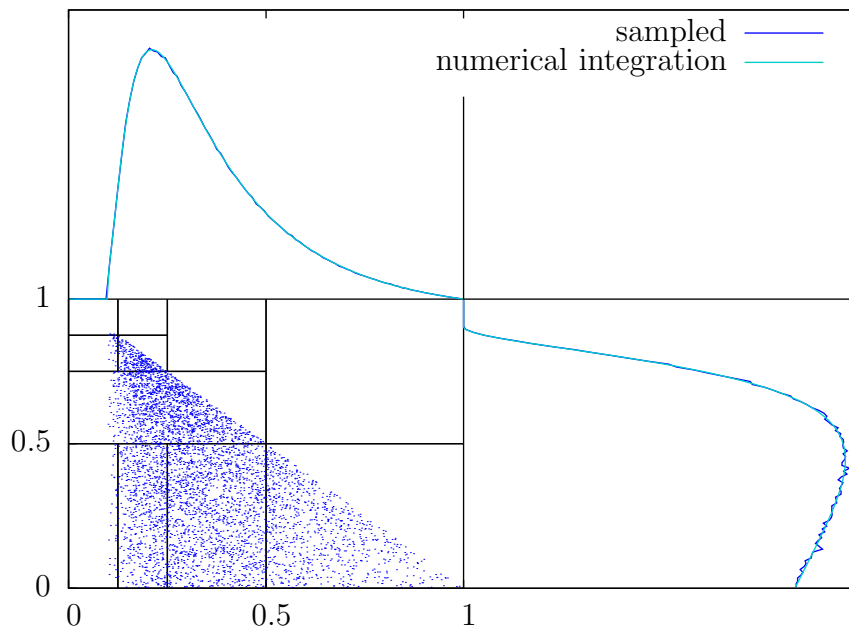
Figure 7.2: A Sudakov-type distribution with a QCD splitting function type kernel density as sampled by exsample using the adaptive Sudakov veto algorithm. The vertical axis corresponds to the evolution variable, the horizontal to a variable similar to a momentum fraction. Shown are few sampled events, projections of the generated distribution versus the result from a numerical integration, and the the cell grid produced.
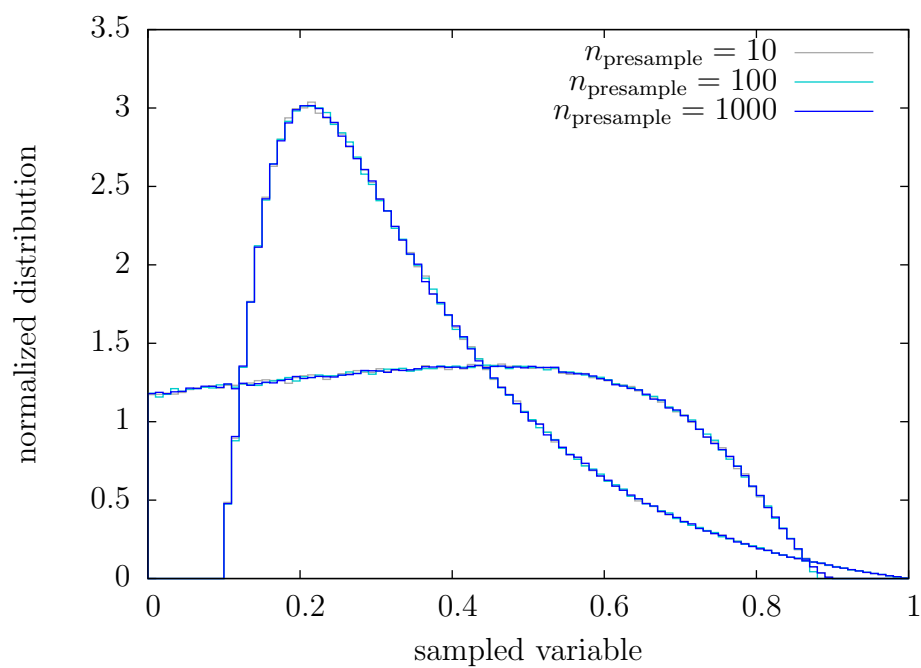
Figure 7.3: The same distributions as shown in figure 7.2, now sampled with a different number of presampling points proving functionality of the compensation procedure.

each random variable separately, but correlated between various variables. Results for three gluons, *i.e.* for 20 required random numbers, obtained from exsample are compared to results obtained from a flat Monte Carlo integration being run with 50 million events. The flat Monte Carlo approach generated a relative error of one per-mille, at the expense of an unweighting efficiency of $\epsilon = 0.00112$.

The error and unweighting efficiency obtained from running exsample are not unique as it depends on the parameters chosen for the number of presampling points, and the threshold values for the gain and efficiency measures. Errors in exsample are estimated in a very conservative way due to the dynamics present during an exsample run. In particular, each run time interval between two cell splits defines an iteration, from which an integral estimate is calculated. All estimates obtained this way are then used to calculate the final integral estimate as an average over iterations. Further, when compensating, points are not considered for integral evaluation due to the bias introduced by the compensation procedure. In general we find, that exsample leads to unweighting efficiencies[3] which are an order of magnitude better than those obtained from the flat Monte Carlo approach, though errors hardly drop below 1% for requesting 500000 unweighted events owing to the conservative way of estimating these. Within uncertainties, the integrals reported by exsample are in complete agreement with the estimate obtained from the standard Monte Carlo integration. Distributions of random numbers as obtained by exsample have been cross-checked against the ones from the standard Monte Carlo and agreement is found also here. Indeed, we find that the relative deviation from the exsample result to the high-statistics flat Monte Carlo run is in the per-mille range, which hints towards overestimated errors for exsample.

7.5 Conclusions

In this chapter advanced Monte Carlo methods have been discussed, focusing on the adaptive sampling of differential cross sections as well as an approach to draw random variates from Sudakov-type densities as encountered in the parton shower evolution or matrix element corrections as present in POWHEG-type matchings. The latter can be sampled from kernels about which no analytic information is required, thus allowing usage of complicated kernels being known only through a function call.

The adaptive sampling algorithms have been implemented in a C++ library, which is used heavily by the shower and matching implementations to be discussed in the next two chapters. Cross-checks on the functionality of the implementation have been performed including the sampling of differential cross sections requiring up to 20 random numbers without mapping out any of their dynamics.

---

[3]The unweighting efficiency in this case is defined as the ratio of generated unweighted events to the number of function evaluations needed to obtain these.

8 The Shower Algorithm in Practise

8.1 Overview

The purpose of this chapter is to describe the parton shower algorithm outlined in chapter 5, as it is implemented in the event generator Herwig++ and used for phenomenological studies as presented in chapter 10.

Section 8.2 describes the initialisation of the algorithm starting from a hard scattering process, the generation of multiple parton emissions and finalising steps, before handing over the generated event to a hadronization model. Section 8.3 will focus on technical issues for the transition to particularly the cluster hadronization model used by Herwig++. It also discusses the modelling of intrinsic transverse momentum, which is needed to obtain a complete simulation of realistic final states at hadron colliders.

8.2 The Complete Algorithm

8.2.1 A Mini-Review of Colour Flows

In order to obtain the initial conditions for the parton shower, information has to be obtained on the colour connection properties of the partons attached to the hard scattering process, at least in the large-N_c limit. Though this is a well-known technique, and facilities are implemented for all hard processes available within Herwig++ [22], we will here briefly review the notion of colour flows and how they are selected for a hard process configuration, primarily to obtain definitions to be used in subsequent sections.

The staring point is to translate all colour factors appearing in a QCD amplitude to the fundamental representation. Within this context, it turns out to be useful to normalise the $SU(N)$ generators according to

$$\text{Tr}[t^a t^b] = \delta^{ab} \tag{8.1}$$

such that the strong coupling has to be rescaled by a factor $1/\sqrt{2}$. The gluon wave functions and the colour factor of the gluon propagator are then rewritten as

$$\epsilon_a^\mu(p) = \epsilon_b^\mu(p)(t^b)^i{}_j(t^a)^j{}_i \equiv \epsilon^{\mu i}{}_j(p)(t^a)^j{}_i \qquad \delta^{ab} = (t^a)^i{}_j(t^b)^j{}_i \ , \tag{8.2}$$

and any combination of generators and structure constants can then be translated into a product of Kronecker symbols by making use of the $SU(N)$ Fierz identity,

$$(t^a)^i{}_j(t^a)^k{}_l = \delta_l^i \delta_j^k - \frac{1}{N}\delta_j^i \delta_l^k \ . \tag{8.3}$$

Here, upstairs indices correspond to the fundamental representation, or outgoing colour, whereas downstairs indices transform according to the anti-fundamental representation and are associated to outgoing anti-colour. Accordingly, a gluon carries colour and anti-colour degrees of freedom. As is evident from the Fierz identity, or from the adjoint representation property, $\mathbf{8} = \mathbf{3} \otimes \bar{\mathbf{3}} \oplus \mathbf{1}$, it cannot be regarded to be formed of an independent colour-anticolour pair. This will only be the case in the large-N limit, where the $\mathbf{1}$ contribution is absent.[1] The net result of the operations above is that any QCD amplitude can be written as

$$\mathcal{M} = \sum_{\sigma \in S_n} \delta_{\sigma(j_1)}^{i_1} \cdots \delta_{\sigma(j_n)}^{i_n} \mathcal{M}(\sigma)_{i_1 \cdots i_n}^{j_1 \cdots j_n} \ . \tag{8.4}$$

We will call each product of Kronecker symbols a *colour flow*, and $\mathcal{M}(\sigma)_{i_1 \cdots i_n}^{j_1 \cdots j_n}$ the corresponding partial amplitude. Colour flows are now simply selected with relative weights determined by the individual partial amplitudes squared. If only large-N_c contributions should be taken into account, the partial amplitudes with a relative suppression to the leading power of N_c are just dropped from this procedure, which for tree level amplitudes guarantees that the singlet contribution for any gluon is absent.

The main definitions which will be needed in the following sections are *colour connectedness* and *colour singlet* within the notion of colour flows $\delta_{\sigma(j_1)}^{i_1} \cdots \delta_{\sigma(j_n)}^{i_n}$:

$$\sigma(j_a) = j_b \quad \Leftrightarrow \quad a \text{ and } b \text{ are colour connected} \ , \tag{8.5}$$

$$\sigma(j_a) = j_b \text{ for all } a, b \in \mathcal{I} \subseteq \{1, ..., n\} \quad \Leftrightarrow \quad \mathcal{I} \text{ is a colour singlet} \ . \tag{8.6}$$

---

[1] We note that this contribution decouples for purely gluonic amplitudes owing to the antisymmetry of the three- and four-gluon vertices.

8.2.2 Starting the Shower

The parton shower will start to evolve from a hard sub-process, which we divide into a set of partons $q_m = \{\hat{q}_1, ..., \hat{q}_m\}$ and non-coloured particles $\hat{q}_{m+1}, ..., \hat{q}_n$. At this level, we do not explicitly distinguish between incoming and outgoing partons or particles, but just assume that this information is present somewhere. Further, a colour flow in the large-N_c limit as defined in the previous subsection is assumed to be assigned to the hard sub-process.

In order to start the evolution, all partons at the hard sub-process are first sorted into colour singlets C_α. Practically, this is done by making use of the fact that a colour singlet is 'simply connected' in the sense of its colour flow topology: Any parton i in C_α can be reached from a parton j in C_α by just following colour lines and changing from a colour to an anti-colour line at an external gluon. Each colour singlet is now an independently evolving entity, and can only split into two colour singlets in the presence of a $g \rightarrow q\bar{q}$ splitting.[2]

In the next step, the partons in each singlet C_α are sorted such that colour connected partons are located at neighbouring positions, when representing C_α as a sequence. Note that these sequences may be open or closed: We will call C_α open, or non-circular, if there exists a circular permutation of the elements in C_α such that the partons at the first and last position are not colour connected. Conversely, if there does not exist such a permutation, C_α is called circular or closed. Once this sorting has been accomplished, we will refer to the C_α as *dipole chains*: each pair of subsequent partons in C_α forms a dipole, which may radiate. For each parton in each dipole, a hard scale is then determined as defined in the previous chapter. The algorithm is defined in a formal way in alg. 4. Examples of dipole chains are shown in fig. 8.1.

8.2.3 Evolution of the Parton Ensemble

The main shower algorithm acts on a set of dipole chains, $\mathcal{C} = \{C_1, ..., C_n\}$, and proceeds as long as this set is non-empty. Dipole chains are removed from the list, if they stopped evolving, *i.e.* if there was no splitting selected with a $p_\perp^2$ above the shower's infrared cutoff μ_{IR}^2. The first entry in $\mathcal{C}$ is taken to be the current chain. For each dipole (i, j) in the current chain (with both possible emitter–spectator assignments, *i.e.* also considering (j, i) along with (i, j)), any possible splitting $(i, j) \rightarrow (i', k, j)$ is considered to compete with all other possible splittings of the chain. For any such splitting, given

---

[2]It is known that for some observables colour singlets cannot be regarded as evolving independently. The 'cross-talk' between two such systems is assumed to be mediated by exchanging any number of soft gluons forming a colour singlet and are implemented in so-called 'colour reconnection' models. We will not consider this possibility in this chapter. Indeed, these models are typically imposed after the parton shower evolution has terminated.
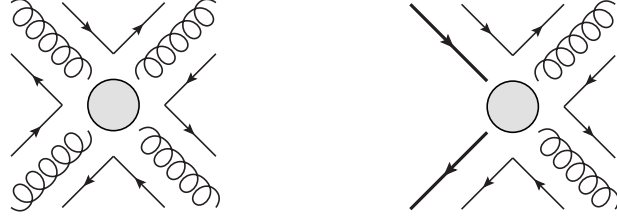
Figure 8.1: Examples of dipole chains. Thin arrowed lines indicate the colour connection properties and may directly be translated to a corresponding δ_j^i. The left figure shows a circular, the right figure a non-circular chain.

Algorithm 4 The initialisation phase of the parton shower.

---

initDipoleShower(event) {

    $\mathcal{P} \leftarrow$ find coloured particles in event

    $\mathcal{C} \leftarrow$ partition $\mathcal{P}$ into colour singlets

    for $C_k \in \mathcal{C}$ **do**

        sort C_k such that subsequent partons are colour connected

        if C_k is non-circular **then**

            shift elements in C_k such that $(C_k)_{\text{first}}$ and $(C_k)_{\text{last}}$ are colour-disconnected

        end if

        $i \leftarrow 1$

        while $i < \text{length}(C_k) \vee (i \leq \text{length}(C_k) \wedge C_k \text{ circular})$ **do**

            $j \leftarrow (i \mod \text{length}(C_k)) + 1$

            $i \leftarrow i + 1$

            $p_{\perp,i,j}^2 \leftarrow$ hard scale for emitter $\hat{q}_i$, spectator $\hat{q}_j$

            $p_{\perp,j,i}^2 \leftarrow$ hard scale for emitter $\hat{q}_j$, spectator $\hat{q}_i$

        end while

    end for

}

---

a hard scale $p_\perp^2$ associated to the emitter under consideration, a scale $q_\perp^2$ is selected with probability given by the Sudakov form factor

$$\Delta_{(i,j)\to(i',k,j)}(q_\perp^2, p_\perp^2) = \exp\left(-\int_{q_\perp^2}^{p_\perp^2} \mathrm{d}q^2 \int_{z_-(q^2)}^{z_+(q^2)} \mathrm{d}z P_{(i,j)\to(i',k,j)}(q^2, z)\right) , \qquad (8.7)$$

where $P_{(i,j)\to(i',k,j)}(q^2, z)$ is the appropriate splitting probability as defined in chapter 5, using the respective dipole splitting function $V_{i',k;j}$.

The splitting with the largest selected value of $q_\perp^2$ is then chosen to be the one to happen, except the largest $q_\perp^2$ turned out to be below the infrared cutoff. In this case the current chain is removed from the set of dipole chains, inserted into the event record and the algorithm proceeds with the next chain. The momentum fraction z is chosen to be distributed according to $\mathrm{d}P_{(i,j)\to(i',k,j)}(q^2, z)$. Since we make use of azimuthally averaged splitting kernels, the azimuthal orientation of the transverse momentum is chosen to be distributed flat.

Since the evolution factors into dipole chains as independently evolving objects, all possible emitters in the chain – after having inserted the generated splitting – now get the selected $q_\perp^2$ assigned as their hard scale, or stay at the kinematically allowed scale $p_{\perp,i,j}^2$ if $q_\perp^2 > p_{\perp,i,j}^2$. If a $g \to q\bar{q}$ splitting has been selected for a circular chain, this chain becomes non-circular. If it has been selected for an already non-circular chain, this chain breaks up into two independent chains exactly between the $q\bar{q}$-pair, owing to the colour structure of this splitting. This situation, along with non-exceptional splittings is depicted in fig. 8.2. The evolution algorithm is formally defined in alg. 5

8.2.4 Finishing the Shower

After the shower evolution has terminated, the incoming partons with momenta $p_{a,b}$ in general have non-vanishing transverse momenta with respect to the beam directions. This necessitates a realignment of the complete event encountered at this stage. Following the arguments of section 5.4, the momenta of the evolved incoming partons $p_{a,b}$ are taken to *define* the frame of the collision at hand, *i.e.* hadron momenta $\tilde{P}_{a,b}$. We then seek a Lorentz transformation to take $\tilde{P}_{a,b}$ to the externally fixed hadron momenta $P_{a,b}$, which is in turn used to realign the complete event.

To construct the momenta of the incoming hadrons $\tilde{P}_{a,b}$, we require the three-momenta of $\tilde{P}_{a,b}$ being collinear to the respective partonic three-momenta and define momentum fractions
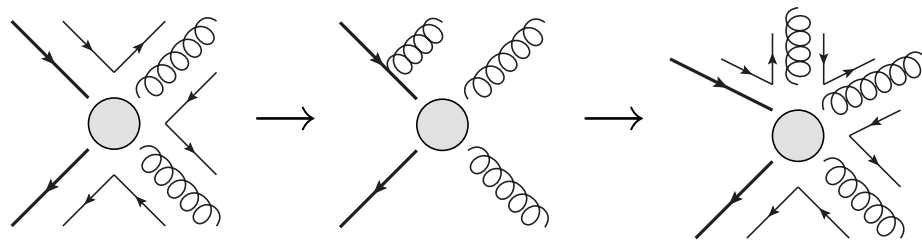
$$x_{a,b} = \frac{2\tilde{P}_{b,a} \cdot p_{a,b}}{S} . \qquad (8.8)$$

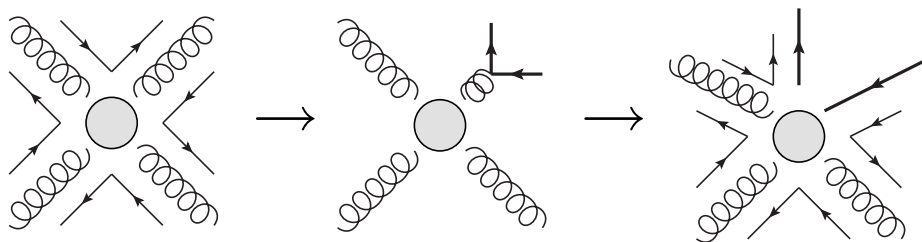The momentum fractions are further constrained by requiring that
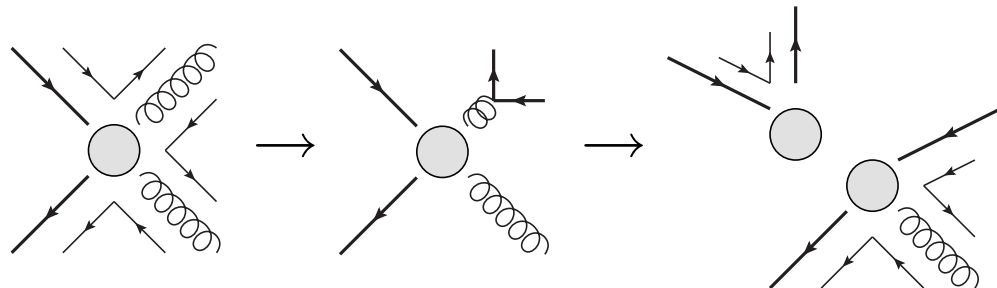
$$(\tilde{P}_a + \tilde{P}_b)^2 = S \qquad (8.9)$$
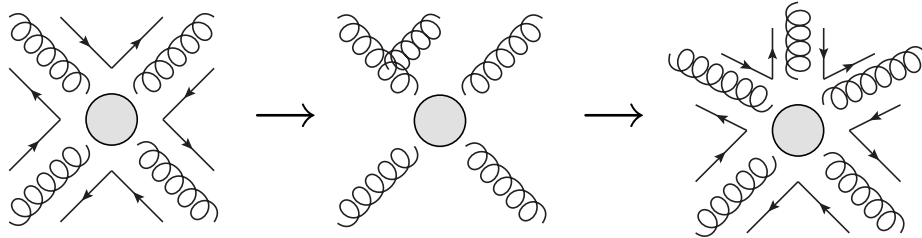
Gluon emission off a circular chain. The chain stays circular.

Gluon emission off a non-circular chain. The chain stays non-circular.

$g \to q\bar{q}$ splitting in a circular chain. The chain becomes non-circular.

$g \to q\bar{q}$ splitting in a non-circular chain, triggering breakup of the chain.

Figure 8.2: Examples of parton emission from dipole chains. In these examples always the upper dipole has been considered for emissions. Note that any dipole may split in two different ways, splitting either of its legs. These competing possibilities are not shown in the transition diagrams.

Algorithm 5 The evolution phase of the parton shower.

---

runDipoleShower$(\mathcal{C})$ {

  $\mathcal{C}_{\text{final}} \leftarrow \{\}$
  while $\mathcal{C}$ non-empty **do**
    $C \leftarrow (\mathcal{C})_{\text{first}}$
    $p_\perp^2 \leftarrow 0$, $(a, b \rightarrow a', c, b) \leftarrow$ undefined
    $i \leftarrow 1$
    while $i < \text{length}(C) \vee (i \leq \text{length}(C) \wedge C$ circular$)$ **do**
      $j \leftarrow (i \mod \text{length}(C)) + 1$, $i \leftarrow i + 1$
      for $(k, l) \leftarrow (i, j), (j, i)$ **do**
        for possible splittings $(k, l \rightarrow k', m, l)$ **do**
          select $q_\perp^2$ from $\Delta_{(k,l \rightarrow k',m,l)}(q_\perp^2, p_{\perp,i,j}^2)$
          if $q_\perp^2 > p_\perp^2$ **then**
            $p_\perp^2 \leftarrow q_\perp^2$, $(a, b \rightarrow a', c, b) \leftarrow (k, l \rightarrow k', m, l)$
          end if
        end for
      end for
    end while
    if $p_\perp^2 < \mu_{\text{IR}}^2$ **then**
      move $(\mathcal{C})_{\text{first}}$ from $\mathcal{C}$ to $\mathcal{C}_{\text{final}}$
      continue
    end if
    select z from $\mathrm{d}P_{(a,b \rightarrow a',c,b)}(p_\perp^2, z)$ and ϕ flat in $[0, 2\pi]$
    calculate momenta $\hat{q}_a$, $\hat{q}_c$, $\hat{q}_b$ from $\hat{p}_a$, $\hat{p}_b$ and $p_\perp^2, z, \phi$
    replace $\hat{p}_a$, $\hat{p}_b$ by $\hat{q}_a$, $\hat{q}_b$ and insert $\hat{q}_c$ between $\hat{q}_a$ and $\hat{q}_b$
    $i \leftarrow 1$
    while $i < \text{length}(C) \vee (i \leq \text{length}(C) \wedge (C)_{\text{first}},(C)_{\text{last}}$ colour-connected$)$ **do**
      $j \leftarrow (i \mod \text{length}(C)) + 1$, $i \leftarrow i + 1$
      $p_{\perp,i,j}^2 \leftarrow \min(p_\perp^2, p_{\perp,i,j}^2)$, $p_{\perp,j,i}^2 \leftarrow \min(p_\perp^2, p_{\perp,j,i}^2)$
    end while
    if $(a \rightarrow a', c) = (g \rightarrow q\bar{q})$ **then**
      if $(C)_{\text{first}},(C)_{\text{last}}$ colour-connected **then**
        shift elements in C such that $(C)_{\text{first}}$ and $(C)_{\text{last}}$ are colour-disconnected
      else
        move $(C)_{c,...,\text{last}}$ to C'
        append C' to $\mathcal{C}$
      end if
    end if
  end while
  return $\mathcal{C}_{\text{final}}$

}

---

where S is the centre-of-mass energy squared of the collision, such that the desired Lorentz transformation does exist.

The second constraint is in principle to be chosen in such a way as to preserve the most relevant kinematic quantity of the hard process which initiated the showering. By default, we choose this to be the rapidity of a system X, which is either the system of non-coloured particles at the hard sub-process, or the complete final state in case of a pure QCD hard scattering.

In practise, one may indeed run into numerical instabilities in the sense that the transverse components of the incoming partons are not zero after applying the realignment transformation. If this case is detected and checked to be compatible with the typical order of magnitude of these instabilities (experience shows that these are of the order of 10^{-6} GeV), the components are put to zero and a small boost is applied to the final state to correct for this change. This step is necessary in order not to cause problems for steps in the simulation downstream of the parton showering.

8.3 The Transition to the Non-Perturbative Domain

8.3.1 Using the Cluster Hadronization Model

The cluster hadronization model, originally proposed in [44], is the hadronization model used by the Herwig++ event generator. The model in its initial stage just after parton showering, performs a splitting of gluons into quark-antiquark pairs such that in the large-N_c limit a set of colour singlet clusters emerge from the event under consideration.

These clusters are then subsequently converted into hadrons, by either splitting them into clusters of lower invariant mass or performing directly the decay to meson pairs, in case another $q\bar{q}$ pair is 'popped' from the vacuum inside the cluster, or baryon pairs, where the creation of a diquark-antidiquark pair is assumed. Further details of the model will not be discussed here.

The main assumption of the model is however, that both quarks are located on their *constituent* mass shell, and gluons are as well assigned a non-vanishing constituent mass, entering as a parameter of the model. In the standard Herwig++ parton shower, acting as a $1 \to 2$ cascade, only scales and momentum fractions of the splittings are determined during the evolution, the full kinematic information being constructed after the end of the perturbative evolution. This setup thus straightforwardly allows to include the constituent masses in this particular step. Since the dipole shower preserves momentum conservation locally to each splitting, ending up with a set of massless partons, such a treatment is not possible.

The way to perform the 'reshuffling' of the massless parton momenta to their con-

stituent mass shells is chosen to be the following algorithm: Let Q_c be the total momentum of all final state partons and perform a boost Λ_c to the centre-of-mass system of Q_c, $\Lambda_c Q_c = (\hat{Q}_c, \mathbf{0})$. The boosted parton momenta p_i are now put on the constituent mass shell, including a global rescaling of their three-momenta,

$$p_i = (|\mathbf{p}_i|, \mathbf{p}_i) \rightarrow p_i' = \left(\sqrt{\xi^2 |\mathbf{p}_i|^2 + m_{c,i}^2}, \xi \mathbf{p}_i \right) \ . \tag{8.10}$$

Momentum conservation then demands ξ being a solution to

$$\hat{Q}_c = \sum_i \sqrt{\xi^2 |\mathbf{p}_i|^2 + m_{c,i}^2} \ , \tag{8.11}$$

which is obtained numerically. Finally the inverse boost Λ_c^{-1} is applied to the new parton momenta p_i'.

8.3.2 Intrinsic $p_\perp$ as an Onset of Non-Perturbative Effects

The parton shower evolution is well-defined only in the perturbative region of QCD with a strong hierarchy of scales,

$$\Lambda_{\mathrm{QCD}}^2 \ll \mu^2 \sim p_\perp^2 \ll Q^2 \ . \tag{8.12}$$

Here $p_\perp$ is the typical transverse momentum of parton shower emissions, Q^2 is a hard scale of the order of several hundreds of GeV, and μ^2 is a soft scale in the region of a few GeV. Typically, μ^2 refers to the infrared cutoff of the parton shower, below which no emissions are generated and the event is passed on to a hadronization model.

At hadron colliders, it is phenomenologically known that the parton shower dynamics alone is not capable of describing those properties of final states, which can directly be related to the generation of transverse momentum in the final state system as being build up by initial state radiation. Examples are the $p_\perp$ distributions for Drell-Yan or $\gamma + \mathrm{jet}$ events in the region of small transverse momenta.

To cure this problem, a distribution of 'intrinsic transverse momentum' carried by the partons entering the hard collision is introduced. These dynamics, taking place after the parton shower evolution has terminated, are attributed to non-perturbative dynamics in the colliding hadrons. The typical distribution is taken to be Gaussian,

$$\frac{d^2 p_\perp}{\pi \Lambda_\perp^2} \exp \left(-\frac{p_\perp^2}{2\Lambda_\perp^2} \right) \tag{8.13}$$

relating to a spatial distribution of partons inside the colliding hadrons with a width $1/\Lambda_\perp$.

For the dipole-type shower outlined previously, this model can be implemented for hadron-hadron collisions, where at the end of the evolution each incoming parton a, b

has a transverse momentum $\vec{p}_\perp^{\,a,b}$ added to its spatial momentum. Determining a boost to transform the outgoing three-momentum $\vec{Q}$ to $\vec{Q} + \vec{p}_\perp^a + \vec{p}_\perp^b$, a rescaling of the incoming parton momenta is then sufficient to restore overall energy-momentum conservation, and Lorentz invariant properties of the final state are preserved.

In collisions involving one incoming hadron only, such as DIS, or for processes where it is assumed that the QCD dynamics of partons from one and the other incoming hadron basically factorise, such as in VBF, this procedure is not applicable anymore owing to the fact that a part of the final-state system not related to the QCD dynamics of the incoming parton of interest would have to absorb part of the recoil of the intrinsic transverse momentum added to the incoming parton. [3]

A different approach, originally followed by [45], is to 'continue' the parton shower dynamics into the non-perturbative region, thereby generating intrinsic transverse momentum through successive soft parton shower emissions. This necessitates assumptions on the infrared behaviour of the strong coupling $\alpha_s(q^2)$, which will have to be regular across the Landau pole $q^2 = \Lambda^2_{QCD}$. In [45], some simple models have been introduced. We will analyse this approach in more detail here. Models using a simple modified α_s are available in the implementation of the dipole-type shower, along with the traditional method applicable for hadron-hadron collisions.

Practically, the parton shower is allowed to generate emissions down to transverse momenta of the order of the QCD scale, and we aim at modelling the *onset* of non-perturbative dynamics by modifying the parton shower dynamics in the region where

$$\Lambda^2_{\text{QCD}} \sim p_\perp^2 \ll \mu^2 \; . \tag{8.14}$$

The soft scale μ^2 now becomes a parameter, which is not related to the termination of parton shower dynamics. Note that we cannot claim to use this approach to model dynamics below the QCD scale, since there the notion of a parton is indeed of no sense anymore, while it may still be regarded valid to some extent in the domain considered here.

For soft gluon emission off an incoming parton i, the distribution of transverse momentum generated by a *single* parton shower emission when backwards evolving from a scale Q^2 can be approximated by

$$\frac{d^2 p_\perp}{2\pi} \frac{\partial}{\partial p_\perp^2} \left\{ \frac{f_{P \leftarrow i}(x, p_\perp^2)}{f_{P \leftarrow i}(x, Q^2)} \exp\left(-\int_{p_\perp^2}^{Q^2} \frac{\mathrm{d}q^2}{q^2} \frac{\alpha_s(q^2)}{2\pi} \Gamma_i(p_\perp^2, Q^2) \right) \right\} \; , \tag{8.15}$$

where Γ_i denotes the Sudakov anomalous dimension, of which we consider here only the

---

[3]In parton showers, which do not conserve energy and momentum locally at each branching, this is not a problem. Here, the intrinsic $p_\perp$ is generated as just being part of the dynamics of the last splitting encountered and hence dealt with by the so-called 'kinematic reconstruction' which determines physical momenta from the parton shower variables generated.

leading logarithmic contribution,

$$\Gamma_{q,g}(p_\perp^2, Q^2) = C_{F,A} \ln\left(\frac{Q^2}{p_\perp^2}\right) \ . \tag{8.16}$$

We are now interested in the distribution resulting in evolution from μ^2, along with modifying the parton distribution functions and the strong coupling in the 'soft' region, *i.e.* we regard this modifications to be power suppressed for scales well in the perturbative region, $p_\perp^2 \gtrsim \mu^2$.

For the parton distributions, a smooth 'freezing' may be applied by replacing $p_\perp^2 \to p_\perp^2 + \mu^2$ in the argument of the PDF in eq. 8.15. Evolving from μ^2 to $p_\perp^2 \ll \mu^2$, the $p_\perp^2$ distribution may then, up to a x-dependent normalisation, be regarded universal,

$$\mathrm{d}P_{q,g}(p_\perp^2) = \frac{d^2 p_\perp}{2\pi} \frac{\partial}{\partial p_\perp^2} \exp\left(-\int_{p_\perp^2}^{\mu^2} \frac{\mathrm{d}q^2}{q^2} \frac{C_{F,A}\tilde{\alpha}_s(q^2, \mu^2, \Lambda_{QCD}^2)}{2\pi} \ln\left(\frac{\mu^2}{q^2}\right)\right) \ . \tag{8.17}$$

Here, $\tilde{\alpha}_s(q^2, \mu^2, \Lambda_{QCD}^2)$ denotes the modified running coupling. We assume that for $q^2 < \mu^2$ the modified coupling can be expanded in terms of a power series,

$$\tilde{\alpha}_s(q^2, \mu^2, \Lambda_{\mathrm{QCD}}^2) = \sum_{k=0}^\infty c_k(\mu^2, \Lambda_{\mathrm{QCD}}^2) \left(\frac{q^2}{\mu^2}\right)^k \ . \tag{8.18}$$

Since $\tilde{\alpha}_s$ is regular across the Landau pole by definition, we can expand the exponent in the region of interest, $p_\perp^2 \sim \Lambda_{\mathrm{QCD}}^2 \ll \mu^2$. In this region, we may also approximate logarithms in $p_\perp^2/\mu^2$ by logarithms in $\Lambda_{\mathrm{QCD}}^2/\mu^2$. The Sudakov exponent then behaves as

$$\mathrm{const} + \frac{C_{F,A}}{2\pi} c_1(\mu^2, \Lambda_{\mathrm{QCD}}^2) \frac{p_\perp^2}{\mu^2} \left(1 + \ln\left(\frac{\mu^2}{\Lambda_{\mathrm{QCD}}^2}\right)\right) + \mathcal{O}\left(\frac{p_\perp^4}{\mu^4}\right) \ . \tag{8.19}$$

One of the simplest modifications of the strong coupling is probably to introduce a smooth freezing here as well,

$$\tilde{\alpha}_s(q^2, \mu^2, \Lambda_{QCD}^2) = \alpha_s(q^2 + \mu^2, \Lambda_{QCD}^2) \ . \tag{8.20}$$

For a one-loop running we then indeed find a Gaussian behaviour,

$$\mathrm{d}P_{q,g}(p_\perp^2) \propto d^2 p_\perp \exp\left(-\frac{p_\perp^2}{2\Lambda_\perp^2}\right) \ , \tag{8.21}$$

with width

$$\Lambda_\perp^2 = \mu^2 \frac{\beta_0 \pi \ln^2(\mu^2/\Lambda_{\mathrm{QCD}}^2)}{C_{F,A}(1 + \ln(\mu^2/\Lambda_{\mathrm{QCD}}^2))} \ . \tag{8.22}$$

The width is smaller for gluons, implying a broader spatial distribution than for quarks, which may also be motivated on more general grounds. For a soft scale $\mu \sim 1$ GeV, three active flavours and $\Lambda_{\mathrm{QCD}} \sim 200...500$ MeV, typical widths range in

$$\Lambda_{\perp} \sim 800 \text{ MeV} ... 1.2 \text{ GeV} \tag{8.23}$$

which is exactly in the right order of magnitude as obtained by fitting the simple Gaussian model to data.

The estimate carried out in this section confirms that modelling the running of α_s in the region where an onset of non-perturbative is expected, may indeed give rise to a distribution of transverse momenta of incoming partons, which is dominated by a Gaussian behaviour. These models – besides the advantage given in the introduction to this section – may however exhibit richer dynamics than the simple Gaussian models themselves, thereby possibly allowing better fits to data.

8.4 Conclusions

In this chapter, the technical details to obtain a complete event simulation using the coherent dipole parton shower introduced in chapter 5 have been given. Besides the precise way, how initial conditions are determined on basis of a hard scattering process and the evolution algorithm itself, issues related to handing over an event to the further process of hadronization have been discussed. Alternative approaches to the generation of intrinsic transverse momentum in context of the dipole parton shower – especially needed for deep inelastic scattering or vector boson fusion processes – have been motivated and shown to produce a distribution compatible with a Gaussian, but probably richer in dynamics than more conservative models.

9 NLO Matching in Practise

9.1 Overview

The purpose of this chapter is to introduce all technical details specifying the implementation of NLO matching in the context of the Catani–Seymour dipole subtraction [9].

In particular, both variants of a purely subtractive matching and a POWHEG-type matching with matrix element corrections will be discussed. Both options have been implemented in the Matchbox add-on module to the Herwig++ event generator. Matchbox additionally provides facilities to automatically setup the subtraction needed for a NLO Monte Carlo simulation, requiring only phase space generators, tree-level, one-loop and real emission amplitudes as external input. Matchbox is documented in appendix C.

The POWHEG variant can be used independently of the shower module used, whereas consistent results from the subtractive matching can only be obtained along with the dipole shower introduced in chapters 5 and 8. The matching has so far been studied numerically for selected processes in chapter 10.

9.1.1 Notation and NLO Calculations in Dipole Subtraction

In this chapter, we will consider NLO calculations carried out using the dipole subtraction method, [9].

Instead of using the notation established there, we unify the indices of all possible dipoles to ease readability, as expressions become quite complicated especially when considering the POWHEG type matching. In addition, we adopt the conventions chosen for the dipole kernels in the chapter 6 for consistency,

$$\mathcal{D}_{ij,k} \,, \mathcal{D}_{ij}^{a} \,, \mathcal{D}_{k}^{ai} \,, \mathcal{D}^{ai,b} \quad \rightarrow \quad \mathcal{D}_{\alpha} \,, \tag{9.1}$$

where the arguments are unified and we make explicit the dependence on either real emission or 'tilde' kinematics, *e.g.*

$$\mathcal{D}_{ij,k}(q_1, ..., q_{n+1}) \quad \rightarrow \quad \mathcal{D}_\alpha(p_n^\alpha(q_{n+1})|q_{n+1}) \ , \tag{9.2}$$

where $p_n^\alpha(q_{n+1})$ and $q_{n+1}^\alpha(q_n; p_\perp^2, z, \phi)$ mark the 'tilde' mapping and its inverse,

$$\tilde{p}_{ij}(q_i, q_j, q_k) \ , \tilde{p}_k(q_i, q_j, q_k) \equiv p_n^\alpha(q_{n+1}) \tag{9.3}$$
$$q_{i,j,k}(\tilde{p}_{ij}, \tilde{p}_k; p_\perp^2, z, \phi) \equiv q_{n+1}^\alpha(p_n; p_\perp^2, z, \phi) \ .$$

Differential cross sections are considered in collinear factorisation and written in the notation of chapter 6,

$$\mathrm{d}\sigma_X(p_n|Q, x_a, x_b, \mu_F) = f_{P \leftarrow a}(x_a, \mu_F) f_{P \leftarrow b}(x_b, \mu_F) \mathrm{d}\sigma_X(p_n|Q) \mathrm{d}x_a \mathrm{d}x_b \tag{9.4}$$

where the partonic cross section is in general of the form

$$\mathrm{d}\sigma_X(p_n|Q) = F(\hat{p}_a, \hat{p}_b) X(p_n) \mathrm{d}\phi(p_n|Q) \ . \tag{9.5}$$

Here $F(\hat{p}_a, \hat{p}_b)$ is the appropriate flux factor and $X(p_n)$ generically denotes any contribution to the cross section which can be cast in the above form, *i.e.* tree-level amplitudes squared, one-loop tree-level interferences, subtraction terms, or the 'deconvoluted' finite collinear terms to be discussed below. As opposed to the previous chapters, the phase space measure $\mathrm{d}\phi(p_n|Q)$ now only refers to final state particles. In latter sections, it will turn out to be useful to rewrite this as

$$\mathrm{d}\sigma_X(p_n|Q, x_a, x_b) = X(p_n) \mathrm{d}F(x_a, \hat{p}_a, x_b, \hat{p}_b) \mathrm{d}\phi(p_n|Q) \tag{9.6}$$
$$\equiv X(p_n) \mathrm{d}\phi_F(p_n|Q, x_a, x_b) \ .$$

where we dropped making explicit the factorisation scale dependence from now on.

The finite collinear terms originating from counter terms to renormalise parton distribution functions and integrated subtraction terms are reported in [9] as convolutions of Born-type cross sections of colour correlated amplitudes with certain 'insertion operators', *e.g.* for the incoming parton a

$$\int_0^1 \mathrm{d}z \ C(p_n^a(z)) \mathrm{d}\phi(p_n|Q^a(z)) \mathrm{d}F(x_a, z\hat{p}_a, x_b, \hat{p}_b) \ , \tag{9.7}$$

where the superscript a along with an argument z indicates, that parton a's momentum is rescaled by z. The insertion operators themselves include +-distributions, and events should be generated according to the rescaled incoming momentum $z\hat{p}_a$. A numerical implementation is at first sight not obvious. Considering however the integration over

the momentum fraction x_a, these contributions can be rewritten in terms of a Born-type cross section multiplied by modified PDFs along the lines of

$$\int_0^1 \mathrm{d}x \int_0^1 \mathrm{d}z f(x) B(xz) P(z) = \int_0^1 \mathrm{d}x B(x) \int_x^1 \frac{\mathrm{d}z}{z} f\left(\frac{x}{z}\right) P(z) \tag{9.8}$$

and the +-distributions can be expressed in a way to allow for numerical implementation. All possible contributions are implemented in the DipolePKOperator class of the Matchbox module documented in appendix C.

Any NLO cross section within the dipole subtraction thus takes the form

$$\sigma_{NLO} = \int |\mathcal{M}_B(p_n)|^2 u(p_n) \mathrm{d}\phi_F(p_n|Q, x_a, x_b) \tag{9.9}$$

$$+ \int \left[2\mathrm{Re}\langle \mathcal{M}_B^*(p_n) \mathcal{M}_V(p_n)\rangle + \right.$$

$$\left. \langle \mathcal{M}_B(p_n)|\mathbf{I}|\mathcal{M}(p_n)\rangle \right]_{\epsilon=0} u(p_n) \mathrm{d}\phi_F(p_n|Q, x_a, x_b)$$

$$+ \int \langle \mathcal{M}_B(p_n)|(\tilde{\mathbf{P}} + \tilde{\mathbf{K}})|\mathcal{M}(p_n)\rangle u(p_n) \mathrm{d}\tilde{\phi}_F(p_n|Q, x_a, x_b)$$

$$+ \int \left(|\mathcal{M}_R(q_{n+1})|^2 u(q_{n+1}) \right.$$

$$\left. - \sum_\alpha \mathcal{D}_\alpha(p_n^\alpha(q_{n+1})|q_{n+1}) u(p_n^\alpha(q_{n+1})) \right) \mathrm{d}\phi_F(q_{n+1}|Q, x_a, x_b)$$

where the insertion operators $\mathbf{I}$ are given in [9] and have been implemented in full generality in the Matchbox module as well. $\tilde{\mathbf{P}}$, $\tilde{\mathbf{K}}$ and $\mathrm{d}\tilde{\phi}_F$ denote the deconvoluted versions of the finite collinear terms originating from the insertion operators $\mathbf{P}$,$\mathbf{K}$ given in [9]. Here, the test functions $u(p_n)$ refer to the class of events to be generated by a Monte Carlo realisation of the above integrals, and $\mathcal{M}_{B,R}$ denote the Born and real emission amplitudes, respectively. The subtraction terms $\mathcal{D}_\alpha$ are automatically generated within the implementation of NLO cross sections in Matchbox.

Since only the structure of the real emission and subtraction terms turns out to be relevant for matching purposes, we from now on collectively denote Born, virtual and insertion operator contributions by

$$\int |\mathcal{M}_{BV}(p_n)|^2 u(p_n) \mathrm{d}\phi_F(p_n|Q, x_a, x_b) \ .$$

Since all the integrals will be dealt with by means of Monte Carlo methods, we consider the integrands to define probability densities[1], and differentials are expressed in terms of

---

[1]Some contributions indeed may turn negative, thus a probabilistic interpretation does not seem to be evident. Contributions of this type can, however, still be treated in a pseudo-probabilistic manner. Details are given in chapter 7.

a Jacobian expressing the physical variables in terms of random numbers and a volume element on the unit hypercube of these random numbers, *e.g.*

$$\mathrm{d}\phi(p_n|Q) = \left| \frac{\partial p_n}{\partial \vec{r}} \right| \mathrm{d}^k r \tag{9.10}$$

and we identify ratios of differentials to actually mean the ratios of the corresponding functions multiplied by the Jacobian in use to express them in terms of random numbers, *e.g.* for two cross sections we define

$$\frac{\mathrm{d}\sigma_X(q_m|Q)}{\mathrm{d}\sigma_Y(p_n|Q)} \equiv \frac{X(q_m)}{Y(p_n)} \frac{\left| \frac{\partial q_m}{\partial \vec{r}_q} \right|}{\left| \frac{\partial p_n}{\partial \vec{r}_p} \right|} \ . \tag{9.11}$$

9.2 Subtractive Matching

The subtractive matching is the simplest variant of the matching schemes considered here. From a computational point of view it is basically identical to the NLO calculation with the only exception that the subtracted real emission does not generate a real emission event associated with a set of Born-type events per subtraction term, but just the real emission event with weight given by the real emission and all subtraction terms. This means just replacing $u(p^\alpha(q_{n+1}))$ by $u(q_{n+1})$ in the general expression of the NLO cross section, eq. 9.9, in accordance with the findings in section 6.4.2, since the shower splitting kernels exactly equal the subtraction terms.

In an algorithmic manner, the matching may thus be expressed very simple:

- Generate Born-type events p_n with density

$$|\mathcal{M}_{BV}(p_n)|^2 \mathrm{d}\phi_F(p_n|Q, x_a, x_b) \ , \tag{9.12}$$

- generate real-emission type events q_{n+1} with density

$$\left(|\mathcal{M}_R(q_{n+1})|^2 - \sum_\alpha \mathcal{D}_\alpha(p_n^\alpha(q_{n+1})|q_{n+1}) \right) \mathrm{d}\phi_F(q_{n+1}|Q, x_a, x_b) \ , \tag{9.13}$$

- and feed either into the dipole shower.

Note that this algorithm does require a minimal change to an already implemented NLO calculation, which consists of just the technical interface to the dipole shower. A subtlety, however, arises here. Since we are interested in describing the hardest emission

according to the exact real emission matrix element, the parton shower should not generate harder emissions than the one fixed from the NLO calculation. Practically, this is implemented by calculating the $p_\perp^\alpha$ as defined by the inverse 'tilde' mapping from each dipole and communicating this as a veto scale to the dipole shower, which is not allowed to generate emissions with $p_\perp > p_\perp^\alpha$ off the emitter, emission and spectator partons used to evaluate $\mathcal{D}^\alpha$.

9.3 Matching with Matrix Element Corrections

9.3.1 The Matrix Element Correction

As discussed in section 6.4.3, the splitting kernels to be used for a matrix element correction are given by the ratio of real emission and Born matrix elements squared, weighted by (in principle) arbitrary weight functions for each kinematic mapping of a subtraction term, *i.e.* for each subtraction term. It is most simple to choose the subtraction terms themselves to define these weight functions. This has the advantage that all divergences but the divergence associated to the subtraction term $\mathcal{D}_\alpha$ are divided out from the real emission matrix element, and dynamical features of the Born matrix element, like peaks owing to unstable particles, are flattened out in the splitting kernel considered.

Within this procedure, on faces three major problems:

- Some of the subtraction dipoles, in particular the ones with initial state emitter and final state spectator or vice versa, are not positive-definite. This makes a Monte Carlo treatment of the corresponding Sudakov-type distribution hard to implement. Since the regions, where these dipole kernels become negative correspond to hard, large angle parton emission, it is clear that this problem can be cured by changing the irrelevant finite terms of the subtraction dipoles, provided they are consistently taken into account in the integrated ones. Within the Matchbox implementation this has so far been carried out for the qq initial-final dipoles, which have been modified to reproduce the the matrix element squared for gluon emission off the corresponding vector current and are thus positive by definition.

- The Born matrix element squared may contain 'radiation zeroes'. In this case, its inverse is obviously ill-defined.

- The implementation of the parton densities at hand, which enter as a ratio in the splitting kernels as well, may not be stable in particular for large x in the sense that the interpolation used oscillates around zero rather than tending to zero smoothly.

This poses a problem similar to the radiation zeroes, however now without any physical interpretation.

The latter two problems can be solved by introducing an auxiliary cross section $\mathrm{d}\sigma_{\mathrm{screen}}(p_n|Q; p_\perp^2)$ which enters into the definition of the splitting kernels

$$\mathrm{d}P_\alpha(p_\perp^2, z, \phi | p_n) = \mathrm{d}^3 r \frac{\mathcal{D}_\alpha(p_n | q_{n+1}^\alpha)}{\sum_\beta \mathcal{D}_\beta(p_n^\beta(q_{n+1}^\alpha) | q_{n+1}^\alpha)}$$

$$\times \frac{\mathrm{d}\sigma_R(q_{n+1}^\alpha | Q, x_a', x_b')}{\mathrm{d}\sigma_B(p_n | Q, x_a, x_b) + \mathrm{d}\sigma_{\mathrm{screen},\alpha}(p_n | Q; p_\perp^2)} , \quad (9.14)$$

where we have already written the splitting kernel differential in the random numbers determining $p_\perp^2$, z and ϕ, and the dependence of $q_{n+1}^\alpha = q_{n+1}^\alpha(p_n; p_\perp^2, z, \phi)$ on the splitting variables is understood implicitly. In order not change the divergence structure implying the resummation of large logarithms, the screening cross section needs to vanish as $p_\perp^2 \to 0$. Since Born zeroes cannot occur for $p_\perp^2 \to 0$ (the QCD singularities factor in this limit with respect to the Born process) eq. 9.14 is free of these problems. If, in addition, the screening cross section does not depend on the parton distributions, the technical issues with PDFs becoming zero are cured as well. A treatment similar to the above one has already been suggested by Nason, though applying only to the matrix elements squared. Our treatment is more general, and does not make necessary the modification of parton distributions to cure numerically ill-defined PDF ratios.

The screening cross section has however to be taken into account for the fixed order calculation in order to reproduce the correct NLO cross section and will thereby spoil the original simplicity of using the NLO K-factor differential in the Born variables to generate events to enter the matrix element corrected shower.

9.3.2 The Fixed Order Calculation

Including the screening cross section the fixed order cross section can then be calculated to be constructed of densities for Born-type and real emission type events. The densities for Born-type events closely resemble the K-factor modification,

$$\mathrm{d}\sigma_{\mathrm{inclusive}}(p_n | Q, x_a, x_b) =$$
$$\mathrm{d}^k r_B \left(\frac{\mathrm{d}\sigma_{BV}(p_n | Q, x_a, x_b)}{\mathrm{d}^k r_B} + \mathrm{d}^3 r \frac{\mathrm{d}\sigma_{R,\mathrm{inclusive}}(p_n | Q, x_a, x_b)}{\mathrm{d}^k r_B \mathrm{d}^3 r} \right) \quad (9.15)$$

where

$$\frac{\mathrm{d}\sigma_{R,\mathrm{inclusive}}(p_n | Q, x_a, x_b)}{\mathrm{d}^k r_B \mathrm{d}^3 r} = \frac{\mathrm{d}\sigma_B(p_n | Q)}{\mathrm{d}^k r_B} \sum_\alpha \frac{\mathcal{D}_\alpha(p_n | q_{n+1}^\alpha)}{\sum_\beta \mathcal{D}_\beta(p_n^\beta(q_{n+1}^\alpha) | q_{n+1}^\alpha)}$$
$$\times \left(\frac{\mathrm{d}\sigma_R(q_{n+1}^\alpha | Q, x_a', x_b')}{\mathrm{d}\sigma_B(p_n | Q, x_a, x_b) + \mathrm{d}\sigma_{\mathrm{screen},\alpha}(p_n | Q; p_\perp^2)} - \frac{\mathrm{d}\phi_F(q_{n+1}^\alpha | Q, x_a', x_b')}{\mathrm{d}\phi(p_n | Q)} \right) . \quad (9.16)$$

To generate events according to these densities, a $k + 3$-dimensional random number point is chosen, where the three additional degrees of freedom are discarded. Owing to the fact that the integration volume in terms of random numbers is the unit hypercube, this procedure produces the integration over the degrees of freedom of the parton emitted in the real emission on average.

Events of real emission type are to be generated with density

$$
\begin{aligned}
\mathrm{d}\sigma_R(q_{n+1}|Q, x_a, x_b) \quad &\times \\
\sum_\alpha \frac{\mathrm{d}\sigma_{\mathrm{screen},\alpha}(p_n^\alpha(q_{n+1})|Q; p_\perp^2)}{\mathrm{d}\sigma_B(p_n^\alpha(q_{n+1})|Q, x_a', x_b') + \mathrm{d}\sigma_{\mathrm{screen},\alpha}(p_n^\alpha(q_{n+1})|Q; p_\perp^2)} \\
&\times \frac{\mathcal{D}_\alpha(p_n^\alpha(q_{n+1})|q_{n+1})}{\sum_\beta \mathcal{D}_\beta(p_n^\beta(q_{n+1})|q_{n+1})} \mathrm{d}^l r_R \;,
\end{aligned}
\tag{9.17}
$$

which is just a reweighting of the real emission contribution. Events of both classes can then be showered by a parton shower using a matrix element correction as defined in the previous section, and a communication of veto scales applies to the real emission contribution along the same lines as for the subtractive matching. Note that the individual contributions are positive, as long as the screening cross section is bounded from above by a reasonable value.

Since this type of matching is independent of the parton shower to act downstream, the actual implementation does not make any reference to the dipole parton shower, and real emission contributions according to the matrix element correction are generated outside any shower module, presenting a real emission sub process supplemented with proper veto scales, or a Born-type sub process to the shower, if radiation has been generated according to the matrix element correction or not, respectively.

Note that, when putting the screening cross section to zero, the original simplicity of the POWHEG-type matching is recovered. The matrix element corrections, inclusive and real-emission type contributions are all setup and calculated in an automated way within the Matchbox implementation. The screening cross section is by default chosen from the corresponding phase space and the dimensionality required by the phase space, *i.e.*

$$
\mathrm{d}\sigma_{\mathrm{screen},\alpha}(p_n^\alpha(q_{n+1})|Q; p_\perp^2) = \frac{(p_\perp^\alpha)^2}{s_\alpha(q_{n+1})} \frac{\mathrm{d}\phi(q_{n+1}|Q)}{(s_\alpha(q_{n+1}))^{n_{\mathrm{out}}}} \;,
\tag{9.18}
$$

where $p_\perp^\alpha$ is the transverse momentum associated to the mapping $p_n^\alpha(q_{n+1})$, and $s_\alpha(q_{n+1})$ is the appropriate mass squared of the emitter-spectator pair in p_n^α. Other choices may be possible.

9.4 Conclusions

In this chapter all technical details for NLO matching as implemented in the Matchbox module have been discussed. Matchbox is capable of setting up NLO calculations in an automated way, with the only need of having Born-, one-loop-, and real emission amplitudes provided.

All manipulations to obtain the quite simple matched calculation for the subtractive scheme, or the more complicated matching with matrix element corrections, can be carried out automatically as well. Problems due to non-positive definite dipole kernels have been solved by modifying finite terms, and a scheme has been introduced to cope with radiation zeroes as well as numerical instabilities in the evaluation of parton distribution functions. Numerical results of applying these matching schemes to simple processes are presented in chapter 10.

10 Simulation Results

10.1 Overview

In this chapter, numerical results from the implementation of the dipole shower algorithm and the automatised NLO matching are presented. Simulation results for e^+e^- annihilation into hadrons as measured by the LEP experiments, deep inelastic scattering as present at the HERA collider and Drell-Yan pair production at Fermilab's Tevatron collider have been compared to data. Both LO and NLO predictions are considered. All software modules involved in the simulation part of hard process generation at LO and NLO as well as the parton showering are documented in appendices A – C. Appendix D gives an overview on validation of the code's functionality.

10.2 Jet Production in e^+e^- Annihilation

In this section we extensively discuss simulation results for jet production in e^+e^- annihilation, in particular as measured by the experiments at the LEP collider running at a centre-of-mass energy of 91.2 GeV. The hard process of interest here, $e^+e^- \to q\bar{q}$, offers the possibility to explicitly test the coherence properties of the parton shower, and the data acquired by the LEP experiments allow to fix parameters entering the hadronization model.

10.2.1 An Explicit Test of Soft Gluon Coherence

In order to test the coherence properties of the dipole shower algorithm we here define an observable, which is sensitive to the very defining property of coherent emission of soft gluons. Though the observable may indeed be defined at hadron level, when supplemented by a proper jet resolution criterion, we here define it on parton level in order to make explicit the behaviour of parton showering only.

To be precise, we select events with four partons in the final state. Since these are produced through e^+e^- annihilation, their overall colour state is a singlet. The required four final state partons are ordered in energies, with one referring to the hardest, four to the softest parton. The observable is defined in terms of angles between the partons in the CMS of the collision, θ_{ij}, and the energy fraction of the softest parton,

$$x_4 = \frac{E_4}{E_{\text{tot}}} \ . \tag{10.1}$$

We require partons two and three to be collinear,

$$\theta_{23} < \theta_c \ , \tag{10.2}$$

and the fourth parton to have an energy below some threshold,

$$x_4 < x_c \ . \tag{10.3}$$

The event topology is sketched in Figure 10.1. We are interested in the correlation between energy and angular ordering. To this extent we consider the difference in opening angles, assuming that partons three and four have been emitted by parton two,

$$\theta^* = \theta_{24} - \theta_{23} \ . \tag{10.4}$$

In order to suppress contributions where the soft parton has most probably been emitted from parton one, we further require

$$\theta_{24} < \frac{\pi}{2} \ . \tag{10.5}$$

The distribution of θ^* is thus expected to be dominated mainly by the angular ordering property, *i.e.* we expect a suppression of events with $\theta^* < 0$. An enhancement towards $\theta^* = 0$ should however be present, since this corresponds to emitting the soft parton collinear to parton three. Note that this singularity is actually screened by the Sudakov form factor, thus we expect a peak towards $\theta^* \gtrsim 0$, providing another important cross check on the connection of the evolution variable to coherence properties.

The manifestation of a coherent evolution is, however, most notably the property that for large-angle emission the colour sub structure of the collinear parton pair cannot be
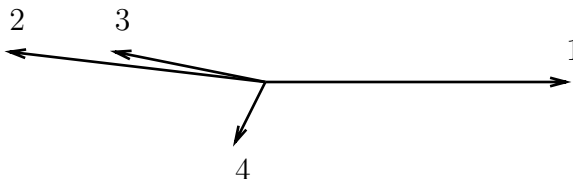
Figure 10.1: The event topology selected for testing coherence properties.

resolved by the soft parton. This implies that it is being preferably emitted as if there were only two hard partons forming the corresponding dipole. In this region, there is no Sudakov suppression in the angular variable, and the distribution of θ^* is to be governed by the corresponding radiation pattern for an emitter being combined of partons two and three. For small θ_{23} the angle to the respective combined emitter may roughly be taken to be θ^* itself, that is we expect a drop of θ^* towards $\theta^* \sim \pi/2$, with a steep fall-off starting from $\theta^* = \pi/2 - \theta_c$, which is just a consequence of the cuts imposed[1]. In particular, there should not be an enhancement towards $\theta^* \sim \pi/2$. For the $p_\perp$ ordered dipole shower we exactly find the expected behaviour, whereas a virtuality ordering does not exhibit the coherence features. The simulation results for $x_c = 0.1$, comparing different orderings are shown in Figure 10.2.

The angular ordered shower of Herwig++ shows the same qualitative behaviour of the θ^* distribution as for the $p_\perp$ ordered dipole shower, confirming that the $p_\perp$ ordering gives rise to a coherent evolution. Note that one cannot expect the showers to be in perfect agreement, since after all these are *different* shower implementations. The differences in the observable considered are influenced by many properties which are not connected to the choice of evolution though significantly differ between both shower implementations. In particular, the kinematic reconstruction at the end of the evolution

---

[1]In this region, the selected events tend to isotropic three-jet configurations, making it impossible for the fourth parton to be soft by the energy-momentum constraint.
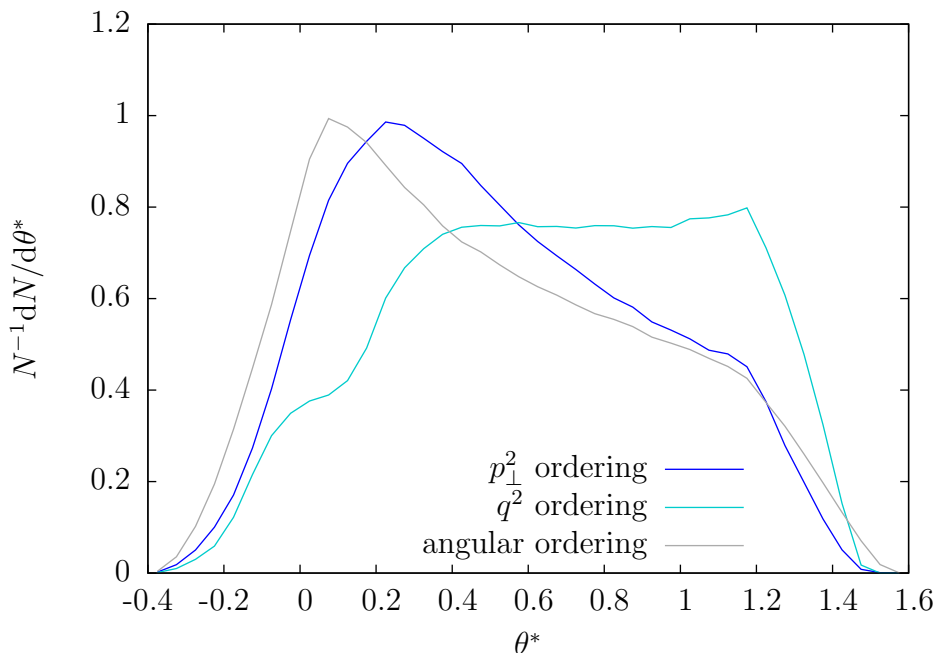
Figure 10.2: The θ^* distribution for $\theta_c = \pi/8$ and $x_c = 0.1$.

present in Herwig++, as opposed to the local recoils implemented in the dipole shower, and the dead phase space region inherent to the angular ordered evolution should be mentioned here.

10.2.2 Tuning of Parameters

The variety of data acquired by the LEP experiments allow for a systematic fir of parameters of the parton shower and the hadronization model. In a preliminary fit, the parameters assumed to mainly determine the description of event shape variables and jet rates as measured by the DELPHI experiment [46] and jet observables as reported by the OPAL collaboration [47] have been fitted using the Rivet [48] and Professor [49] systems. The parameters and ranges considered are given in table 10.1, along with a short description. Parameters which are known to mainly affect individual hadron multiplicities have not been varied, and fragmentation parameters for heavy quarks have been set equal to the values of those for light quarks. A simple modification of the running of α_s in the infrared has been adopted by replacing its argument $q^2 \rightarrow q^2 + \mu_{\text{soft}}^2$, cf. section 8.3.2, since there is no reason of assuming that this model should not be valid for final state radiation.

Separate fits have been performed for LO and NLO predictions. LO predictions have

Parameter	Range	Description
$\alpha_s(M_Z^2)$	$0.1 - 0.13$	Input α_s at Z mass.
$\mu_{IR,FF}$	0.5 GeV $- 2.0$ GeV	Infrared cutoff for final-final dipoles
$\mu_{\text{soft},FF}$	0.0 GeV $- 1.2$ GeV	Soft scale for final-final dipoles
$m_{g,c}$	0.67 GeV $- 3.0$ GeV	Gluon constituent mass
Cl_{max}	0.5 GeV $- 10$ GeV	Maximum cluster mass
Cl_{pow}	$0.0 - 10.0$	Cluster mass exponent
Cl_{smr}	$0.0 - 10.0$	Cluster direction smearing
P_{split}	$0.0 - 1.4$	Cluster mass splitting parameter

Table 10.1: The parameters varied for the fit to LEP data.

Parameter	LO	NLO
$\alpha_s(M_Z^2)$	0.113185 ± 0.007281	0.117550 ± 0.005053
$\mu_{IR,FF}$	(1.416023 ± 0.306430) GeV	(1.245196 ± 0.226821) GeV
$\mu_{\text{soft},FF}$	(0.242725 ± 0.202069) GeV	0.0 GeV [2]
$m_{g,c}$	(1.080386 ± 0.499546) GeV	(1.007680 ± 0.265565) GeV
Cl_{max}	(4.170320 ± 0.589504) GeV	(3.664004 ± 0.639504) GeV
Cl_{pow}	5.734681 ± 1.006965	5.687022 ± 0.869322
Cl_{smr}	4.548755 ± 2.350193	3.115744 ± 2.436793
P_{split}	0.765173 ± 0.074008	0.771329 ± 0.074248

Table 10.2: Parameters for LO and NLO fits to LEP data.

been obtained by running just the parton shower, using a one-loop running α_s. NLO prediction have been obtained by means of supplementing the shower with the matrix element correction matching without using the Born screening cross section and a two-loop running α_s. In total we find that the NLO simulation gives a marginally better fit than the LO one, though the description of data is completely comparable within experimental uncertainties.

The fitted parameter values are displayed in table 10.2. Most notably, the hadronization parameters for the LO and NLO fit do not significantly differ. For both predictions, a modification of the infrared running of α_s seems not to be preferred.

The infrared cutoff of the parton shower is determined more precisely by the NLO fit, which prefers a smaller cutoff. In other words, it prefers that more of the dynamics are modelled by a QCD prediction than by the phenomenological hadronization model. Also $\alpha_s(M_Z^2)$ is determined more precisely by the NLO fit. Both α_s values obtained are compatible with the world average [50] of 0.1184, where the NLO result is closer to this

---

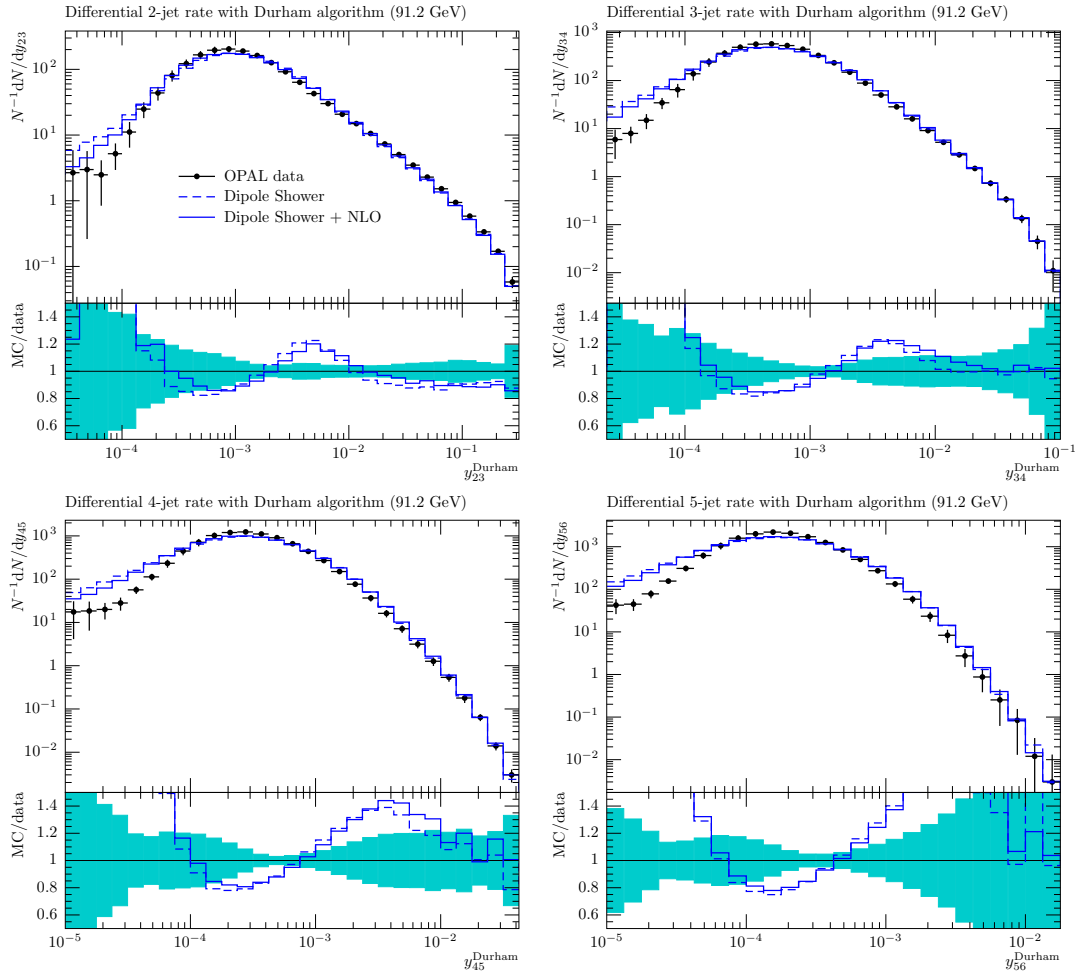[2]This parameter was predicted negative by Professor though consistent with zero and has thus been fixed.

Figure 10.3: Differential jet rates as predicted by the leading order and next-to-leading order simulations. Note that the small y_{ij} bins correspond to invariant masses in the vicinity of or below the QCD scale and are thus almost only subject to non-perturbative modelling. More sophisticated models or a more systematic fit may reveal an even better description of data in this phasespace region.
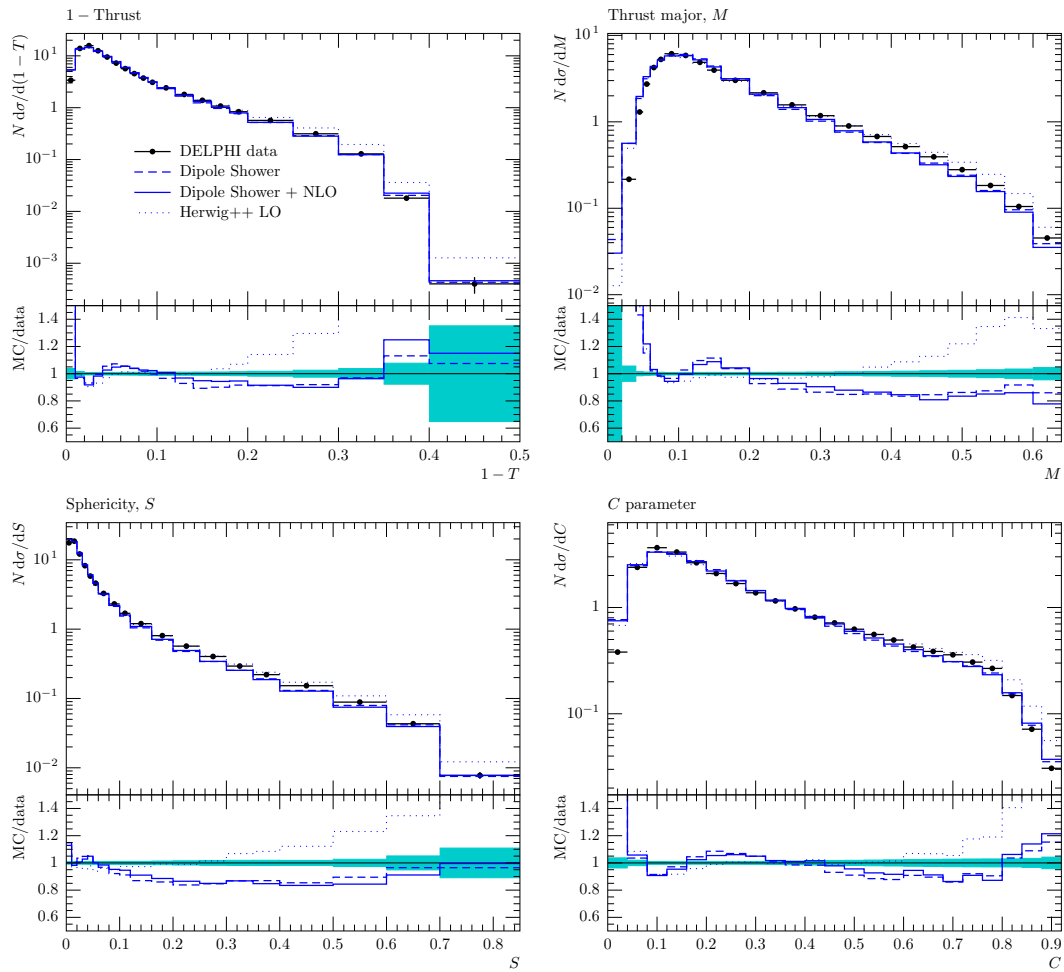
Figure 10.4: Some event shape variables as predicted by the leading order and next-to-leading order simulations. Here, we additionally compare to the standard Herwig++ shower, showing that the dipole shower gives a significantly improved description already at leading order.
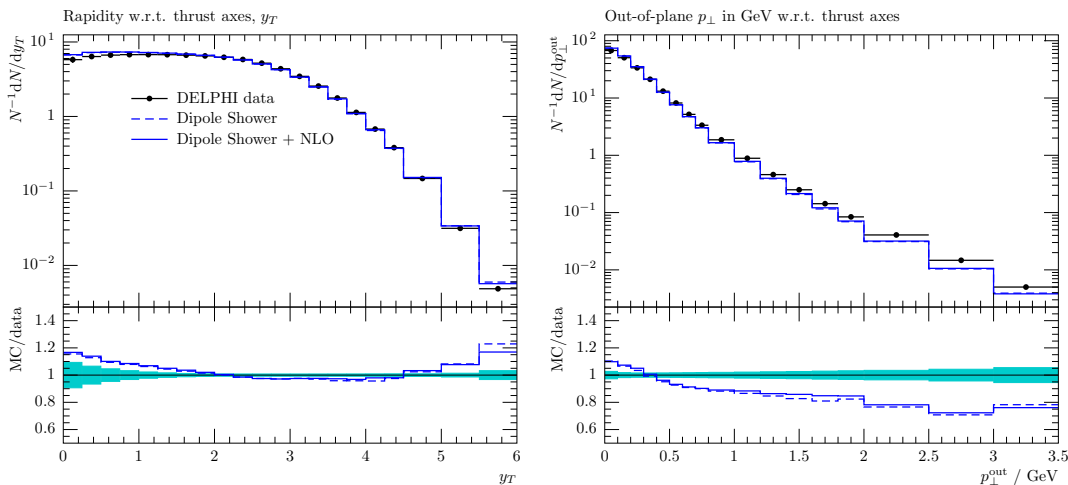
Figure 10.5: $p_\perp$ and rapidity distributions with respect to the thrust axis.

value. In figures 10.3 and 10.4 the LO and NLO simulation results are compared for selected observables.

In figure 10.5 the $p_\perp$ and rapidity distributions with respect to the thrust axis are displayed. Figure 10.6 shows two observables, which have not been included in the fit and thus test the predictivity of the simulation to some extent. For the energy-energy correlation we find an almost perfect description. The correlation of the out-of-plane $p_\perp$ and the hadron energy fraction x_p is not described properly. This is the case for the Herwig++ shower as well, though interestingly this is the only observable to show significant improvements by the NLO matching. We trace back this to the fact that the NLO prediction gives an improved description of three-jet final states, entering this observable in the definition of the thrust axis and event plane.

10.2.3 Comparison of Matching Strategies

The Matchbox framework provides to switch between the POWHEG-type matching with matrix element corrections including or excluding the auxiliary Born screening cross section, and subtractive matching. For reasons of systematics it is instructive to compare these approaches. No separate fit for the variants not considered so far has been performed and the NLO fit values as given in the previous section have been used. The different matching strategies give completely comparable results. If there are small visible differences, there is no clear tendency that either variant would give a better description than any of the others. Figure 10.7 compares the matching strategies for two jet rate observables. To this extent, the subtractive matching could be preferred amongst the POWHEG-type ones owing to its smaller computational complexity. This
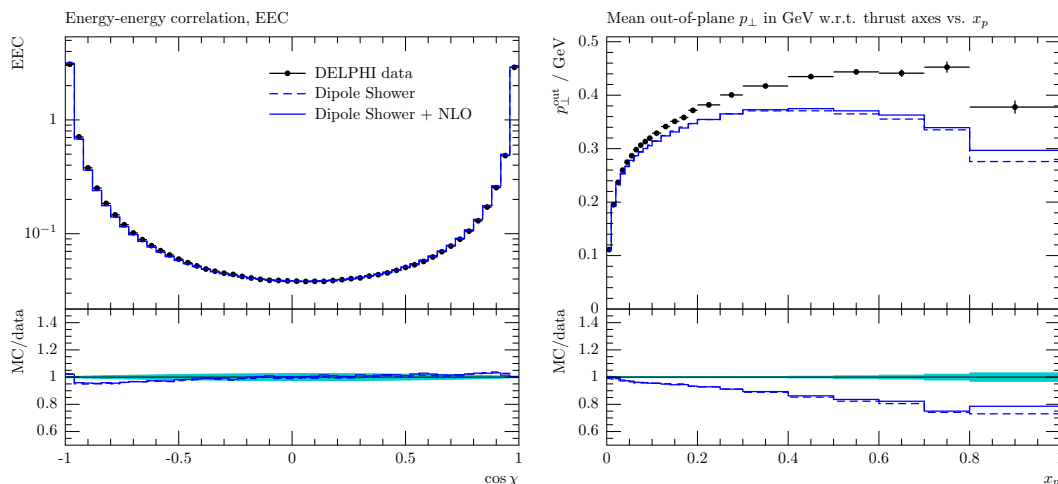
Figure 10.6: Energy-energy correlation and out-of-plane $p_\perp$ correlation w.r.t. the thrust axis. These observables have not been included in the fit and thus provide a test of the predictivity of the simulation. The $p_\perp$ correlation is the only observable showing a significant improvement by the NLO matching. It should be noted that this observable turns out to be problematic also for the Herwig++ shower.

Parameter	LO	NLO
$\mu_{IR,FI}$	(0.796205 ± 0.333340) GeV	(0.718418 ± 0.210448) GeV
$\mu_{\text{soft},FI}$	(1.355894 ± 0.432515) GeV	(1.003714 ± 0.252398)GeV

Table 10.3: Parameters for LO and NLO fits to HERA data.

statement of course includes that negative weighted events do not pose a major problem and also has to be decided in a process dependent matter since there is no hint, if the behaviour observed here is a general feature.

10.3 Deep Inelastic Scattering

Owing to the approximation underlying the parton shower, cf. chapter 5, diagrams contributing to parton emission of a given dipole (i, j) may be considered a gauge invariant subset in the soft and/or collinear limits for $N_c \to \infty$. This motivates that the infrared cutoffs and soft scales entering the emission probabilities need not be the same for all dipoles. The emitter-spectator configurations forming gauge invariant quantities in this sense are the two emitter choices for final-final dipoles, initial-initial dipoles, and the
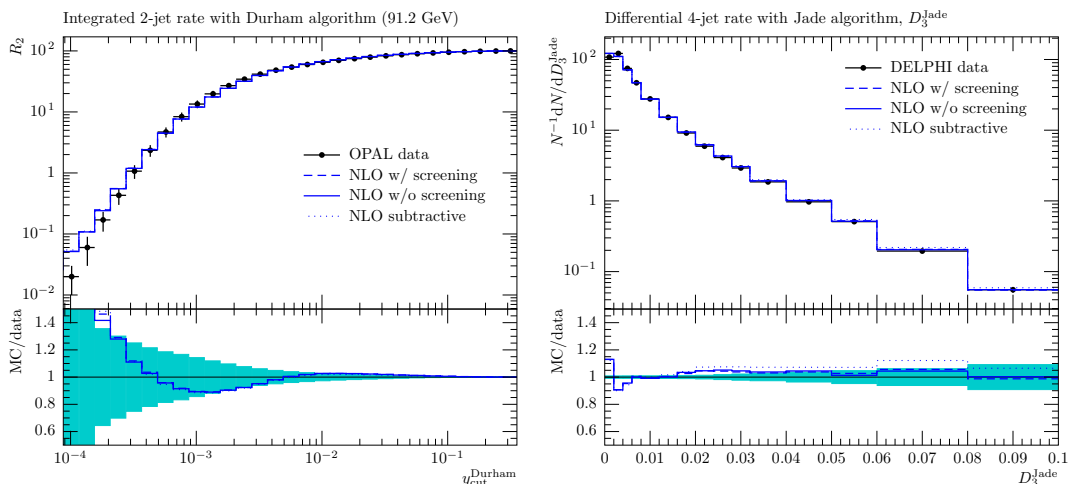
Figure 10.7: Comparison of matching strategies exemplified for the Durham two-jet rate and JADE differential four-jet rate.

combination of initial-final and final-initial configurations. Fitting DIS data therefore allows to fix the infrared cutoff and soft scale for the latter, before finally constraining the same parameters for initial-initial dipoles at a hadron collider, which is considered in the next section.

For the fit described here, the same technique as for LEP, and data accumulated by the H1 experiment [51] have been used. For LO and NLO, the default Herwig++ PDFs, MSTW 2008 LO [52] and MRST 2002 NLO [53], have been used. The same PDFs were considered for hadron collider data to be discussed in the next section. The NLO fit was obtained by running the matching with matrix element correction.

The findings are similar as for the fit to LEP data. The matched NLO prediction gives a comparable fit to the LO simulation, while preferring both a smaller infrared cutoff and screening scale. The fitted parameters are given in table 10.3.

In figures 10.8 and 10.9 simulation results are compared to transverse energy flows $dE_\perp/d\eta$ in various bins of the Bjorken variable x and momentum transfer Q^2. Both predictions give a comparable and reasonable description of HERA data over the whole range of the (x, Q^2) plane.

Figure 10.10 shows the average transverse energy as a function of Q^2 in both the central and forward detector regions. These observables are clearly improved by the NLO matching at small momentum transfers, though the description of the forward region may be improved. The fact that this region is not properly described by an ordinary parton shower is not surprising: in this region, large logarithms of the Bjorken variable have a major impact and need to be resummed by a CCFM-type evolution, see *e.g.* [54].
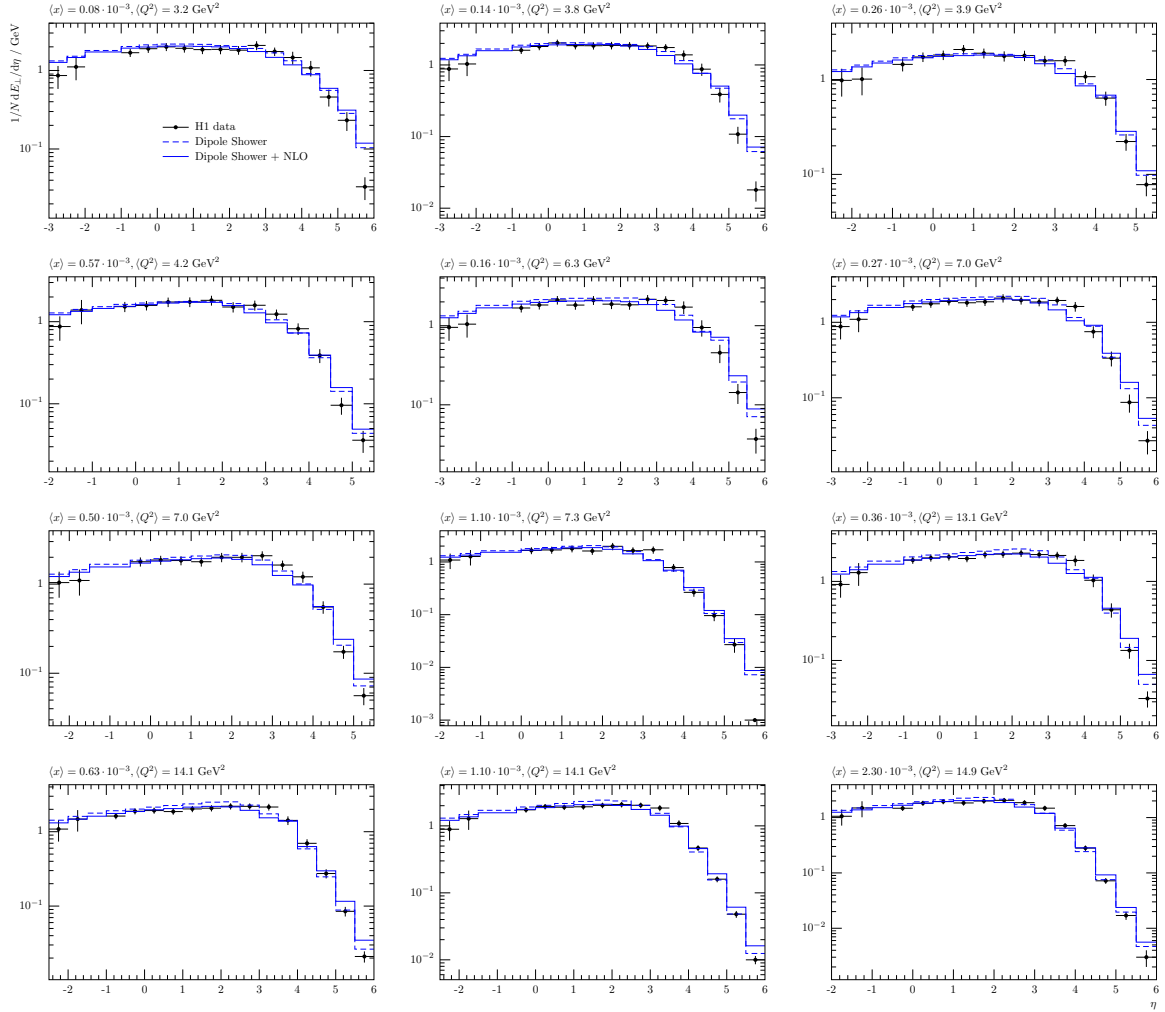
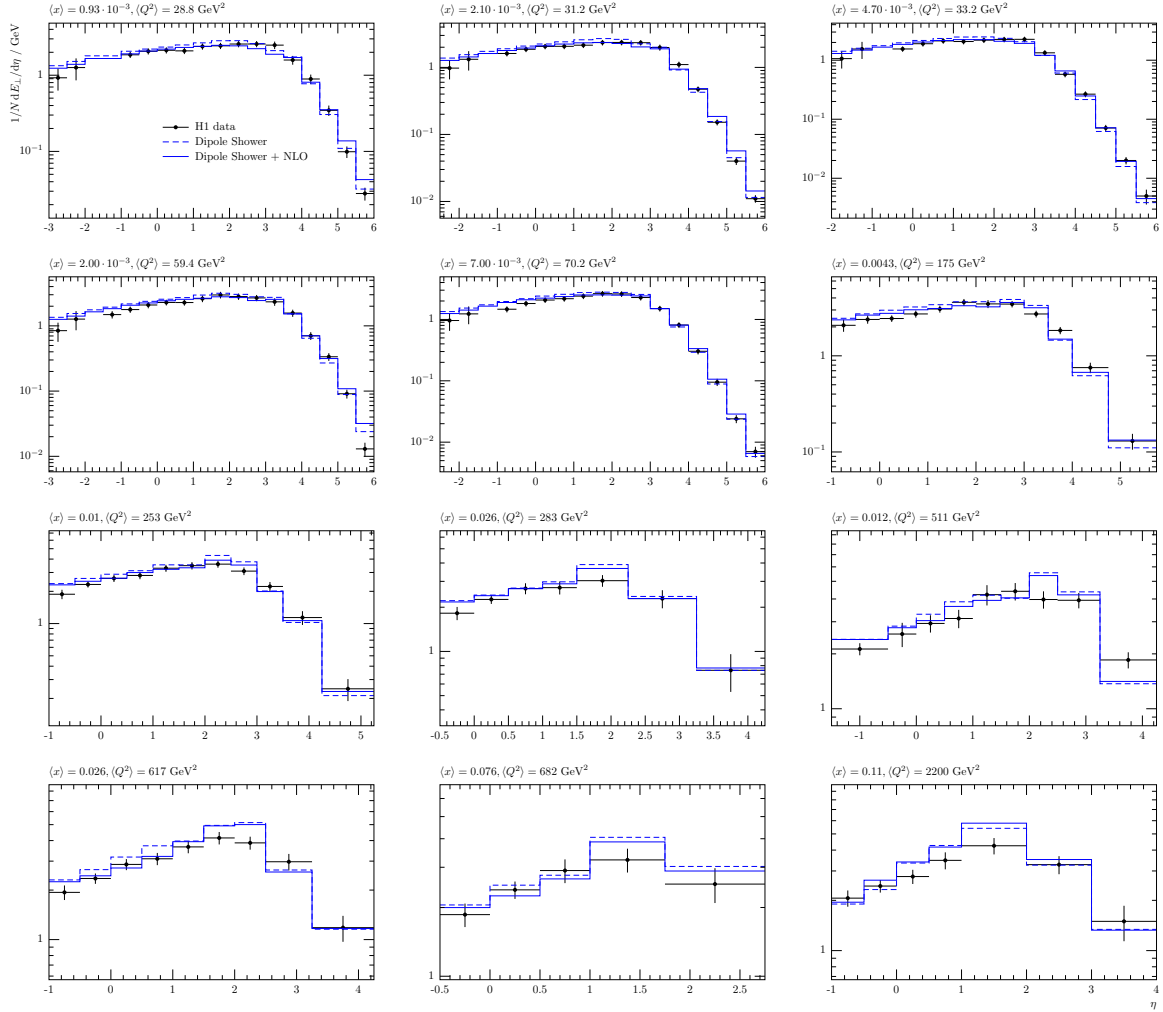Figure 10.8: Transverse energy flows as measured by H1 compared to LO and NLO simulations.

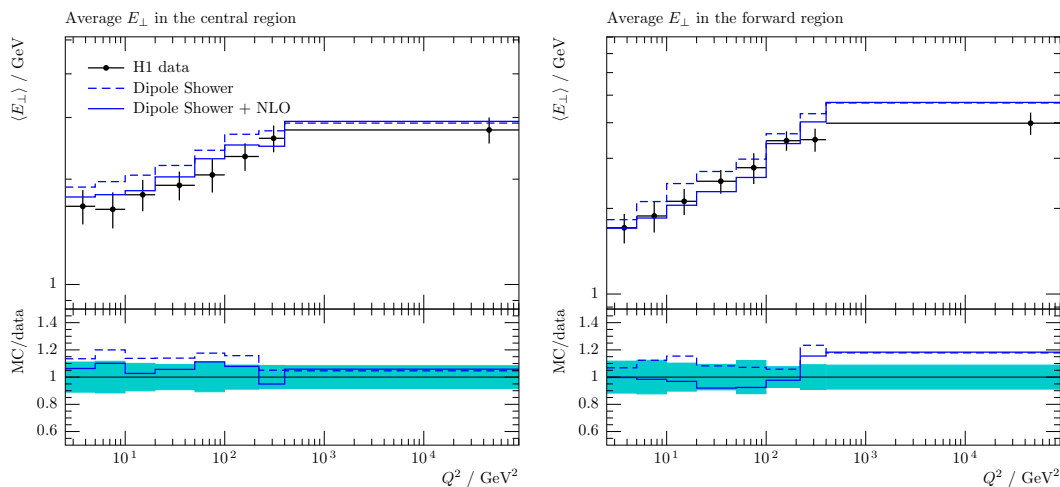Figure 10.9: Transverse energy flows as measured by H1 compared to LO and NLO simulations.

Figure 10.10: Average transverse energy in the central and forward regions as measured at HERA and compared to leading order and next-to-leading order predictions. In the central region, the NLO prediction is fully contained within the experimental uncertainties.

10.4 Vector Boson Production at Hadron Colliders

In this last section of comparing data to simulation results, we investigate the dipole shower's and matching performance in hadron-hadron collisions. Specifically, the $p_\perp$ spectrum of Z bosons produced at the Tevatron is considered. Before comparing to data, we analyse the impact of the new kinematic prescription for initial state radiation by considering a parton level analysis only.

10.4.1 The Relevance of the Recoil Scheme

The effects of the altered recoil scheme for initial state radiation can most prominently be analysed by looking at the predictions for the $p_\perp$ spectrum of the Z boson in $p\bar{p} \rightarrow Z+X$ events. Events have been generated at parton level without inclusion of intrinsic $p_\perp$. So-called 'forced splittings' to valence quarks are however present, which to some extent contribute transverse momentum to the final state system. We analyse the effect on the $p_\perp$ spectrum by constraining the parton shower evolution to generate a fixed number of initial state emissions according to the proposed recoil scheme, comparing to the recoil scheme which keeps the initial state emitter aligned with the beam axis. We will refer to the first scheme as 'non-collinear', the second will be called the 'collinear' scheme.
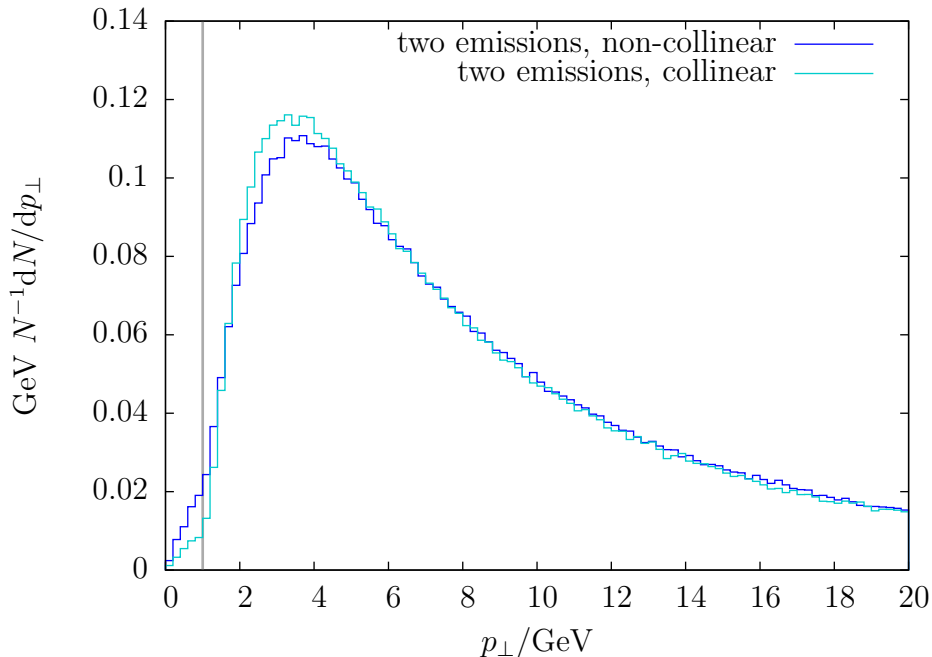
Figure 10.11: The Z $p_\perp$ spectrum when limiting the shower to two initial state emissions, which is the first contribution to show differences between the recoil schemes. The vertical grey line marks the infrared cutoff. Note that the non-collinear scheme shows a much more smooth transition to the non-perturbative domain.

For a single initial state emission we expect no difference in the distributions, since the two parametrisations for one emission are related by a boost, which in the case of the non-collinear scheme is applied after the emission has been generated. We exactly find the expected agreement, which provides a cross check of our implementation. Starting from two emissions, differences are clearly visible. Figure 10.11 shows the example of two emissions, and we find the same systematics for higher multiplicities and the overall spectrum. Though visible at parton level, the effect may be screened at hadron level owing to non-perturbative modelling, in particular intrinsic transverse momentum, leading to comparable results when the full simulation is taken into account. The influence of the different schemes on constraining non-perturbative parameters such as the width of the intrinsic $p_\perp$ distribution to reasonable ranges would have to be studied in a dedicated fit to data.

10.4.2 The Drell-Yan $p_\perp$ spectrum

After having determined the simulation parameters for hadronization, final state radiation, and radiation off an final-initial dipole by fitting LEP and HERA data, two parameters remain to be determined: the infrared cutoff and soft scale for radiation off an initial-initial dipole. The best observable to constrain these parameters is probably the $p_\perp$ spectrum of e^+e^- Drell-Yan pair production as measured by the CDF collaboration [55]. Since the Drell-Yan process receives rather large QCD corrections of order 20% from leading to next-to-leading order and a still considerable correction at NNLO, both fits have been performed by normalising the simulation to the measured cross section. The matrix element matching including the Born screening cross section has been used here, as for the DIS data.

The cubic interpolation used by Professor turned not to be able to describe the simulation dynamics over a wide parameter range for this observable. Therefore a different method to obtain a preliminary fit has been used here: out of a sample of 200 randomly generated points in parameter space the point with smallest χ^2 has been chosen. When normalised to data, we find that LO and NLO simulations are again comparable, with the NLO fit surprisingly being worse than the LO one. Further, though finding a reasonable description of the hard tail of the $p_\perp$ spectrum for both predictions, the peak position is not reproduced properly. Since the peak position is known to be determined almost completely by non-perturbative models of the distribution of incoming parton momenta, there are basically two possible reasons for this result:

- The modelling of intrinsic $p_\perp$ by the simple modification of shifting the argument of α_s may not be sufficient, and other models would have to be considered. In particular models, where the running of the strong coupling in the infrared region exhibits a peak somewhere below a soft scale instead of just a plateau could be promising.[3] These models would enhance soft emissions at intermediate transverse momenta while suppressing the occurrence of too low $p_\perp$ emissions – resulting in shifting the peak to higher $p_\perp$ as required by the data.

- The model may be sufficient for Hadron-Hadron and DIS data separately, but the DIS data prefer a different parameter set for final-initial (FI) dipoles. This can be constrained by either a simultaneous fit to both experiment's data or by re-fitting the FI parameters to the CDF data.

Either case implies a shortcoming of the non-perturbative models involved, and improving these will be subject to future work. In order to get a first handle on the systematics, further fits have been done: first a fit of the initial-initial (II) parameters while including the traditional Gaussian model for intrinsic $p_\perp$, and a re-tune of both

---

[3]This behaviour is motivated by results for α_s obtained from lattice simulations.

Fit Strategy	Parameter	LO	NLO
HERA→ TVT + $\langle p_\perp \rangle$	χ^2	3.00315	1.73401
	$\mu_{IR,II}$	0.367359 GeV	0.275894 GeV
	$\mu_{\text{soft},II}$	0.205854 GeV	0.254028 GeV
	$\Lambda_{\perp,\text{valence}}$	1.68463 GeV	1.26905 GeV
	$\Lambda_{\perp,\text{sea}}$	1.29001 GeV	1.1613 GeV
HERA→ TVT	χ^2	2.97787	3.42818
	$\mu_{IR,II}$	0.307381 GeV	0.210811 GeV
	$\mu_{\text{soft},II}$	0.22353 GeV	0.563621 GeV
TVT only	χ^2	1.63246	3.05275
	$\mu_{IR,FI}$	0.252593 GeV	0.252309 GeV
	$\mu_{\text{soft},FI}$	0.690434 GeV	1.5097 GeV
	$\mu_{IR,II}$	0.363603 GeV	0.502962 GeV
	$\mu_{\text{soft},II}$	0.495252 GeV	0.392963 GeV

Table 10.4: Parameters for LO and NLO fits to CDF $p_\perp(Z)$ data. The notation HERA→TVT indicates FI parameters fixed by the HERA fit. Note that uncertainties could not be determined owing to the different fit method used here. This results reveal that there is a huge impact of non-perturbative models in describing this particular observable, and more sophisticated models and a more systematic fit will have to be considered.

FI and II parameters to the CDF data. The results are given in table 10.4, where 300 parameter points have been used for the latter fits. Figure 10.12 compares the different predictions. By including intrinsic $p_\perp$ we find reasonable values for the width of the Gaussian distribution $\Lambda_\perp$, with the NLO matching preferring smaller widths. Here, the expected hierarchy with the NLO fit being better than the LO one is apparent, and we find $\Lambda_{\perp,\text{sea}} < \Lambda_{\perp,\text{valence}}$, *i.e.* a broader spatial distribution for sea partons as compared to valence partons. By re-tuning the FI parameters, we again find the counter-intuitive fact of a NLO prediction being worse than a LO one, though more points in parameter space would have to be considered to obtain a definite statement. In total, this study reveals that there is a huge impact of non-perturbative models in describing the Z $p_\perp$ spectrum and the simple modified-α_s model does indeed not seem to be sufficient to describe these dynamics. Figure 10.13 compares LO and NLO simulations run with parameters from the fit including intrinsic $p_\perp$, while keeping FI parameters as obtained from HERA data.
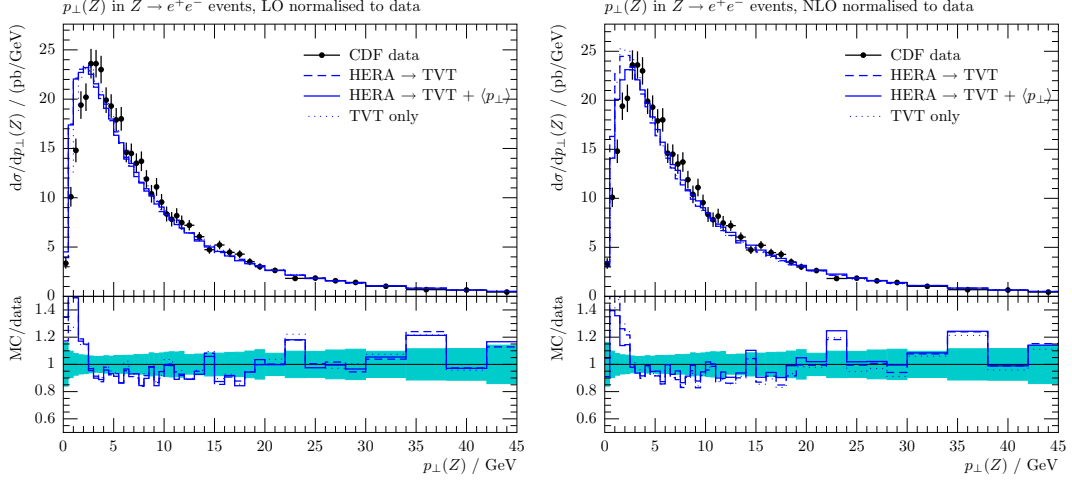
Figure 10.12: Fit strategies for LO and NLO compared to CDF data. See text and table 10.4 for details.
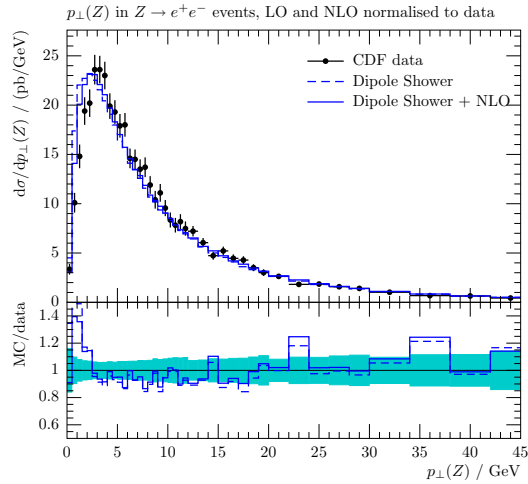

Figure 10.13: LO and NLO predictions for the Z $p_\perp$ spectrum. The FI parameters have been fixed by the HERA fit, and II parameters and intrinsic $p_\perp$ width have been varied.

10.5 Conclusions

In this chapter, we have presented simulation results obtained by an implementation of the dipole shower and matching algorithms described in detail in the previous chapters. Parameters of the simulation have been obtained by successive fits to data acquired at LEP, HERA and the Tevatron, constraining first hadronization parameters, the value of α_s at the Z mass and the parameters entering radiation off final-final dipoles from LEP data. This fit exhibits a very good description of several observables at LEP. The predictivity has been tested by looking at observables not included in the fit and a reasonable description is obtained also here. The three possible matching schemes have been compared and shown to yield comparable results, though this may not be regarded a process independent statement.

The parameters entering radiation off final-initial and final-initial dipoles have been constrained from data acquired by the H1 experiment. The transverse energy flows measured there are reasonably described over the complete (x, Q^2) plane. In the last step, parameters for radiation off initial-initial dipoles have been obtained from the Z $p_\perp$ spectrum as measured by CDF. Non-perturbative modelling is shown to have a major impact in describing this observable, and more sophisticated models will have to be considered here.

In all cases we find that the NLO predictions give results comparable to LO predictions, with no or few improvements visible. This may be attributed to the 'simplicity' of the processes studied here in the sense that only two coloured partons are involved in the Born process yielding trivial colour correlations and factoring vertex corrections only. The programs developed within the context of this work allow however to study more complex processes, which will be looked at in future work.

11 Outlook

The collider experiments being currently operated, most notably these at CERN's Large Hadron Collider, require theoretical predictions for final states as encountered in reality. Up to recent work, these predictions – being carried out by using Monte Carlo methods – have mostly only been available at the leading order of QCD perturbation theory. The increasing precision of data acquired at collider experiments, including those from experiments not being in operation anymore, require a similar precision for theoretical predictions. Including higher-order QCD corrections into parton shower simulations has thus emerged to be a vital field of research. In this thesis, a twofold approach has been presented to improve simulations to the next-to-leading order in QCD perturbation theory.

This includes on the one hand theoretical development and the implementation of a parton shower algorithm which eases the combination with higher order QCD corrections, while maintaining the correct description of multiple parton emission. On the other hand, a detailed and rigorous theoretical basis for deriving matching conditions to higher orders has been formulated. Within this calculational formalism, the most general form of matching parton showers and NLO calculations, and, for the first time also NNLO corrections, have been calculated.

The new parton shower algorithm and a framework for setting up NLO calculations and performing parton shower matching either through matrix element corrections or subtractive matching in a fully automated way have been implemented within the event generator Herwig++. The NLO framework requires solely a code calculating the respective tree-level and one-loop amplitudes, for which automated approaches are available as well besides many specialised and optimised codes for certain classes of processes. This opens up possibilities to provide a self-contained event simulation at NLO with less or no additional work required, as opposed to other approaches. A major technical obstacle to achieve such a level of automation has been solved by the development of dedicated Monte Carlo methods and a flexible library implementing these to sample the required

distributions without analytic knowledge about matrix element properties.

The simulation has been validated for simple processes at all major collider types, *i.e.* for e^+e^- annihilation into jets, deep inelastic scattering, and Drell-Yan lepton pair production at hadron colliders. Reasonable agreement has been found with data acquired by the LEP experiments, H1 and CDF. For this class of processes, the impact of NLO corrections turned out not to be significant besides the overall normalisation after having performed independent fits at LO and NLO precision. Since this is certainly not a general statement and readily traced back to the fact that in these processes no non-trivial colour correlations nor non-factoring virtual corrections are involved, the study of more complex processes is mandatory. The software libraries developed enable these studies in a straightforward way, and one of the 'non-trivial' processes to be considered next will certainly be the inclusion of NLO QCD corrections to jet pair production at hadron colliders, a process which is of interest for example when extracting parton distributions.

A further improvement of the simulation would be the consistent combination of NLO QCD corrections to processes being accompanied by an additional number of jets. Such a combination has successfully been achieved at LO already within the context of CKKW/L merging, and a similar merging at NLO is thus of utmost importance. Again, the simulation developed in this thesis work may form the basis of such an algorithm. Having at hand the theoretical basis to perform matching at NNLO, and the recent developments in turning NNLO calculations into fully differential Monte Carlo programs, a first attempt to implement such a matching will certainly be undertaken in the near future.

A The Exsample Library

This appendix documents the main structure of the **exsample** library used to sample events from differential cross sections and Sudakov-type densities. The main **exsample** classes are described in table A.1. The next sections describe the most important classes for a user of **exsample**, *i.e.* the interface to the density to be sampled, the interface to parameters steering the adaption behaviour and the usage of the generator classes for standard sampling or Sudakov-type sampling as discussed in chapter 7. **exsample** provides an interface of the standard sampling generator to **ThePEG**'s **SamplerBase** interface used in generating events.

A.1 The Density Interface

All **exsample** classes heavily make use of the **template** facilities provided by C++ to act in a very generic way. To this extent, there is no base class for a class representing a density to be sampled. The **exsample** generator classes instead expect the density object to meet a certain concept, which is defined in the following. In addition, the **exsample** generator classes are templated with the type of container representing a point in the sampling volume. This defaults to **std::vector** which we will assume has been used here. A density object then needs to provide the following methods:

- **pair<vector<double>,vector<double> > support() const** Return the boundaries of the sampling volume as a pair of the lower left and upper right corner.

- **size_t dimension() const** Return the number of variables the density depends on

- **unsigned long maxtry() const** Return the maximum allowed number of attempts to draw an event from the density.

Class Name	Description
binary_tree	Generic binary tree class used to build up sampling trees. Contains implementation of the sub-tree hashing algorithm and selection of tree leafs according to a **selector** object.
cell	A sampling cell.
sampling_selector	Selector class passed along a **binary_tree** to sample cells in the standard sampling context.
parametric_sampling_selector	Selector class passed along a **binary_tree** to sample cells with some variables fixed.
linear_interpolator	Implementation of a simple linear interpolation and its inversion, used to generate the next evolution variable in the Sudakov veto algorithm.
statistics	Generic statistics class used to accumulate information in the Monte Carlo estimate of a density's integral and overall efficiencies.
adaption_info	Container for parameters steering the adaption behaviour of the **exsample** algorithm.
generator	Main class for standard sampling of densities.
exponential_generator	Main class for Sudakov-type sampling.

Table A.1: The main classes of the **exsample** library.

- unsigned long presampling_points() const Return the number of presampling points which should be used for the density.

- void start_presampling() Informs the density object that exsample is about to presample the density.

- void stop_presampling() Informs the density object that exsample is done with presampling the density.

- double evaluate(const vector<double>&) Evaluate the density at the given point.

Additional functions to be supplied for Sudakov-type sampling are

- vector<bool> variable_flags() const Indicate which of the variables are not considered parameters, including the evolution variable.

- size_t evolution_variable() const Indicate which of the variables corresponds to the evolution variable.

- size_t evolution_cutoff() const Return the lower boundary on the evolution variable.

- vector<double> parameter_point() const Return the parameter values at which the next event should be generated.

A.2 The Generator Classes

The main interface of the generator classes, with a template parameter Function representing the density object, consists of the following methods:

- void function(Function* f) Set the density object.

- Function& function() Return the density object.

- adaption_info& sampling_parameters() Access the adaption parameters (see next section for details).

- void initialize() Initialize the generator.

- double generate() Generate an event and return the sign of its weight (for standard sampling), or zero or one for Sudakov-type sampling indicating if the event has been selected below or above the evolution variable cutoff.

- const vector<double>& last_point() const Return the last generated event.

- void reject() Indicate that the last generated event has been rejected by the code using the generator. Rejections of this type will be included in optimizing the efficiency.

- void finalize() Finalize the generator performing cleanup and calculation of final statistics accumulated.

Methods special to generator are:

- const statistics& stats() const Return the statistics object accumulating information on integral estimates and efficiency.

- double integral() const Return the estimate of the density's integral.

- double integral_variance() const Return the variance on the integral estimate.

- bool compensating() const Return true, if the generator is in a compensating state, *i.e.* if there are cells with a non-zero number of missing events.

A.3 Adaption Parameters

The parameters steering the adaption are contained in a simple adaption_info structure, providing the following members:

- double efficiency_threshold Lower limit on the unweighting efficiency below which a cell will be considered for splitting.

- double gain_threshold Value of the gain measure, eq. 7.2, above which a cell split is considered worth being performed.

- unsigned long freeze_grid The number of accepted events after which the adaption procedure should be stopped. If zero, adaption is always being performed.

- vector<bool> adapt False values indicate that the corresponding variable should not be included in the adaption procedure. No efficiency is recorded for such variables, nor are splits being performed along the corresponding hypercube dimension.

B The DipoleShower Module

This appendix documents the DipoleShower add-on module to the Herwig++ event generator. DipoleShower has been developed as part of this thesis, and will be made publicly available in the near future. It implements the dipole shower algorithm defined in chapters 5 and 8 and is well integrated with Herwig++'s structure to handle multiple interactions for hadron collisions.

Section B.1 gives an overview of the main classes of the module, whereas section B.2 introduces more details of the work flow how an event is handled. Finally, section B.3 introduces the module from a user's point of view.

B.1 General Structure and Main Classes

The DipoleShower modules maps the physical ingredients of the parton shower algorithm almost one-to-one to an object hierarchy. The corresponding classes are however implemented in a more abstract way such as to allow for additional flexibility, when *e.g.* considering ordering variables other than the transverse momentum or to allow for the implementation of splitting kernels for emission off massive quarks.

The most basic object entering is probably the Dipole class, representing a dipole formed by two partons. Dipole objects are assembled in DipoleChain objects, as introduced in chapter 8.

The splitting probabilities are defined by an object of class DipoleShowerSplittingKernel, representing the azimuthally averaged dipole splitting function, together with a DipoleSplittingKinematics object implementing the kinematic parametrization and the phase space weight to accompany the splittings described, and a ThePEG::AlphaS object implementing the running strong coupling. DipoleShower provides one- and two-loop

running α_s implementations, where the threshold matching is simply performed by requiring continuity of $\alpha_s(q^2)$ along m_n^2, where m_n is the mass of the n'th flavour to become active.

Splittings for a dipole are generated by DipoleSplittingGenerator objects, assembling DipoleShowerSplittingKernel, DipoleSplittingKinematics and ThePEG::AlphaS objects to completely define a splitting probability[1]. The needed Sudakov-type distribution is sampled by making use of the Exsample library. Any sensible choice of evolution for the dipole cascade can be implemented in objects deriving from the DipoleEvolutionOrdering class.

The complete showering of a sub process is managed by the DipoleShowerHandler class. Several utility classes are provided for special tasks within the evolution and management of the event record. The main physics classes are listed in table B.1, along with a short description making use of the notation as introduced in chapter 8. The list of utility classes can be found in table B.2.

B.2 Work Flow

The general initialization and evolution algorithms have already been formalized in 8.2. This section gives an overview of how the components described in the previous section act together such as to implement these algorithms. This work flow is depicted in figure B.1.

In the initialization phase, the colour ordering is performed by making use of ThePEG's representation of colour flows. Colour flows are represented by colour lines containing references to the particles which are connected to these lines. Colour ordering can thus be implemented relatively straightforward, by noting that a colour singlet is 'simply connected' with respect to its colour flow topology, *i.e.* walking along colour lines (being the equivalent of a fundamental-representation Kronecker-δ), any parton in the singlet can be reached by following colour lines, changing from a colour to an anti-colour line on an external gluon. Along this 'walk', the referred ThePEG::Particle objects are already appended to a list. A new list is opened, when the end of a colour singlet is reached.

The colour ordered partons are then sorted in dipole chains, and the hard scales are reported by the DipoleEvolutionOrdering object, given additional parameters such as the type of the splitting through a reference to a DipoleSplittingKernel object.

During the evolution stage, a performance-critical issue is the efficient generation of candidate splittings for each dipole – this is much more important than in a traditional parton shower, since in dipole-type showers all dipoles in a chain are competing for splittings at any stage at the evolution, giving a multiple of the candidate splittings to

---

[1] The ThePEG::AlphaS object is actually contained in the DipoleSplittingKernel objects.

Class Name (← Inherits from)	Description
DipoleSplittingKinematics ← ThePEG::HandlerBase	Base class for kinematic parametrisations and phase space weight $$\hat{q}_{a,c,b}(\hat{p}_{a,b}, p_\perp^2, z, \phi) \ , \qquad \mathrm{d}\phi_1(\hat{p}_{a,b}, p_\perp^2, z)$$
DipoleSplittingKernel ← ThePEG::HandlerBase	Base class for azimuthally averaged splitting kernels $$\langle \mathbf{V}_{a,c,b}\rangle(\hat{p}_{a,b}, p_\perp^2, z)$$.
DipoleSplittingGenerator ← ThePEG::HandlerBase	Assembles DipoleSplittingKernel, DipoleSplittingKinematics, ThePEG::AlphaS and PDFRatio objects to sample $p_\perp^2, z$ points according to the density $$\mathrm{d}P_{(a,b\to a',c,b)}(p_\perp^2, z)\Delta_{(a,b\to a',c,b)}(p_\perp^2, p_{\perp,a,b}^2)$$
Dipole	Class representing a dipole $\hat{q}_a, \hat{q}_b$. Associates to a pair of ThePEG::Particle objects information on momentum fractions and PDF's for incoming partons, and a DipoleIndex object for each emitter-spectator assignment.
DipoleChain	Represents a dipole chain C and provides implementations of inserting dipole splittings, rotating or a chain which became non-circular or splitting a non-circular chain.
DipoleEventRecord	Represents a collection of dipole chains, $\mathcal{C}$. Provides implementations for colour ordering and chain finding of partons at a hard sub process, and filling the ThePEG event record after the showering has terminated.
DipoleEvolutionOrdering ← ThePEG::HandlerBase	Base class for selecting hard scales, assigning scales after a splitting and determining a winner splitting.
DipoleShowerHandler ← Herwig::ShowerHandler	Main class steering the showering of a ThePEG::SubProcess object as passed from the Herwig::ShowerHandler class.

Table B.1: Main classes of the DipoleShower module.

Class Name (← Inherits from)	Description
DipoleIndex	Indexes a emitter-spectator selection for a dipole of flavours a, b, along with references to ThePEG::PDF objects for incoming partons. Used to index different splitting generators capable of selecting splittings of a dipole of given type.
DipoleSplittingInfo	Contains full information on a splitting to be performed, *i.e.* a DipoleIndex object, a reference to a DipoleSplittingKinematics object, and the selected values of $p_\perp^2$, z and ϕ.
DipolePartonSplitter	Performs $1 \to 2$ parton splittings with the proper selection of colour information.
PDFRatio ← ThePEG::HandlerBase	Numerical stable implementation of ratios of the form $$\frac{f_{P \leftarrow a}(x/z, q^2)}{f_{P \leftarrow b}(x, q^2)}$$
IntrinsicPtGenerator ← ThePEG::HandlerBase	Traditional approach to Gaussian-distributed intrinsic transverse momentum of incoming partons. Applicable to hadron-hadron collisions only.
ConstituentReshuffler ← ThePEG::HandlerBase	Performs the transformation ('reshuffling') of partons from their pole to constitutent mass shells in order to make use of the cluster hadronization model possible.

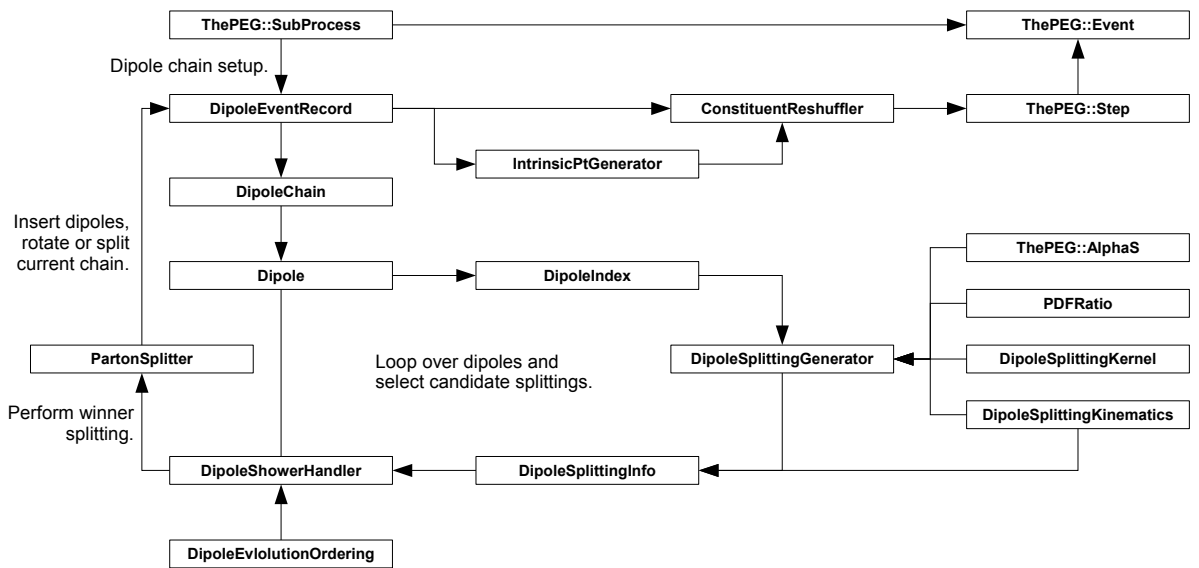Table B.2: Utility classes of the DipoleShower module.

Figure B.1: Work flow in the DipoleShower module.

be generated to reach the same multiplicities, as if there where only individually evolving partons undergoing $1 \rightarrow 2$ splittings.

The Exsample library enables a very efficient sampling of a single splitting kernel, though it needs a certain 'adaption' phase and nonetheless a non-negligible amount of memory. The task is therefore to keep the number of Exsample::exponential_generator objects as small as possible.

To this extent, new generators are firstly only built and initialized, if a splitting of a certain type occurs for the first time during running the generator. This avoids a long initialization phase potentially presampling kernels which will never be used in the evolution. Secondly, each DipoleSplittingKernel can flag a certain splitting type to be equivalent to another splitting type. In this case, generation of the equivalent splitting is automatically redirected for the already running Exsample::exponential_generator object. Examples of this type are all splittings with a massless final state spectator, making no reference to the flavour of the spectator.

B.3 User Interaction

This section describes the most relevant interfaces of the main DipoleShower classes steerable from input files. For a complete documentation the reader is referred to the source code documentation.

B.3.1 'End User' Interfaces

DipoleSplittingKinematics interfaces:

- IRCutoff: Set the $p_\perp$ infrared cutoff in units of GeV

DipoleSplittingKernel interfaces:

- AlphaS: The α_s implementation to be used.

- SplittingKinematics: The kinematics parametrization to be used.

- PDFRatio: The PDFRatio object for numerical stable evaluation of PDF ratios.

- Flavour: The quark flavour to be produced, if ambiguous (*e.g.* in $g \rightarrow q\bar{q}$ the flavour cannot be obtained from the flavours of the splitting dipole).

- ScreeningScale: Optional soft scale μ in units of GeV for a simple modification of α_s in the infrared region, $\tilde{\alpha}_s(q^2) = \alpha_s(q^2 + \mu^2)$.

- PresamplingPoints: The number of points used for presampling the splitting kernel.

- MaxTry: The maximum number of attempts to generate a splitting.

DipoleShowerHandler interfaces:

- Kernels: Vector of splitting kernels to be considered.

- EvolutionOrdering: The evolution ordering to be used.

- ConstituentReshuffler: The object to transform partons to constitutent mass shells.

- IntrinsicPtGenerator: Intrinsic $p_\perp$ generation for hadron-hadron collisions.

- GlobalAlphaS: When used, the ThePEG::AlphaS objects of *all* splitting kernels are overridden by the object set through this interface.

- DoFSR: Switch On or Off final state radiation.

- DoISR: Switch On or Off initial state radiation.

IntrinsicPtGenerator interfaces:

- ValenceIntrinsicPtScale: The mean intrinsic $p_\perp$ for valence quarks in GeV.

- SeaIntrinsicPtScale: The mean intrinsic $p_\perp$ for sea quarks and gluons in GeV.

B.3.2 Developer Interfaces

DipoleSplittingKernel interfaces:

- MCCheck: Set a DipoleMCCheck object to numerically cross check sampled distributions.

DipoleShowerHandler interfaces:

- NEmissions: Limit the number of emissions to be generated.

- DiscardNoEmissions: When switched On, events which did not radiate are discarded. If NEmissions> 0 only events with exactly NEmissions emissions are accepted.

- Verbosity: Different levels of verbosity ranging from 1 to 3 to print debug information on the showering being performed. 0 disables debug output.

B The DipoleShower Module

C The Matchbox Module

This appendix documents the **Matchbox** add-on module to the Herwig++ event generator. **Matchbox** has been developed as part of this thesis, and will be made publicly available in the near future.

Along with the **Matchbox** development, several extensions to the **ThePEG** software framework, on which both Herwig++ and **Matchbox** are based, have been implemented in order to enable the processing of NLO Monte Carlo event generation within **ThePEG**.

The outline of this appendix is as follows: section C.1 discusses the general structure, main classes and gives a brief overview of the NLO extensions to the**ThePEG** framework. Section C.2 introduces the interface to matrix elements provided by external codes, while section C.3 outlines, how **Matchbox** automatically generates subtraction terms. Section C.4 sketches the work flow of the complete module when running 'plain' or matched NLO calculations, before section C.5 introduces a user's view on **Matchbox**.

C.1 General Structure and Main Classes

Being developed within the paradigm of an object-oriented library, **Matchbox** closely resembles the structure of a NLO calculation, and the matching schemes already discussed.

The ingredients for a standard NLO calculation are grouped into generic interfaces to (tree-level) matrix elements and interferences of one-loop and Born amplitudes, contributions of the dipole subtraction acting at the level of virtual corrections, *i.e.* the so-called insertion operators $\mathbf{I}$, $\mathbf{P}$ and $\mathbf{K}$, and subtracted real emission matrix elements. Phase space generators are considered part of the corresponding tree-level matrix element interface.

All these contributions are assembled into a ThePEG::SubProcessHandler object by the NLOFactory class, which is then handled by ThePEG's standard event generation chain. In addition, Matchbox provides utilities for coding amplitudes using contemporary techniques based on the spinor helicity formalism. The main classes for performing NLO calculations are listed in tables C.1, C.2 and C.3, along with a short description of the physics object they represent.

C.1.1 NLO Extensions for the ThePEG Framework

The ThePEG framework has been designed to provide a toolkit for the full simulation of events in a high-energy physics experiment, starting from a hard sub process, going on to parton showers, multiple parton interaction models, hadronization and decays of unstable particles. It provides enormous flexibility for this whole chain of event simulation, but so far has been implemented and maintained with only leading order cross sections in mind. Though recently support has been added for merging tree-level matrix elements of different multiplicity and parton showers, native support for NLO calculations and matching to parton showers has so far been missing.

During the development of Matchbox, several obstacles with regard to NLO calculations have been removed and additional functionality to natively support NLO calculations has been added to ThePEG. In particular, the frequently encountered grouping of a real emission phase space point along with a set of Born-type phase space points originating from subtraction terms is now possible. The corresponding functionality has, however, been implemented in a generic way, as such groupings may not only appear in the context of subtracted real emission matrix elements and are indeed also used by Matchbox to calculate inclusive NLO cross sections as entering POWHEG-type matchings. The main extensions are described in table C.4.

C.1.2 Matching with Matrix Element Corrections

Matchbox is in particular capable of automatically turning a NLO calculation into a POWHEG-type matching, or 'matching with matrix element correction'. Again, the class structure closely resembles the contributions entering this matching scheme. A crucial concept within this context are the various forms of ratios of a matrix element squared, or a subtraction dipole, divided by a sum of subtraction dipoles. These contributions are all represented by objects of type ME2byDipoles. The inclusive QCD cross section is evaluated by making use of a specialized ThePEG::MEGroup class, the 'finite' real emission contributions – if a screening of the Born process due to radiation zeroes or vanishing flux factors is in order – are represented by ordinary MatchboxMEBase objects, re-weighted by the required ME2ByDipoles objects.

Class Name ($\leftarrow$ **Inherits from**)	Description
MatchboxMEBase $\leftarrow$ThePEG::MEBase	Base class for tree-level matrix elements. Represents • amplitudes squared, $\|\mathcal{M}\|^2$ • correlated amplitudes, $\langle\mathcal{M}_\mu\|C^{\mu\nu}\mathbf{T}_i\cdot\mathbf{T}_j\|\mathcal{M}_\nu\rangle$, • and a phase space generator for the process implemented.
MatchboxVirtualMEBase $\leftarrow$ThePEG::HandlerBase	Base class for virtual corrections. Represents • one-loop/Born interference, • or insertion operators.
MatchboxNLOME $\leftarrow$ ThePEG::MEBase	Assembles a MatchboxMEBase and several MatchboxVirtualMEBase objects calculating the Born process and virtual corrections, respectively.
SubtractionDipole $\leftarrow$ ThePEG::MEBase	Base class for subtraction dipoles $\mathcal{D}_{ij,k}$.
TildeKinematics $\leftarrow$ ThePEG::HandlerBase	Base class for the 'tilde' mapping, $\tilde{p}_{ij}(q_i,q_j,q_k),\tilde{p}_k(q_i,q_j,q_k)\equiv p_n^\alpha(q_{n+1})$.
SpinCorrelationTensor	A Lorentz tensor of the form $c\eta^{\mu\nu}+k^\mu l^\nu$ used for spin-correlated amplitudes.
SubtractedME $\leftarrow$ ThePEG::MEGroup	Assembles a MatchboxMEBase and several SubtractionDipole objects calculating a subtracted real emission matrix element.

Table C.1: The main classes used to perform NLO calculations within Matchbox.

Class Name (← Inherits from)	Description
DipoleRepository	Contains the different SubtractionDipole objects and insertion operators available. Any dynamically loaded library may register subtraction dipoles or insertion operators with the DipoleRepository.
DipoleIOperator ← MatchboxVirtualMEBase	The insertion operator $\mathbf{I}$, capable of dealing with arbitrary processes for massless quarks.
DipolePKOperator ← MatchboxVirtualMEBase	The sum of the insertion operators $\mathbf{P}$ and $\mathbf{K}$, capable of dealing with arbitrary processes for massless quarks.
NLOFactory ← ThePEG::SubProcessHandler	Assembles all contributions to a NLO calculation into a ThePEG::SubProcessHandler object to be used by the standard event generation chain.

Table C.2: Classes used for the automated dipole subtraction provided by Matchbox.

Class/Namespace Name	Description
SpinorHelicity (namespace)	Provides implementations of the Weyl spinors $|p\rangle$ and $|p]$, spinor inner products $\langle pq \rangle$, $[pq]$ and currents $\langle p|\gamma^\mu|q]$, $[p|\gamma^\mu|q\rangle$.
AmplitudeCache	Caching facilities for invariants, spinor products and off-shell currents.

Table C.3: Support for implementing spinor helicity amplitudes in Matchbox.

Class Name (← Inherits from)	Description
MEGroup ← MEBase	Base class for a 'matrix element group', consisting of a 'head' matrix element (*e.g.* a real emission matrix element) and a set of 'dependent' matrix elements (*e.g.* subtraction terms)
StdXCombGroup, StdDependentXComb ← StandardXComb	Information on phase space points associated to a MEGroup object.
SubProcessGroup ← SubProcess	A group of a 'head' and a set of 'dependent' hard sub process objects, as generated by a MEGroup object.

Table C.4: Main NLO extensions to ThePEG.

Again, all pieces are assembled automatically into a ThePEG::SubProcessHandler by the PowhegFactory class. A specialized PowhegSplittingGenerator class acts as a so-called post sub-process handler within ThePEG, generating real emission radiation according to the matrix element correction Sudakov form factor, eventually replacing a Born-type with a real emission type sub-process. The main classes relevant for the automatised POWHEG matching are listed in table C.5.

C.2 The Matrix Element Interface

One of the main design criteria in the development of Matchbox has been to use already existing programs for calculating the amplitudes for certain processes and to facilitate the efficient generation of phase space points – leaving the main task of matching calculations to Matchbox, while not imposing unnecessary constraints on the fixed-order codes.

The interface between both is Matchbox's generic matrix element handling, defined through the MatchboxMEBase and MatchboxMEVirtualBase base classes, which are described in more detail in this section. The interface closely complies with parts of a proposal raised by the author at the Les Houches workshop 2009, [56].

Besides the functionality required by ThePEG::MEBase, which includes implementing a phase space generator through

$$\text{ThePEG::MEBase::generateKinematics(const double * r)} \equiv \left| \frac{\partial \phi(p_n)}{\partial \vec{r}} \right| , ^1 \qquad (C.1)$$

and the tree-level matrix element squared through

$$\text{ThePEG::MEBase::me2()} \equiv |\mathcal{M}|^2 , \qquad (C.2)$$

MatchboxMEBase requires amongst minor bookkeeping issues the implementation of colour- and potentially colour- and spin-correlated amplitudes,

$$\text{MatchboxMEBase::colourCorrelatedME2(pair<int,int> ij)} \equiv \langle \mathcal{M} | \frac{\mathbf{T}_i \cdot \mathbf{T}_j}{\mathbf{T}_i^2} | \mathcal{M} \rangle , \quad (C.3)$$

$$\text{MatchboxMEBase::spinColourCorrelatedME2} \qquad (C.4)$$
$$\text{(int g, pair<int,int> ij, SpinCorrelationTensor C)} \equiv \langle \mathcal{M}_{\mu_g} | C^{\mu_g \nu_g} \frac{\mathbf{T}_i \cdot \mathbf{T}_j}{\mathbf{T}_i^2} | \mathcal{M}_{\nu_g} \rangle .$$

---

[1]Storing generated momenta in ThePEG::MEBase::meMomenta(), and the actual value of the Jacobian through ThePEG::MEBase::jacobian(double x).

Class Name ($\leftarrow$ **Inherits from**)	Description
ME2byDipoles $\leftarrow$ MatchboxReweightBase	Base class for objects of type $$\frac{X(q_{n+1})}{\sum_\alpha \mathcal{D}(p_n^\alpha(q_{n+1})|q_{n+1})}$$
InvertedTildeKinematics $\leftarrow$ ThePEG::HandlerBase	Base class for the inverted 'tilde' mapping, $q_{i,j,k}(\tilde{p_{ij}}, \tilde{p_k}; p_\perp^2, z, \phi) \equiv q_{n+1}^\alpha(p_n)$
PowhegInclusiveReweight $\leftarrow$ ME2byDipoles	Re-weights a subtraction dipole, $$\mathcal{D}_\alpha(p_n|q_{n+1}^\alpha(p_n)) \times \frac{|\mathcal{M}_R(q_{n+1}^\alpha(p_n))|^2}{\sum_\beta \mathcal{D}_\beta(p_n^\beta(q_{n+1}^\alpha(p_n))|q_{n+1}^\alpha(p_n))}$$ to obtain a contribution to the inclusive NLO cross section.
PowhegRealReweight $\leftarrow$ ME2byDipoles	Re-weights a real emission matrix element, $$|\mathcal{M}_R(q_{n+1})|^2 \times \frac{\mathcal{D}_\alpha(p_n^\alpha(q_{n+1})|q_{n+1})}{\sum_\beta \mathcal{D}_\beta(p_n^\beta(q_{n+1})|q_{n+1})}$$ contributing to the 'finite' real emission.
PowhegSplittingKernel $\leftarrow$ ME2byDipoles	Represents the matrix element correction kernel, $$\frac{\mathcal{D}_\alpha(p_n|q_{n+1}^\alpha(p_n))}{|\mathcal{M}_B(p_n)|^2} \times \frac{|\mathcal{M}_R(q_{n+1}^\alpha(p_n))|^2}{\sum_\beta \mathcal{D}_\beta(p_n^\beta(q_{n+1}^\alpha(p_n))|q_{n+1}^\alpha(p_n))}$$
PowhegInclusiveME $\leftarrow$ ThePEG::MEGroup	Assembles a MatchboxNLOME, a MatchboxMEBase and a set of SubtractionDipole objects to calculate the NLO inclusive cross section.
PowhegSplittingGenerator $\leftarrow$ ThePEG::StepHandler	Samples the real emission according to the matrix element correction Sudakov form factor, eventually replacing a Born-type by a real emission ThePEG::SubProcess object.
PowhegFactory $\leftarrow$ ThePEG::SubProcessHandler	Given a NLOFactory object, assembles all contributions to the fixed-order cross section into a ThePEG::SubProcessHandler object and a set of PowhegSplittingKernel objects to be used by a PowhegSplittingGenerator.

Table C.5: Matchbox's facilities for automatic POWHEG matching. For the notation the reader is referred to chapter 9.

The interface to virtual corrections requires the implementation of differential cross sections similar to ThePEG::MEBase, though the communication of the corresponding sub-process is simplified through the

<p align="center">bool MatchboxVirtualMEBase::apply(...)</p>

method, which is given a flavour assignment for a certain sub-process and shall return true, if the virtual correction is to be included for the process, and false otherwise.

With respect to the automated dipole subtraction, it is important for the virtual correction implementation to communicate, if it uses conventional dimensional regularization (CDR) or dimensional reduction (DR) through the

<p align="center">bool MatchboxVirtualMEBase::isDR()</p>

method, which should return true for the case of DR and false for the case of CDR.

C.3 Automatic Generation of Subtraction Terms

The automatic generation of subtraction terms is based on ThePEG's built-in functionality of communicating tree-level Feynman diagrams through the ThePEG::Tree2toNDiagram class. Within the development of Matchbox this class has been enhanced to support 'mergings' of two external partons attached to the same vertex. A ThePEG::Tree2toNDiagram is now capable of trying to merge an 'emission' particle and an 'emitter' particle, returning either failure, if emission and emitter are not connected to the same vertex, or the diagram resulting from the merging, including identifying the emitter after the merging through the

<p align="center">ThePEG::Tree2toNDiagram::mergeEmission(int emitter, int emission)</p>

method. Within a real emission matrix element, all possible mergings are checked, eventually giving rise to inclusion of the corresponding dipole if the merging returned a valid 'underlying Born process' from the merging. The corresponding dipole is then looked up from the global DipoleRepository object and inserted into the SubtractedME object to be built by the NLOFactory object.

Further, all insertion operators known to the DipoleRepository are queried, if they apply to the Born process at hand and are inserted into the corresponding MatchboxN-LOME object to be built by the NLOFactory.

C.4 Work Flow for NLO Calculations and Matching

The work flow of Matchbox to perform NLO calculations and matching to parton showers has been outlined in detail in the previous sections. The purpose of this section is to restore the global view in terms of a simple work flow diagram, given here:
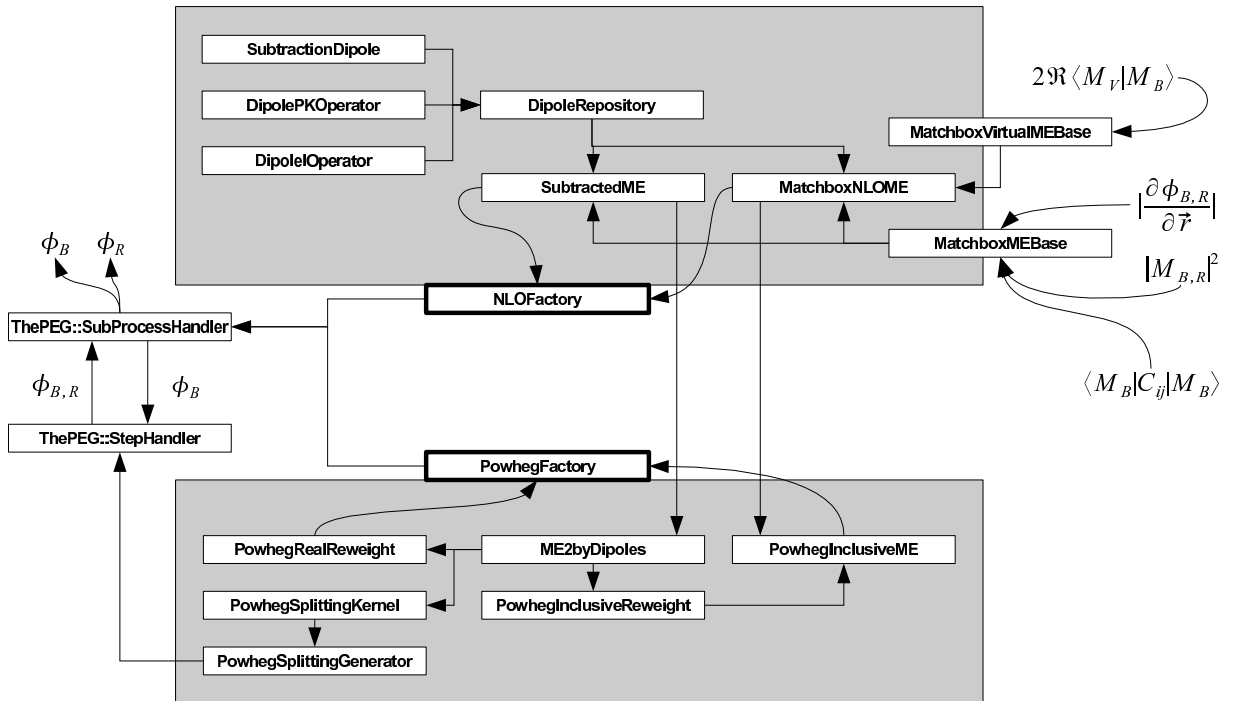
C.5 User Interaction

This section describes the most relevant interfaces of the main Matchbox classes steerable from input files. For a complete documentation the reader is referred to the source code documentation.

C.5.1 'End User' Interfaces

MatchboxMEBase interfaces:

- FactorizationScaleFactor: Factor to rescale the factorization scale μ_F.

- RenormalizationScaleFactor: Factor to rescale the renormalization scale μ_R.

NLOFactory interfaces:

- BornMEs: A vector of MatchboxMEBase objects implementing the Born processes to be considered.

- Virtuals: A vector of MatchboxVirtualMEBase objects implementing virtual corrections to the Born processes set in BornMEs.

- RealEmissionMEs: A vector of MatchboxMEBase objects implementing real emission corrections to the Born processes set in BornMEs.

- SubProcessGroups: When switched On, ThePEG::SubProcessGroups are created by the NLOFactory for running a 'plain' NLO calculation. Otherwise, real emission events are generated with a weight determined by the sum of real emission and subtraction term weights. The latter option (Off) can be used to run the DipoleShower on such events, performing the subtractive matching scheme.

PowhegFactory interfaces:

- NLOFactory: Set the NLOFactory object from which a matching with matrix element corrections should be built.

C.5.2 Developer Interfaces

NLOFactory interfaces:

- SubtractionData: Set a path where real emission phasespace points along with real emission and subtraction contributions are written to text files for checking the subtraction.

- Verbose: When switched On, the NLOFactory object will dump information on the automatic setup of the NLO calculation to standard output.

- Mode: Switch to select only parts of the NLO calculation. Options are All to take into account all contributions, BornVirtual for only Born and virtual corrections, or SubtractedReal for only subtracted real emission contributions.

PowhegFactory interfaces:

- Verbose: When switched On, the PowhegFactory object will dump information on the automatic setup of the matched calculation to standard output.

C The Matchbox Module

D Code Validation

This appendix gives an overview of the validation of the quite complex simulation code. Almost all classes available in the DipoleShower and Matchbox modules provide the possibility to extensively print out diagnostic information through both initialisation and event generation phases. The first test of functionality has been performed by looking in detail at these logs, and no malfunction has so far been recognised.

On the fixed order side, the performance of exsample on integrating cross sections has been cross-checked against ThePEG's built in ACDCSampler.[1] Full agreement has been found. In the following we will discuss validations of the shower implementation as present in the DipoleShower module as well as the NLO and matching code as present in Matchbox.

D.1 Shower Kernels

The sampling of shower splitting kernels has been explicitly verified *in situ*, meaning using the full implementation as present in the simulation code, against an independent implementation using a numerical integration to obtain the Sudakov-type distributions. Figure D.1 shows that full agreement has been found for the final-final splitting kernels, where the test has been performed using 'dummy' matrix elements producing a certain dipole of fixed invariant mass or in a range of masses. A similar test for kernels involving initial state partons is hard to implement owing to the limitations imposed by the ThePEG framework, as matrix elements cannot decide themselves on the distribution of incoming partons. Since the structures handling and sampling the splitting kernels are

---

[1]Where possible, since ACDCSampler is unable to handle differential cross sections of indefinite sign.

implemented in a completely generic way, treating final-final and other dipole splitting types on equal footing, no discrepancy is expected if the test was possible.

D.2 NLO Corrections

For the processes discussed in chapter 10, all leading-order cross sections have been checked to agree with the built in Herwig++ matrix elements.

In a next step, the functionality of the subtraction terms has been tested. Figures D.3 and D.3 show two typical examples of the ratio of subtraction to real emission cross section, plotted against each of the invariants entering the propagator denominators, proving full functionality of this part.

The 'plain' NLO cross section, and the inclusive one entering the matching with matrix element correction have been checked to agree, with and without the usage of the Born 'screening' cross section. The NLO cross section for $e^+e^- \to$ jets has been validated against the analytically known K-factor of $1 + \alpha_s/\pi$. The NLO cross section for Drell-Yan has been checked against the existing POWHEG implementation in Herwig++. For deep inelastic scattering, the subtraction terms have been modified in order to have positive definite dipole kernels, finite terms of the integrated subtraction terms have been changed accordingly. The functionality of the subtraction has been checked with both variants, and the NLO cross sections with and without modifications are found to agree.

A non-trivial cross check of the matrix element correction code and exsample as the underlying 'working horse', is to consider the spectra for a gluon emission off a $q\bar{q}$ dipole as generated by the shower, which is validated against a numerical integration of the expected distribution implemented in a completely independent code. By putting the real emission matrix element entering the matching to be equal to the sum of dipoles (the correctness of which has been checked by verifying that the cross section of the subtracted real emission matrix element is consistent with zero), the matrix element correction must produce the same spectrum as the shower code. Figure D.4 shows that this is indeed the case. It should be stressed that the machinery underlying the setup of the matrix element correction is much more complex than the shower implementation, and, that the splitting kernel entering the matrix element correction does depend on more parameters[2] than the one parameter of the shower kernel (corresponding to the dipole invariant mass). Again, a similar check for hadron collisions is hard to implement, but the same argument of the generic code structure handling all ingredients, as given in the previous section, applies also here.

---

[2]In a realistic application these are not two random numbers needed for the Born process, but indeed six, since photon radiation is generated of each incoming lepton, requiring two random numbers per incoming lepton.
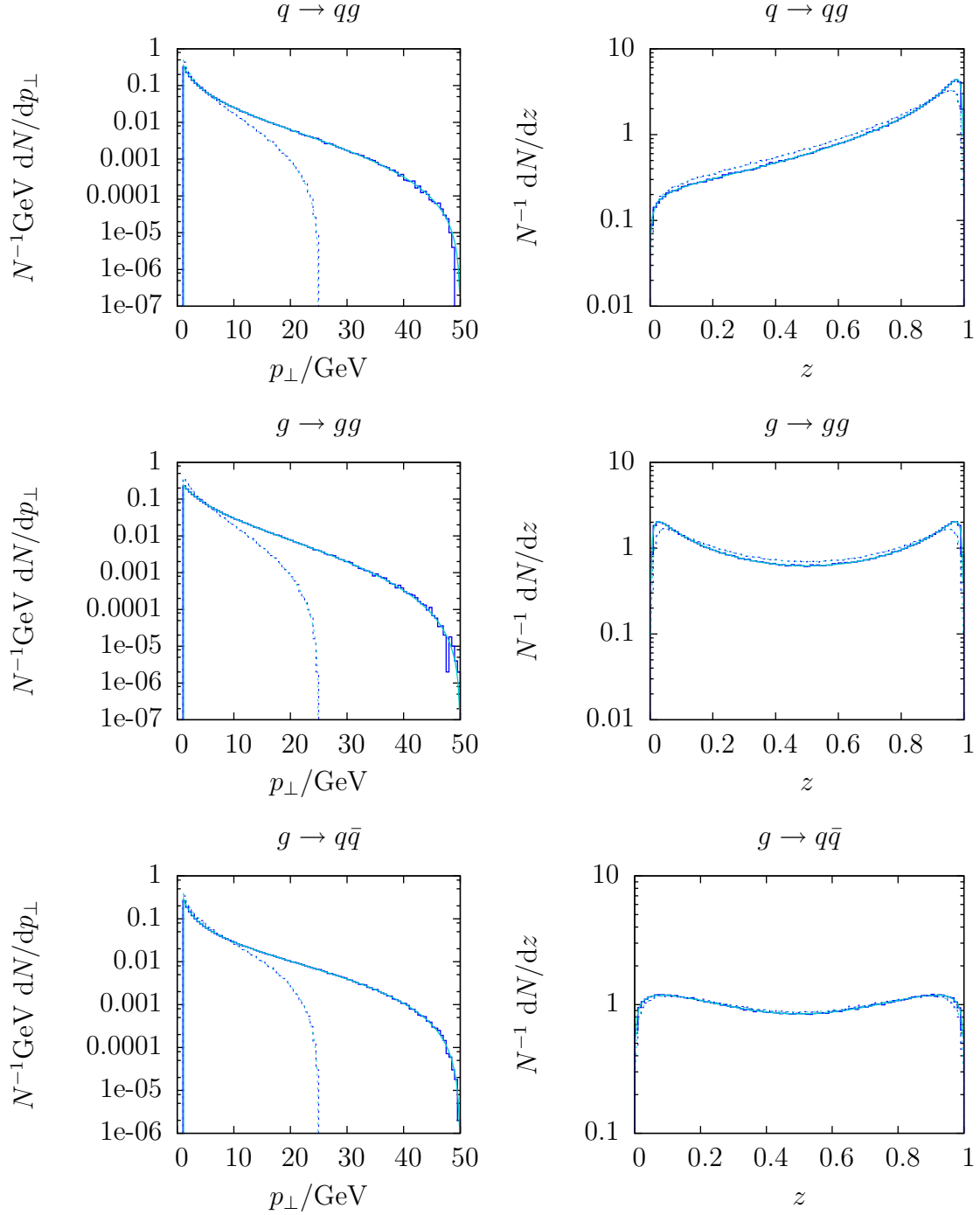
Figure D.1: Comparison of sampled final-final splitting kernels (blue lines) versus results from a numerical integration (turquoise lines) at two different dipole masses, $s_{ij} = (100\text{GeV})^2$ (continuous lines) and $s_{ij} = (50\text{GeV})^2$ (broken lines).
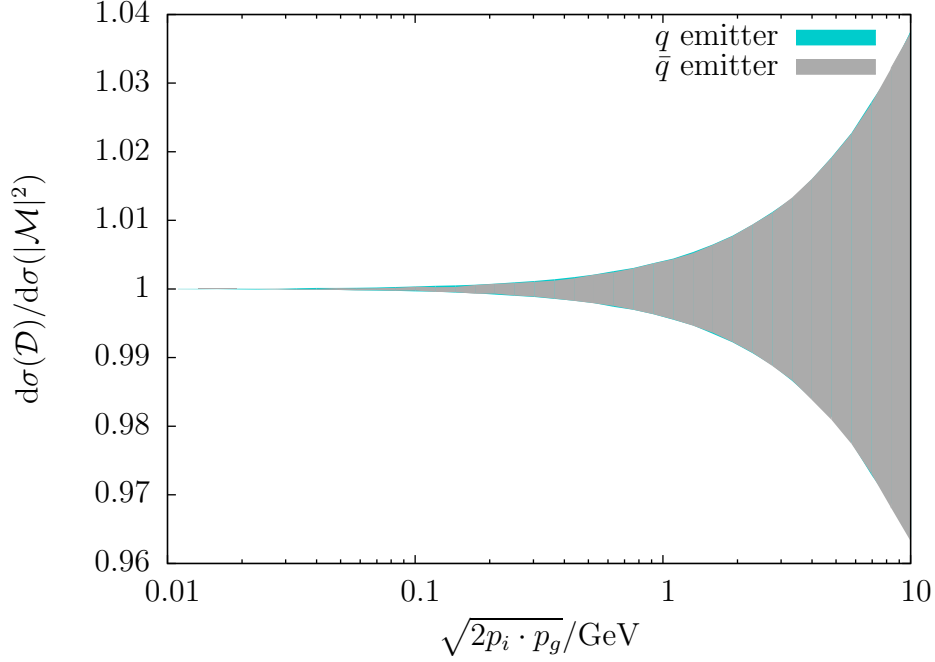
Figure D.2: Envelopes of the ratio of the subtraction to the real emission cross section versus the propagator denominator for both possible combinations in $e^+e^- \to 3$ jets events.
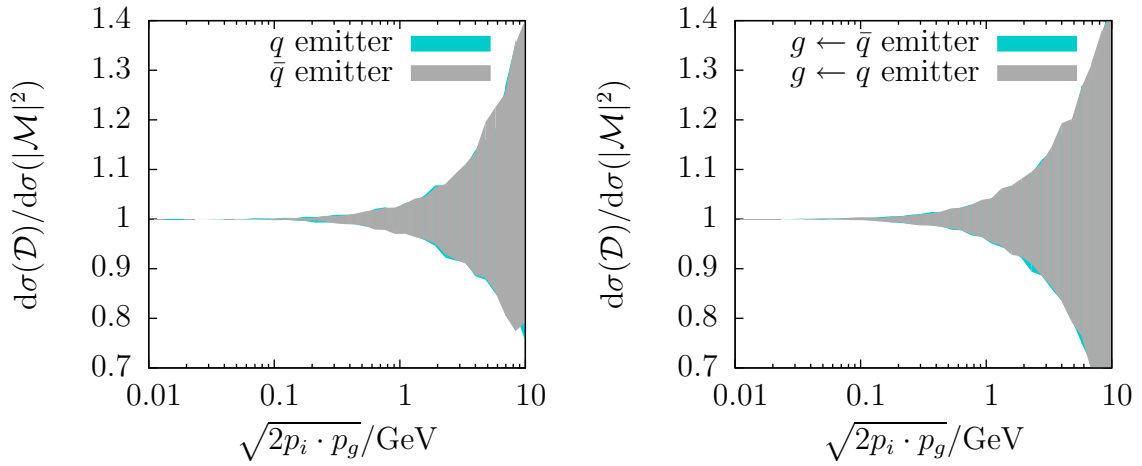

Figure D.3: Envelopes of the ratio of the subtraction to the real emission cross section versus the propagator denominator for all singular configurations in $Z + \mathrm{jet}$ production.
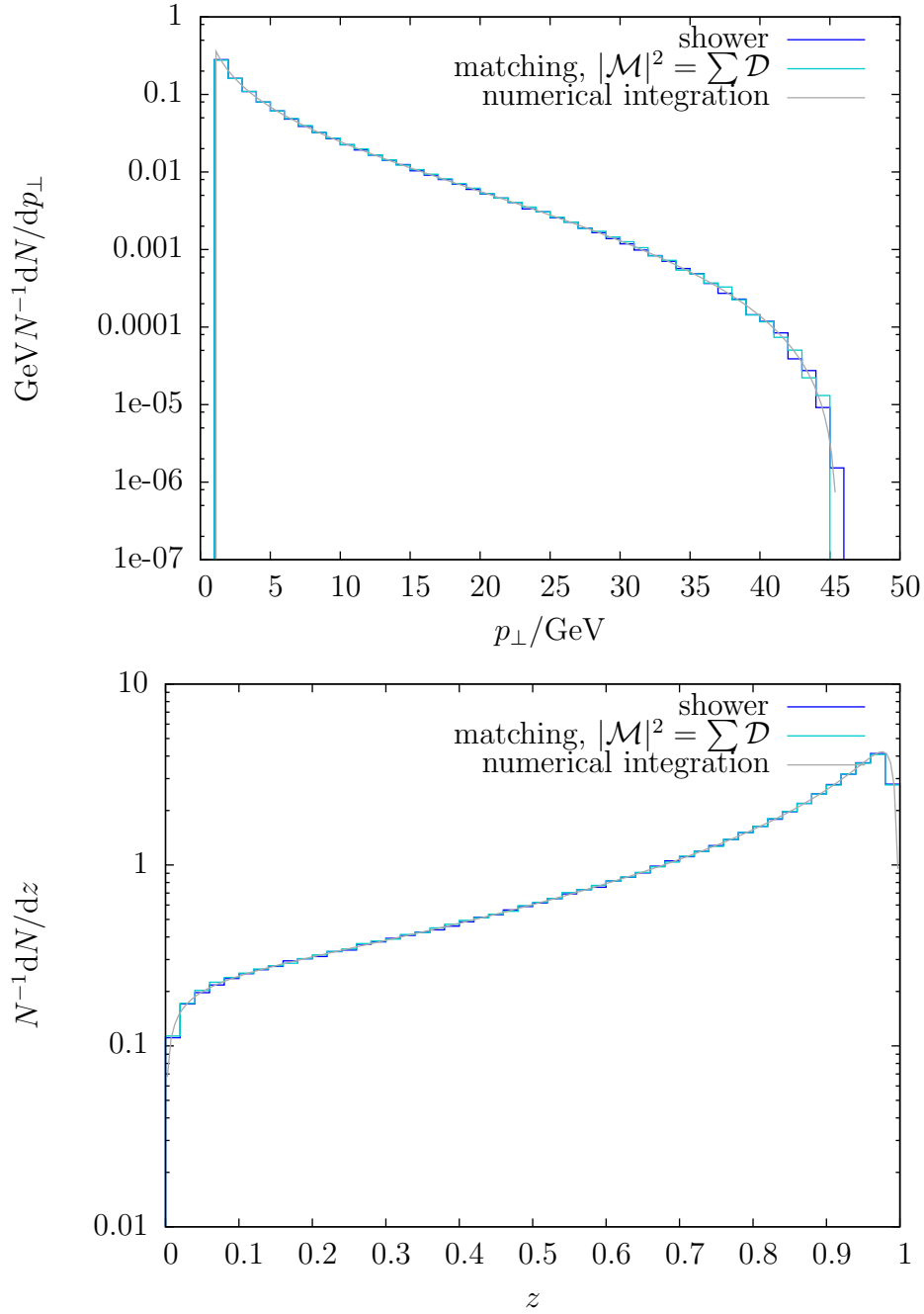
Figure D.4: $p_\perp$ and z spectra as generated from a final state $q\bar{q}$ dipole in LEP events. Putting the real emission matrix element to be equal to the sum of subtraction dipoles needs to reproduce the shower distribution (up to a normalisation) and thus provides a non-trivial cross check of the matching implementation, the complexity of which is much larger compared to the shower implementation.

D Code Validation

References

[1] C.N. Yang und R.L. Mills, *Conservation of isotopic spin and isotopic gauge invariance*, Phys. Rev. **96** (1954) 191–195.

[2] D.J. Gross und F. Wilczek, *Ultraviolet behaviour of non-Abelian gauge theories*, Phys. Rev. Lett. **30** (1973) 1343–1346.

[3] G.C. Callan und D.J. Gross, *Bjorken scaling in quantum field theory*, Phys. Rev. **D8** (1973) 4383–4394.

[4] J. C. Collins, D. E. Soper, and G. F. Sterman, *Factorization of Hard Processes in QCD*, Adv. Ser. Direct. High Energy Phys. **5** (1988) 1–91, [`hep-ph/0409313`].

[5] T. Kinoshita, *Mass singularities of Feynman amplitudes*, J. Math. Phys. **3** (1962) 650–677.

[6] S. Frixione, Z. Kunszt, and A. Signer, *Three jet cross-sections to next-to-leading order*, Nucl. Phys. **B467** (1996) 399–442, [`hep-ph/9512328`].

[7] D. A. Kosower, *Antenna factorization of gauge-theory amplitudes*, Phys. Rev. **D57** (1998) 5410–5416, [`hep-ph/9710213`].

[8] A. Gehrmann-De Ridder and M. Ritzmann, *NLO Antenna Subtraction with Massive Fermions*, JHEP **07** (2009) 041, [`arXiv:0904.3297`].

[9] S. Catani and M.H. Seymour, *A general algorithm for calculating jet cross sections in NLO QCD*, Nucl. Phys. **B485** (1997) 291–419, [`hep-ph/9605323`].

References

[10] S. Catani, S. Dittmaier, M. H. Seymour, and Z. Trocsanyi, *The dipole formalism for next-to-leading order QCD calculations with massive partons*, Nucl. Phys. **B627** (2002) 189–265, [hep-ph/0201036].

[11] G. 't Hooft, *A planar diagram theory for strong interactions*, Nucl. Phys. **B72** (1974) 461.

[12] G. Bozzi, S. Catani, D. de Florian, and M. Grazzini, *The q(T) spectrum of the Higgs boson at the LHC in QCD perturbation theory*, Phys. Lett. **B564** (2003) 65–72, [hep-ph/0302104].

[13] Z. Nagy and D. E. Soper, *Parton showers with quantum interference: leading color, with spin*, JHEP **07** (2008) 025, [arXiv:0805.0216].

[14] Z. Nagy and D. E. Soper, *Parton showers with quantum interference: leading color, spin averaged*, JHEP **03** (2008) 030, [arXiv:0801.1917].

[15] Z. Nagy and D. E. Soper, *Parton showers with quantum interference*, JHEP **09** (2007) 114, [arXiv:0706.0017].

[16] Z. Nagy and D. E. Soper, *Matching parton showers to NLO computations*, JHEP **10** (2005) 024, [hep-ph/0503053].

[17] S. Gieseke, P. Stephens and B.R. Webber, *New formalism for QCD parton showers*, JHEP **12** (2003) 045, [hep-ph/0310083].

[18] G. Marchesini and B.R. Webber, *Simulation of QCD Jets Including Soft Gluon Interference*, Nucl. Phys. **B238** (1984) 1.

[19] A. Bassetto, M. Ciafaloni and G. Marchesini, *Jet Structure and Infrared Sensitive Quantities in Perturbative QCD*, Phys. Rept. **100** (1983) 201–272.

[20] S. Schumann and F. Krauss, *A Parton shower algorithm based on Catani-Seymour dipole factorisation*, JHEP **03** (2008) 038, [arXiv:0709.1027].

[21] M. Dinsdale, M. Ternick and S. Weinzierl, *Parton showers from the dipole formalism*, Phys. Rev. **D76** (2007) 094003, [arXiv:0709.1026].

[22] M. Bähr et al., *Herwig++ Physics and Manual*, Eur. Phys. J. **C58** (2008) 639–707, [arXiv:0803.0883].

[23] S. Frixione and B. R. Webber, *Matching NLO QCD computations and parton shower simulations*, JHEP **06** (2002) 029, [hep-ph/0204244].

[24] S. Catani, F. Krauss, R. Kuhn, and B. R. Webber, *QCD Matrix Elements + Parton Showers*, JHEP **11** (2001) 063, [hep-ph/0109231].

[25] L. Lönnblad, *Correcting the colour-dipole cascade model with fixed order matrix elements*, *JHEP* **05** (2002) 046, [hep-ph/0112284].

[26] N. Lavesson and L. Lonnblad, *Extending CKKW-merging to One-Loop Matrix Elements*, *JHEP* **12** (2008) 070, [arXiv:0811.2912].

[27] P. Nason, *A new method for combining NLO QCD with shower Monte Carlo algorithms*, *JHEP* **11** (2004) 040, [hep-ph/0409146].

[28] P. Nason and G. Ridolfi, *A positive-weight next-to-leading-order Monte Carlo for Z pair hadroproduction*, *JHEP* **08** (2006) 077, [hep-ph/0606275].

[29] M. H. Seymour, *Matrix element corrections to parton shower algorithms*, *Comp. Phys. Commun.* **90** (1995) 95–101, [hep-ph/9410414].

[30] M. Bengtsson and T. Sjostrand, *Coherent Parton Showers Versus Matrix Elements: Implications of PETRA - PEP Data*, *Phys. Lett.* **B185** (1987) 435.

[31] M. Bengtsson and T. Sjostrand, *A Comparative Study of Coherent and Noncoherent Parton Shower Evolution*, *Nucl. Phys.* **B289** (1987) 810.

[32] G. Miu and T. Sjostrand, *W production in an improved parton shower approach*, *Phys. Lett.* **B449** (1999) 313–320, [hep-ph/9812455].

[33] S. Catani and M. Grazzini, *Infrared factorization of tree level QCD amplitudes at the next-to-next-to-leading order and beyond*, *Nucl. Phys.* **B570** (2000) 287–325, [hep-ph/9908523].

[34] A. Gehrmann-De Ridder, T. Gehrmann, and E. W. N. Glover, *Antenna subtraction method for jet calculations at NNLO*, *Nucl. Phys. Proc. Suppl.* **157** (2006) 32–36, [hep-ph/0601145].

[35] G. Somogyi, Z. Trocsanyi, and V. Del Duca, *A subtraction scheme for computing QCD jet cross sections at NNLO: regularization of doubly-real emissions*, *JHEP* **01** (2007) 070, [hep-ph/0609042].

[36] S. Weinzierl, *NNLO corrections to 3-jet observables in electron-positron annihilation*, *Phys. Rev. Lett.* **101** (2008) 162001, [arXiv:0807.3241].

[37] A. Gehrmann-De Ridder, T. Gehrmann, E. W. N. Glover, and G. Heinrich, *Jet rates in electron-positron annihilation at $O(\alpha_s^3)$ in QCD*, *Phys. Rev. Lett.* **100** (2008) 172001, [arXiv:0802.0813].

[38] Z. Bern, V. Del Duca, W. B. Kilgore, and C. R. Schmidt, *The infrared behavior of one-loop QCD amplitudes at next-to-next-to-leading order*, *Phys. Rev.* **D60** (1999) 116001, [hep-ph/9903516].

References

[39] S. Jadach, *Foam: A general purpose cellular Monte Carlo event generator*, *Comput. Phys. Commun.* **152** (2003) 55–100, [`physics/0203033`].

[40] L. Lonnblad, *ACDC – Auto Compensating Divide-and-Conquer Phase Space Generator*, *Part of the ThePEG framework, unpublished*.

[41] G. P. Lepage, *VEGAS: AN ADAPTIVE MULTIDIMENSIONAL INTEGRATION PROGRAM*, . CLNS-80/447.

[42] T. Sjöstrand, S. Mrenna, and P. Skands, *PYTHIA 6.4 Physics and Manual*, *JHEP* **05** (2006) 026, [`hep-ph/0603175`].

[43] R. Kleiss, W. J. Stirling, and S. D. Ellis, *A NEW MONTE CARLO TREATMENT OF MULTIPARTICLE PHASE SPACE AT HIGH-ENERGIES*, *Comput. Phys. Commun.* **40** (1986) 359.

[44] B. R. Webber, *A QCD Model for Jet Fragmentation Including Soft Gluon Interference*, *Nucl. Phys.* **B238** (1984) 492.

[45] S. Gieseke, M. H. Seymour, and A. Siodmok, *A Model of non-perturbative gluon emission in an initial state parton shower*, *JHEP* **06** (2008) 001, [`arXiv:0712.1199`].

[46] **DELPHI** Collaboration, P. Abreu *et. al.*, *Tuning and test of fragmentation models based on identified particles and precision event shape data*, *Z. Phys.* **C73** (1996) 11–60.

[47] **JADE** Collaboration, P. Pfeifenschneider *et. al.*, *QCD analyses and determinations of alpha(s) in e+ e- annihilation at energies between 35-GeV and 189-GeV*, *Eur. Phys. J.* **C17** (2000) 19–51, [`hep-ex/0001055`].

[48] A. Buckley *et. al.*, *Rivet user manual*, `arXiv:1003.0694`.

[49] A. Buckley, H. Hoeth, H. Lacker, H. Schulz, and J. E. von Seggern, *Systematic event generator tuning for the LHC*, *Eur. Phys. J.* **C65** (2010) 331–357, [`arXiv:0907.2973`].

[50] **Particle Data Group** Collaboration, K. Nakamura *et. al.*, *The Review of Particle Physics*, *J. Phys. G* **37** (2010) 075021.

[51] **H1** Collaboration, C. Adloff *et. al.*, *Measurements of transverse energy flow in deep inelastic- scattering at HERA*, *Eur. Phys. J.* **C12** (2000) 595–607, [`hep-ex/9907027`].

[52] A. D. Martin, W. J. Stirling, R. S. Thorne, and G. Watt, *Parton distributions for the LHC*, *Eur. Phys. J.* **C63** (2009) 189–285, [`arXiv:0901.0002`].

[53] R. S. Thorne, A. D. Martin, W. J. Stirling, and R. G. Roberts, *Update of MRST parton distributions*, *Acta Phys. Polon.* **B33** (2002) 2927–2932, [hep-ph/0207067].

[54] S. Catani, F. Fiorani, and G. Marchesini, *Small x Behavior of Initial State Radiation in Perturbative QCD*, *Nucl. Phys.* **B336** (1990) 18.

[55] **CDF** Collaboration, A. A. Affolder *et. al.*, *The transverse momentum and total cross section of e^+e^- pairs in the Z boson region from $p\bar{p}$ collisions at $\sqrt{s} = 1.8$ TeV*, *Phys. Rev. Lett.* **84** (2000) 845–850, [hep-ex/0001021].

[56] J. M. Butterworth *et. al.*, *The Tools and Monte Carlo working group Summary Report*, arXiv:1003.1643.

Acknowledgements

I would like to thank all members of ITP for a very inspiring environment in which this work has been carried out. Many thanks go to Dieter Zeppenfeld for giving me the opportunity to do a PhD, and many valuable comments and advice on my work.

Mike Seymour, Yuri Dokshitzer and Leif Lönnblad have indirectly contributed to the progress of this work through various discussions and remarks. I would especially like to thank Leif for many encouraging comments.

Last not least I would like to express my deep thanks to Stefan Gieseke for all his great support and confidence in my work, for giving me many opportunities to enlarge and share my knowledge through the possibility to attend numerous workshops and conferences and a very fruitful period of work at CERN.

Danksagung

Bei Matthias Steinhauser möchte ich mich für die Übernahme des Korreferats bedanken.

Bei Peter Marquard möchte ich mich bedanken für eine sehr gute Zusammenarbeit und spannende Zeit während der Administration der Rechner und Server am ITP und TTP – und auch für viele interessante Diskussionen über Zwei-Loop Integrale.

Grosser Dank gebührt meinen Eltern und meiner Schwester für die jahrelange Unterstützung während Studium und Promotion.

Ganz herzlich möchte ich mich bei Stephanie Manz für all die schönen Momente ausserhalb meiner Arbeit und die grossartige Unterstützung und Ermutigung bedanken, die unmessbar zu meiner Motivation beigetragen haben.

November 2, 2010